Physico-Chemical Properties of Silicate Melts

INAUGURALDISSERTATION

ZUR ERLANGUNG DES DOKTORGRADES

DER FAKULTÄT FÜR GEOWISSENSCHAFTEN

DER LUDWIG-MAXIMILIANS-UNIVERSITÄT MÜNCHEN

VORGELEGT VON

MARCEL POTUŽÁK

München, May 2006

"No matter how much you do, you never do enough…"

Die vorliegende Arbeit wurde in der Zeit von Dezember 2001 bis Dezember 2005 am Department für Geo und Umweltwissenschaften der Ludwig-Maximilians-Universität, München angerichtet.

Tag des Rigorosums: 07. 07. 2006

Promotionskomissions-
vorsitzender: Prof. Dr. H. Igel

1. Berichterstatter: Prof. Dr. D.B. Dingwell
2. Berichterstatter: Priv. Doz. Dr. T. Kunzmann

Übrige Promotions-   Prof. Dr. P. Gille
komissionsmitglieder: Prof. Dr. T. Fehr

Content

Thanks to

Prof. Dr. Donald Bruce Dingwell to accept me in Munich, offering and supervising this very interesting study. Many thanks to him for finding a sources to cover expenses of the scientific conferences and for rare but very intensive, useful and open discussions. My first supervisor p.g. Petr Jakeš PhD to sending me to Munich. I am very sad that I can not to tell him personally how much I appreciate his introduction to the problems of „Simulating the Earth".

My parents, František and Blanka, who enabled this scientific life by always supporting me. My grandmother Marie to keep my mind open even if my life situation was critical. My sister Dominika and brother Lukáš for going through the Potužák´s way of education.

My colleagues in office, lab and field Daniele Giordano, Philippe Courtial, Kai-Uwe Hess, Werner Ertel-Ingrisch, Alex Rocholl, Oliver Spieler, Ben Kennedy, Lothar Schwarzkopf, Betty Scheu, Sebastian Müller, Alfonso Davila, Jacopo Taddeucci, Benoit Cordonnier, Thomas Dorfner, Antonia Wimmer, Yan Lavallée, Dominique Richard, Jan Pawlowski, Conrad Gennaro and many more unmentioned but not forgotten.

Special thanks to Alex Nichols alias "Sir Bamboo" for his specific British humour and countless English correction of my very first article. Many thanks to Ulli Küppers for listening me and for frequent help and assistance in any kind of never-ending bureaucratic tasks.

Very special thanks to Anny Mangiacapra for her strong support during a good and even during a bad period of my stay in Germany.

Kelley J. Rusell, R.S.J. Sparks, G. Boudon, B. Villemant, Claudia Romano, Mette Solvang, Dave Clague, Roberto Moretti, Jonathan Castro, François Beauducel, Cliff Shaw, Brenda Ledda, Joe Gottsmann, Meritxell Aulinas I Junca, Antonio Costa, Andrea Di Muro, Luca Caricchi for their help, sample providing, collaboration and scientific discussion.

The institute's secretaries and mechanics Wolfgang and Martin for helping me out whenever something had broken or got stuck.

Libor Stránský alias "Švartna" and Pavel Chromý alias "Paša" with his family to stay as a friends across the distance and the life-roads which divided us.

x

Preamble

Parts of the data presented in this thesis have been published in scientific journals or are in the process of reviewing. Below, these papers are listed in alphabetic order of their first authors:

Giordano D., Mangiacapra A., Potuzak M., Russell J.K., Romano C., Dingwell D.B., Di Muro A., (2006) A model for silicate melt viscosity: A treatment for metaluminous, peraluminous and peralkaline liquids, Chemical Geology, 229, 42-56.

Potuzak, M., Dingwell D.B., (2006) Temperature Dependent Thermal Expansivities of Multicomponent Natural Melts Between 993 and 1803 K, Chemical Geology, 229, 10-27.

Potuzak, M., Dingwell D.B., Ledda B., Courtial P., (2006) A partial molar volume for ZnO in silicate melts, American Mineralogist, 91, 366-374.

Potuzak M., Solvang M., Dingwell D. B., (2006) Temperature Independent Thermal Expansivities of Calcium Aluminosilicate Melts between 1150 and 1973 K in the System Anorthite-Wollastonite-Gehlenite (An-Wo-Geh): A density model, Geochimica et Cosmochimica Acta, 70, 3059-3074 .

Zusammenfassung

Scherviskosität, Dichte, thermische Ausdehnung und spezifische Wärmekapazität sind einige aus einer ganzen Reihe von Faktoren, die das rheologische, morphologische und texturelle Erscheinungsbild von vulkanischen Laven beeinflussen. Diese physikalischen Eigenschaften einer Silikatschmelze hängen von ihrer chemischen Zusammensetzung, ihrem Gehalt an Wasser, Kristallen und Blasen und letztlich auch von dem auf sie ausgeübten Stress ab. In den letzten Jahren wurde erkannt, dass gerade der angelegte Stress eine wichtige Rolle bezüglich des Glasübergangsbereiches von silikatischen Schmelzen spielt. Diese kinetische Grenze zwischen duktilem und sprödem Verhalten hat einen wesentlichen Einfluss auf das eruptive Verhalten eines Vulkans.

Genaue Kenntnis der ablaufenden physikalischen Prozesse ist sehr wichtig für die im Falle eines Ausbruchs verantwortlichen Stellen. Nur so können Zivilschutz oder ähnliche Stellen angepasstes Risikomanagement betreiben und die Verluste an Menschenleben und Sachwerten zu minimieren versuchen. Darüber hinaus stellen natürliche magmatische Gesteine den Hauptrohstoff für die Produktion von Mikrofasern und Endlosfasern dar. Im Vergleich zu "normalen" Glasfasern (z.B. CAS) haben Gesteinsfasern (in der Regel basaltische Zusammensetzung) eine bemerkenswert hohe thermische Stabilität (→ Brandschutz), Säure- und Laugenresistenz sowie Wärme- und Schallisolierfähigkeit. Derartige Gesteinsfasern können Metall und Holz ersetzen und werden in Zukunft wohl in zunehmendem Maße verbaut werden. Darüber hinaus können natürliche basaltische Gesteine als Beimengung von Zement, für den Unterbau von Eisenbahngleisanlagen, bei der Herstellung von Geotextilien, Fliesen, säureresistenten Werkzeugen für die Schwerindustrie, Gesteinswolle, flexiblen Rohren sowie Materialverstärkung, Dachfilzen („Ruberoid"), Laminaten (als Schutzüberzug) und Dämmmaterialien verwendet werden.

Seit Bottinga und Weill (1970) vorgeschlagen hatten, die Dichte einer Silikatschmelze in 2- oder 3-Elementsystemen zur Bestimmung des partiellen Molvolumens einer Oxidkomponente heranzuziehen, wurden in der einschlägigen Literatur mehrere Modelle diesbezüglich vorgestellt. Darauf aufbauend wurde die Dichte von 8 Zink-haltigen Silikatschmelzen im Temperaturintervall von 1363 bis 1850 K ohne Schutzatmosphäre bestimmt. Die gewählten Schmelzzusammensetzungen (Natrium-Di-Silikat [NS2] - ZnO; Anorthit-Diopsid [im 1 atm-Eutektikum-Verhältnis] - ZnO; und Diopsid-Petedunnit) wurden

auf Grundlage des existierenden, experimentellen Datensatzes, ihrer petrologischen Relevanz und des unterschiedlichen strukturellen Zustands des ZnO ausgewählt. Die ZnO-Konzentration betrug bis zu 25 mol % für Natriumdisilikat und Petedunnit sowie 20 mol % für die Anorthit-Diopsid-Mischung. Das molare Volumen und der Ausdehnungskoeffizient wurde für alle Proben bestimmt. Erstere nehmen mit zunehmendem ZnO-Gehalt ab. Das partielle Molvolumen von ZnO, bestimmt über volumetrische Untersuchungen, war für alle Proben innerhalb der Fehlergrenzen konstant und wurde bei 1500 K mit 13.59 +/- 0.55 cm^3/mol bestimmt. Die Ergebnisse der volumetrischen Untersuchungen lieferten keinen Hinweis auf einen Einfluss des Alkalien- oder Aluminiumgehalts auf die Koordination von ZnO.

Das hier bestimmte partielle Molvolumen von ZnO kann in Mehrelementmodelle eingebunden werden, die zur Vorhersage des Volumens einer Silikatschmelze herangezogen werden. Hochtemperaturdichtebestimmungen ZnO-haltiger Silikatschmelzen zeigen, dass ein einzelner Wert ausreicht, um die volumetrischen Eigenschaften dieser Komponente zu beschreiben. Die Anwesenheit von Alkalien und/oder Aluminium scheint das partielle Molvolumen von ZnO innerhalb des untersuchten Temperaturintervalls nicht zu beeinträchtigen. Weiterhin gibt es keinen volumetrischen Hinweis auf eine zusammensetzungsabhängige Veränderung der Strukturelle Rolle von ZnO.

Als weitere physikalische Eigenschaft wurde im Rahmen der vorliegenden Arbeit die thermisch bedingte Ausdehnung von 10 Schmelzzusammensetzungen innerhalb des Anorthit-Wollastonit-Gehlenit (An-Wo-Geh)-Dreiecks untersucht. Da bis dato keine experimentellen Daten der thermischen Expansivität im Temperaturfeld unterkühlter Schmelzen existierten, konzentrierte sich diese Arbeit auf die Untersuchung dieses Parameters mittels einer Kombination kalorimetrischer und dilatometrischer Methoden.

Die Volumina bei Raumtemperatur wurden nach dem Tauchprinzip von Archimedes bestimmt. Hierfür wurden bei 298 K Gläser verwendet, die zuvor mit einer Abkühlrate von 10 K/min abgeschreckt worden waren.

Der thermische Ausdehnungskoeffizient des Glases im Temperaturintervall von 298 K bis zum Glasübergang wurde mit einem Dilatometer gemessen, die Warmkapazität zwischen 298 und 1135 K mittels dynamischer Differenzkalorimetrie. Der thermische Ausdehnungskoeffizient und die spezifische Wärme wurden bei einer Aufheizrate von 10 K/min an Gläsern gemessen, die vorher mit derselben Rate abgekühlt worden waren. Die Dichte der unterkühlten Schmelze, das molare Volumen und die molare thermische Ausdehnung wurden indirekt durch dilatometrische und kalorimetrische Messungen

bestimmt, unter der Annahme, dass die Kinetik der Enthalpie- und der Volumen- Relaxation gleich sind.

Die für die unterkühlten Schmelzen ermittelten Daten wurden verglichen mit Werten, die die Modelle von Lange & Carmichael (1987), Courtial und Dingwell (1995) und Lange (1997) vorhergesagt hatten. Der beste lineare Fit kombiniert die im Rahmen dieser Arbeit experimentell ermittelten Werte und die Vorhersagen des Modells von Courtial & Dingwell (1995).

Die Kombination dilatometrischer und kalorimetrischer Meßmethoden zur Bestimmung der thermischen Ausdehnung unterkühlter Schmelzen vergrößert das abdeckbare Temperaturintervall beträchtlich und verbessert dadurch die Präzision und das Verständnis der thermodynamischen Prozesse in Ca-Al-Si-Schmelzen. Diese erhöhte Genauigkeit liefert klare Hinweise auf eine Temperaturunabhängigkeit der Schmelzausdehnung im System An-Wo-Geh. Dies steht im deutlichen Gegensatz zu den ermittelten Ergebnissen im Anorthit-Diopsid-System und wirft die Frage auf, welchen kompositionellen bzw. strukturellen Ursprung die Temperaturabhängigkeit der thermischen Ausdehnung in mehrelementigen Silikatschmelzen hat.

Darüber hinaus wurden das partielle Molvolumen und die thermische Ausdehnung von 10 Proben der An-Wo-Geh-Mischkristallreihe bestimmt. Die gewonnenen Ergebnisse sind in existierende Mehrelement-Modelle zur Vorhersage des Volumens von Silikatschmelzen eingeflossen. Die ermittelten Volumina unterkühlter Schmelzen bei Glasübergangstemperaturen (1135-1200 K) und darüber wurden so kombiniert, dass man die thermische Ausdehnung temperaturunabhängig ermitteln konnte.

Aufbauend auf den ermittelten Ergebnissen und in der Literatur genannter Werte ist der Schluss zulässig, dass die thermische Ausdehnung von Schmelzen sowohl binärer als auch ternärer Systeme bei Atmosphärendruck temperaturunabhängig ist. Wenn man Hochtemperatur-Dichtedaten aus der Literatur mit Ausdehnungsdaten bei T_{sc} kombiniert, kann man ein großes Temperaturintervall abdecken. Im An-Wo-Geh-System gibt es in diesem Temperaturintervall keinen volumetrischen Hinweis auf eine temperaturunabhängige thermische Ausdehnung.

In einer weiteren Versuchsreihe wurde zum ersten Mal überhaupt die thermische Ausdehnung dreier natürlicher, magmatischer Proben im Temperaturbereich von 298-1803 K bestimmt. Die Proben stammen vom Vesuv (Tephriphonolit, Ausbruch von 1631), Ätna (Trachybasalt, Ausbruch von1992) und Slapany (Basanit, oligozäner-miozäner Lavastrom).

Die Niedrigtemperatur-Volumina wurden durch Dichtemessungen an Gläsern bestimmt, die mit 5 K/min auf 298 K abgekühlt worden waren. Die thermische Ausdehnung der Gläser wurde oberhalb 298 K bis zum jeweiligen Glasübergangsintervall bestimmt. Das Volumen der unterkühlten Schmelzen und die molare thermische Ausdehnung wurden durch dynamische Differenzkalorimetrie und dilatometrische Messungen bestimmt. Zu diesem Zweck wurde angenommen, dass sich die Enthalpie-Kinetik und die Scherrelaxation entsprechen (Webb, 1992). Die Hochtemperaturdichte wurde nach dem Prinzip von Archimedes mit einem Platin-Lot gemessen. Zusätzlich wurde der Oxidationsgrad von Eisen nasschemisch bestimmt. Zu diesem Zweck wurden in regelmäßigen Temperaturabständen während der Dichtemessung kleine Schmelztropfen durch kurzes Eintauchen einer Al_2O_3-Stange entnommen. Die gemessenen Dichtewerte wurden verglichen mit Werten, die mit dem Modell von Lange & Carmichael (1987) und Lange (1997) berechnet worden waren.

Die ermittelten Werte für das Volumen einer Flüssigkeit nahe des Glasübergangs (993 - 1010 K) und bei Temperaturen von unterkühlten Schmelzen (1512 - 1803 K) wurden zusammengefügt, um den Einfluss der Temperatur auf das Ausdehnungsverhalten im Temperaturbereich von unterkühlten und stabilen Flüssigkeiten zu veranschaulichen. Die vorliegenden Ergebnisse bestätigen die Untersuchungen von Knoche et al. (1992a, 1992b), Toplis & Richet (2000), Liu & Lange (2001) und Gottsmann & Dingwell (2002). Die Molvolumina weisen in der Regel auf eine negative Abhängigkeit der Ausdehnung von der Temperatur hin. Die thermische molare Ausdehnung der Gläser nimmt mit steigendem SiO_2-Gehalt (Basalte/Basanite bis Tephri-Phonolite) zu, wobei dieser Anstieg im selben Maße für unterkühlte Schmelzen wie für die dazugehörigen Gläser zu beobachten ist. Im Gegensatz dazu nimmt die molare thermische Ausdehnung der Schmelzen oberhalb des Liquidus mit zunehmendem SiO_2-Gehalt ab. Oberhalb des Glasübergangs konnte für alle untersuchten Proben eine nicht-lineare Abhängigkeit des Molvolumens festgestellt werden. Die entsprechenden Werte zwischen Temperaturen knapp oberhalb des Glasübergangs bis etwa 1873 K können mit einer nicht-linearen logarithmischen Kurve vorhergesagt werden.

Im Rahmen der vorliegenden Arbeit wurden die Ausdehnung und das Molvolumen relativ basischer Proben untersucht. Die Untersuchung von SiO_2-reicheren Proben ist experimentell sehr schwierig, da die hohe Viskosität die Verwendung von Immersions-Meßmethoden erschwert oder unmöglich macht. Man kann das Problem umgehen, indem man die Hochtemperatur-Dichte an Proben misst, die in einem Magnetfeld oder heißen Gas- oder Luftstrom schweben. Derartige Untersuchungen sollten in Zukunft mit Nachdruck betrieben werden, da sie wichtige Informationen liefern würden, die zu einem besseren Verständnis des

Verhaltens hochviskoser Flüssigkeiten beitragen würden.

Abschließend wurde eine neue Methode zur Viskositätsmessung wasserfreier Proben mit großer kompositioneller Bandbreite entwickelt. Sie erlaubt die Untersuchung von Ryolithen, Trachyten, Moldaviten, Andesiten, Latiten, Pantelleriten, Basalten und Basaniten. Mit Hilfe der Mikropenetration und der konzentrischen Zylinder-Viskosimetrie kann eine Viskositätsbandbreite von 10^{-1} bis 10^{12} Pas und eine Temperaturbandbreite von 973 bis 1923 K abgedeckt werden. Zusammen mit Literaturwerten bilden die so ermittelten Ergebnisse nun eine große Datenmenge von ca. 800 Datenpunkten von 44 gut untersuchten Schmelzzusammensetzungen. Mit dieser Datenmenge konnte das Modell von Giordano & Dingwell (2003a) zur Vorhersage der Viskosität natürlicher silikatischer Schmelzen verfeinert werden. Die vorliegenden neuen Ergebnisse zeigen deutlich, dass

1) die Abhängigkeit von Viskosität und Temperatur mit der VFT-Gleichung über den gesamten untersuchten Bereich an chemischer Zusammensetzung sehr gut nachvollzogen werden kann,

2) die Verwendung eines konstanten Wertes „A" der VFT-Gleichung bei hohen Temperaturen von den experimentellen Ergebnissen bestätigt wird,

3) die Viskosität stark von der chemischen Zusammensetzung abhängt und eine Einteilung der untersuchten Proben in 3 Gruppen (peralkalisch, metaluminös, peraluminös) zur Folge hat, und

4) die Viskosität einer metaluminösen Schmelze sehr gut mathematisch mit einen kompositionellen Parameter (SM) beschrieben werden kann. Dies gilt nicht im gleichen Maße für peralkalische und peraluminöse Proben. Für Letztere wurde ein temperaturabhängiger Parameter auf Grundlage des Alkalienüberschusses (relativ zu Aluminium) in das Modell aufgenommen. Daraufhin konnten sämtliche experimentellen Ergebnisse mit einem Fehler von weniger als 5 % reproduziert werden.

Auf Grundlage der umfassenden Datenbank aus eigenen und Literaturwerten wurde die Temperaturabhängigkeit des Viskosität Verhaltens von „langen" und „kurzen" Schmelzen über eine große kompositionelle Bandbreite bestimmt. Es konnten drei unterschiedliche Probengruppen mit unterschiedlichen Verhalten bestimmt werden: peralkalisch, metaluminös, peraluminös.

Diese Daten erlauben eine Verfeinerung des Modells von Giordano & Dingwell (2003a) durch

1) eine größere, dem Modell zugrunde liegende Datenmenge,

2) eine Ausweitung der kompositionellen Bandbreite,

3) eine Ausweitung der Temperaturbandbreite, und

4) die Erkenntnis, dass der präexponentielle Faktor A (und damit die Viskosität der Schmelze) bei unendlich hohen Temperaturen unabhängig von der chemischen Zusammensetzung einen gemeinsamen, bisher unbekannten Wert (A = -4,07) annimmt.

Die Datenmenge für peralkalische und peraluminöse Proben im Temperaturintervall 949 - 2653 K wurde stark vergrößert. Es zeigte sich weiterhin, dass die vereinfachende Annahme eines zusammensetzungsunabhängigen Wertes für "A" zulässig ist. Diese Verbesserung zeigt die starke Verknüpfung der einzelnen Datenreihen und vergrößert damit die Gesamtaussagekraft. Es konnte gezeigt werden, dass der strukturelle Parameter SM (Giordano & Dingwell, 2003a) nur auf metaluminöse, nicht aber auf peralkalische und peraluminöse Proben angewendet werden kann. Dies lässt den Schluss zu, dass Unterschiede im rheologischen Verhalten auf grundlegende strukturelle Unterschiede in diesen drei Schmelzzusammensetzungen zurückzuführen sind. Deshalb wurde ein weiterer kompositioneller Parameter (AE) in das "SM-Modell" (Gleichung 7.7) eingeführt, um den Einfluss des Alkalienüberschusses in Bezug auf den Aluminiumgehalt auszudrücken. Dieses Modell reproduziert die gesamte experimentelle Datenmenge innerhalb des statistischen Qualitätsfaktors RMSE von 0,45 logarithmischen Einheiten. Das vorliegende Modell eignet sich daher sehr gut zur Vorhersage der Viskosität wasserfreier Silikatschmelzen.

Abstract

The shear viscosity, density, thermal expansivity and specific heat capacity are important factors controlling the morphology, rheology, and texture of volcanic flows and deposits. These physical properties of silicate melts largely depend on chemical composition, water content, crystal content, bubble content and stress applied to the melt. Recently, it has been recognized that the applied stress plays an important role in the so called "glass transition" area of silicate melts. This kinetic boundary between brittle and ductile behavior affects the eruptive style. Thorough knowledge of the physical processes that occur at this brittle/ductile transition can affect the decision making of governments during volcanic crises and help to reduce and/or avoid loss of life and assets. Scientific knowledge from this research can be directly applied to the geomaterial industry. In addition, natural magmatic rocks are the major raw material in the production of microfibres and continuous fibres. Compared to normal glass fibres, rock fibres have a remarkable high temperature endurance, acid and alkali resistance and anti-heat impact. Rock products can be used as substitutes for metal and timber. They are likely to become more widely used in the near future. Further use for natural magmatic rocks include crushed stone, concrete aggregate, railroad ballast, production of high quality textile fibres, floor tiles, acid-resistant equipment for heavy industrial use, rockwool, basalt pipers, basalt reinforcement bars, basalt fibre roofing felt (ruberoid), basalt laminate (used as a protective coating), heat-insulating basalt fibre materials and glass wool (fibre glass).

Since Bottinga and Weill (1970) first suggested that the density of melts in two or three component systems could be used to determine partial molar volumes of oxide components in silicate liquids, several models based upon this approach have been proposed in the Earth sciences literature. Considering that knowledge the densities of 8 Zn-bearing silicate melts have been determined, in equilibrium with air, in the temperature range of 1363 to 1850 K. The compositional joins investigated [sodium disilicate (NS2)- ZnO; anorthite-diopside 1 atm eutectic (AnDi)-ZnO; and diopside-petedunnite] were chosen based on the pre-existing experimental density data set, on their petrological relevance, and in order to provide a test for significant compositionally induced variations in the structural role of ZnO. The ZnO concentrations investigated range up to 25 mol% for sodium disilicate, 20 mol% for the anorthite-diopside 1 atm eutectic, and 25 mol% for petedunnite. Molar volumes and expansivities have been derived for all melts. The molar volumes of the liquids decrease with

increasing ZnO content. The partial molar volume of ZnO derived from the volumetric measurements for each binary system is the same within error. A multicomponent fit to the volumetric data for all compositions yields a value of 13.59(0.55) cm^3/mol at 1500 K. I find, no volumetric evidence for compositionally induced coordination number variations for ZnO in alkali-bearing vs. alkali-free silicate melts nor for Al-free vs. Al-bearing silicate melts.

The partial molar volume of ZnO determined here may be incorporated into existing multicomponent models for the prediction of silicate melt volume. High temperature density determinations on ZnO-bearing silicate melts indicate that a single value for the partial molar volume of ZnO is sufficient to describe the volumetric properties of this component in silicate melts. The presence of alkalies and Al does not appear to influence the partial molar volume of ZnO within the temperature range investigated here. There is no volumetric evidence across this temperature range presented for composition to influence the coordination polyhedron of ZnO in silicate melts.

The next physical property to be studied was thermal expansivity. Ten compositions from within the anorthite-wollastonite-gehlenite (An-Wo-Geh) compatibility triangle were investigated. Due to the lack of information about the thermal expansivities at supercooled liquid temperatures this study focused on the measurement of thermal expansivity using a combination of calorimetric and dilatometric methods.

The volumes at room temperature were derived from densities measured using the Archimedean buoyancy method. For each sample density was measured at 298 K using glass that had a cooling-heating history of 10-10 K min^{-1}.

The thermal expansion coefficient of the glass from 298 K to the glass transition interval was measured by a dilatometer and the heat capacity was measured using a differential scanning calorimeter from 298 to 1135 K. The thermal expansion coefficient and the heat flow were determined at a heating rate of 10 K min^{-1} on glasses that were previously cooled at 10 K min^{-1}.

Supercooled liquid density, molar volume and molar thermal expansivities were indirectly determined by combining differential scanning calorimetric and dilatometric measurements assuming that the kinetics of enthalpy and shear relaxation are equivalent.

The data obtained on the supercooled liquids were compared to high-temperature predictions from the models of Lange and Carmichael (1987), Courtial and Dingwell (1995) and Lange (1997). The best linear fit combines the supercooled liquid data presented in this study and the high temperature data calculated using the Courtial and Dingwell (1995) model.

This dilatometric/calorimetric method of determining supercooled liquid molar thermal expansivity greatly increases the temperature range accessible for thermal expansion. It represents a substantial increase in precision and understanding of the thermodynamics of calcium aluminosilicate melts. This enhanced precision demonstrates clearly the temperature independence of the melt expansions in the An-Wo-Geh system. This contrasts strongly with observations for neighboring system such as Anorthite-Diopside and raises the question of the compositional/structural origins of the temperature dependence of thermal expansivity in multicomponent silicate melts.

In addition, the partial molar volumes and the thermal expansivities of 10 samples from within the An-Wo-Geh compatibility triangle have been determined. They have been incorporated into existing multicomponent models in order to predict silicate melt volume. The resulting supercooled liquid volumes near glass transition temperatures (1135 - 1200 K) and at superliquidus temperature were combined to yield temperature independent thermal expansivities over the entire temperature range.

In light of results presented in this study, together with the published data, it seems that binary and ternary systems have temperature independent thermal expansivities from the supercooled liquid to the superliquidus temperature at 1 atmosphere. By combining the high temperature densitometry data (i.e., above liquidus) from the literature with volume and expansivity data obtained at T_{sc}, a wide temperature range is covered. There is no volumetric evidence across this temperature range for temperature independent thermal expansivities in the An-Wo-Geh compatibility triangle.

Furthemore, the thermal expansivities of three multicomponent glasses and liquids have been obtained over a large temperature interval (298 - 1803 K) which involved combining the results of low and high temperature measurements. The sample compositions investigated were derived from three natural lavas; Vesuvius 1631 eruption, Etna 1992 eruption and an Oligocene-Miocene lava flow from Slapany in the Bohemian massif. The original rocks are tephri-phonolite, trachybasalt and basanite, respectively. This is the first time this calorimetric/dilatometric method has ever been applied to natural magmatic melts. The low temperature volumes were derived from measurements of the glass density of each sample after cooling at 5 K.min^{-1} at 298 K, followed by measurements of the glass thermal expansion coefficient from 298 K to the samples´ respective glass transition interval. Supercooled liquid volumes and molar thermal expansivities were determined by combining scanning calorimetric and dilatometric measurements, assuming that the kinetics of enthalpy

and shear relaxation are equivalent (Webb, 1992). High temperature densities were measured using Pt double bob Archimedean densitometry. In addition, the oxidation state of iron was analyzed using a wet chemistry method. Small amounts of samples were taken from the liquids using a "dip" technique at regular temperature steps during high temperature densitometry. The measured high temperature densities have been compared with predicted densities across the same temperature interval calculated using the multicomponent density models of Lange and Carmichael (1987) and Lange (1997).

The resulting data for liquid volumes near glass transition temperatures (993 - 1010 K) and at super-liquidus temperatures (1512 - 1803 K) are combined to yield temperature dependant thermal expansivities over the entire supercooled and stable liquid range. These results confirm the observation of Knoche et al. (1992a); Knoche et al. (1992b); Toplis and Richet (2000); Liu and Lange (2001); Gottsmann and Dingwell (2002) of the temperature dependence of thermal expansivity. The molar volumes indicate, in general, a significant negative temperature dependence of the expansivity. The thermal molar expansivity of the glasses increase from SiO_2-poor (basalt-basanite composition) to relatively SiO_2-rich melts (tephri-phonolite composition). The thermal molar expansivity at supercooled liquid temperatures increases in the same manner as the glasses. In contrast, the thermal molar expansivity of the superliquidus liquid decrease from SiO_2-poor to relatively SiO_2-rich melts. Non-linear dependency of molar volume has been observed for all studied samples above the glass transition area. Molar volume from just above the glass transition area to about 1873 K can be predicted by a non-linear logarithmic curve.

This study examined the expansivities and molar volumes of relatively basic compositions. Extending such a study to more SiO_2-rich, but still geologically relevant, compositions remains a challenge, because the high viscosities of such melts preclude the use of immersion techniques. This problem can be solved using a high temperature densitometry where the volume is measured on levitated sample. I would like to urge studies of this sort in the future. Results from such studies should provide important information regarding a number of geological processes, which occur in such extremely high viscous liquids.

A new viscosity measurement for melts spanning a wide range of anhydrous compositions including: rhyolite, trachyte, moldavite, andesite, latite, pantellerite, basalt and basanite are discussed in the last chapters. Micropenetration and concentric cylinder viscometry measurements cover a viscosity range of 10^{-1} to 10^{12} Pas and a temperature range from 973 to 1923 K. These new measurements, combined with other published data, provide a

high-quality database comprising ~800 experimental data on 44 well -characterized melt compositions. This database is used to recalibrate the model proposed by Giordano and Dingwell [Giordano, D., Dingwell, D. B., 2003a. Non-Arrhenian multicomponent melt viscosity: a model. Earth Planet. Sci. Lett. 208, 337–349] for predicting the viscosity of natural silicate melts. The recalibration shows that:

a) the viscosity (η)–temperature relationship of natural silicate liquids is very well represented by the VFT equation [log η=A+B/ (T−C)] over the full range of viscosity considered here,

b) the use of a constant high-T limiting value of melt viscosity (e.g., A) is fully consistent with the experimental data.

There are 3 different compositional suites (peralkaline, metaluminous and peraluminous) that exhibit different patterns in viscosity, the viscosity of metaluminous liquids is well described by a simple mathematical expression involving the compositional parameter (SM) but the compositional dependence of viscosity for peralkaline and peraluminous melts is not fully controlled by SM. For these extreme compositions we refitted the model using a temperature-dependent parameter based on the excess of alkalies relative to alumina (e.g., AE/SM). The recalibrated model reproduces the entire database to within 5% relative error.

On the basis of this extended database the T-variation of the viscous response of strong and fragile liquids within a wide range of compositions shows three clearly contrasting compositional suites (peralkaline, metaluminous and peraluminous). As a result, I present an extended model to calculate the viscosity of silicate melts over a wide range of temperatures and compositions. This model constitutes a significant improvement with respect to the Giordano and Dingwell (2003a) study in that:

1) The number of experimental determinations over which the model is calibrated is larger.

2) The range of investigated compositions is larger.

3) The investigated temperature range is larger.

4) The assumption is made that at infinite temperature, the viscosity of silicate melts converges to a common, but unknown value of the pre-exponential factor (A=−4.07, Equation (7.1)). In particular the compositional range involves a large number of viscosity determinations for peralkaline and peraluminous compositions in a temperature interval between 949 and 2653 K. Furthermore, it is shown that the assumption of a common value of the pre-exponential parameter A produces an equally good representation of the experimental data as that produced by each melt having its own specific A-value. This optimization also

induces a strong coupling between data sets that stabilizes the range of solutions and allows the different rheological behaviour of extreme compositions (peralkaline and peraluminous vs. metaluminous) to be discriminated. It was demonstrated that, although the parameter SM (Giordano and Dingwell, 2003a) can be used to model compositional controls on the viscosities of metaluminous liquids, it does not capture the viscosity of peralkaline and peraluminous liquids. The differences in the rheological behaviour of these extreme compositions reflect important differences in the structural configuration of metaluminous, peralkaline and peraluminous melts. Subsequently, a second regression of the experimental data was performed involving a second compositional parameter (AE) that accounts for the excess of alkali oxides over the alumina. Incorporating this temperature-dependent compositional parameter (i.e., AE) into the SM-based model (Equation 7.7) appears to account for the anomalous rheological behaviour of peralkaline and peraluminous liquids. The resulting model reproduces the entire experimental database to within an average RMSE of 0.45 log units. The model presented here is recommended for the estimation of the viscosity of anhydrous multicomponent silicate melts of volcanic interest.

1. Introduction

A molecular liquid below its melting point will crystallize if the process of cooling is relatively slow. At a certain temperature, the average kinetic energy of molecules no longer exceeds the binding energy between neighbouring molecules and growth of an organized solid crystal begins. Formation of an ordered system takes a certain amount of time since molecules must move from their current location to energetically preferred point at crystal nodes. However, the cooling process can also be relatively fast and as temperature falls, molecular motion slows down. So called supercooled liquid appears at temperature above the glass transition. It is formed by the process of fast cooling of the liquid below its melting point, without it becoming solid. If the fast cooling process continues, molecules never reach their destination - the substance enters into dynamic arrest and a disordered, glassy solid forms. Such arrest apparently takes place across a range of temperatures, which is called the glass transition interval, T_g. Glass is a uniform amorphous solid material, usually produced when the viscous molten material cools to below its glass transition temperature, without sufficient time for a regular crystal lattice to form. Glass in its pure form is a transparent, strong, hardwearing, essentially inert, and biologically inactive material which can be formed with very smooth and impervious surfaces. However, glass is brittle and will break into sharp shards. This property of glass was observed by Humans at very early stage of our history. Naturally occurring glass, such as obsidian, has been used since the Stone Age to make primitive stone tools. As time passed, it was discovered that if glass is heated until it becomes semi-liquid, it can be shaped and left to cool in a new, solid shape. Glass making instructions were first documented in Egypt around 1500 BC when glass was used as a glaze for pottery and other items. In the first century BC at the eastern end of the Mediterranean the technique of blowing glass was developed. During the Roman Empire many forms of glass were created, usually for vases and bottles where the glass was made from sand, plant ash and lime. Our ancestors quickly realized that glass is strong, unreactive and, in general, a very useful material. Today, we tend to take glass for granted. Many household items are made from glass, such as drinking glasses, bowls, bottles, windows, light bulbs, mirrors, cathode-ray tubes and flat screens of monitors, televisions and mobiles. In science, flasks, test tubes, lenses and many other essential pieces of laboratory equipment are made of glass.

Clearly, there is a need for detailed studies and analyses of the behavior and properties of glass. Numerical or analytical models are frequently applied to predict these properties.

In this study I have characterized and parameterized physico-chemical properties of silicate melts and glasses. The aim of this study was to contribute in determining the V-T (volume-temperature) and T-t (temperature-time) relationships relevant during technological, petrological and volcanological processes using thermoanalytical techniques. Dilatometry and calorimetry are applied to determine the volume-temperature dependence of silicate liquids within the anorthite-wollastonite-gehlenite compatibility triangle. A new density model for CAS system is introduced.

Furthemore, the thermal expansivities of three multicomponent glasses and liquids have been obtained over a large temperature interval. Physical and chemical properties of glass can be modified or changed with the addition of other compounds. Taking into account this knowledge and based on the assumption that the density of silicate melts in two or three component system could be used to determine partial molar volumes of oxide component, an 8 Zn-bearing silicate melts densities were synthesized and measured. The derived partial molar volume of ZnO may be incorporated into existing multicomponent models for the prediction of silicate melt volume.

Understanding how the magma below an active volcano evolves with time is crucial for hazard assessment and risk mitigation in these areas. The viscous response of magmatic liquids to stresses applied to the magma body controls the fluid dynamics of magma ascent. Approximately half a billion people live in close proximity to a historically active volcano. Catastrophic volcanic crises have occurred in historic and even recent times all around the word (e.g., Vesuvius, 79 A.D. [Italy], Laki, 1792-94 [Iceland], Mt. Unzen, 1792 and 1990-95 [Japan], Tambora, 1815 and Krakatao, 1883 [Indonesia], Mt. Pelee, 1902 [France], Mt. St. Helens, 1980 [USA], El Chichon, 1982 [Mexico], Nevado del Ruiz 1986 [Colombia], Pinatubo, 1991 [Phillipines], Soufriere Hills, 1995-2002 [Montserrat, U.K.], etc.). Clearly there is a need for detailed studies and analysis of the eruptive record of volcanoes adjacent to populated areas to assess hazards and risks during potential volcanic crises.

However, the current viscosity models for describing magmas rheology are still poor and limited to a very restricted compositional range. Therefore, new viscosity measurements for melts spanning a wide compositional range were performed. On the basis of an extended database comprising the viscosity of natural multicomponent silicate melts a new viscosity model is introduced in the last chapter.

2.   Theoretical Background

2.1. Relaxation theory

It is crucial that the enthalpy relaxation processes at the glass transition interval are understood, in order to interpret the results derived from dilatometry and differential scanning calorimetry measurements. However, initially we need to consider the evolution of enthalpy in a glass-forming liquid as it is cooled to form the glass state, in order to understand what we are measuring when we reheat the sample from the glass state back across the glass transition.

The work presented here deals with two properties, the volume and enthalpy of structurally relaxed and un-relaxed silicate melts. The transition between these two states is known as the glass transition. The glass transition is the temperature interval over which the properties of a melt change from a liquid-like state to a solid-like (glassy) state (Dingwell and Webb, 1989; 1990; Moynihan, 1995). In terms of rheology this is the brittle-ductile transition, a change from an elastic response to stress and strain to a viscous response. In glassy lava flows this transition represents the freezing, or cessation of flow. The glass transition temperature interval can be recognised by comparing the rate at which a property re-equilibrates at a new temperature after a change in temperature cooling, with the rate at which it was cooled. The timescale (τ) for structural relaxation of a given property (e.g. enthalpy) can be approximated using the Maxwell (1867) relationship:

$$\tau = \frac{\eta_N}{G_\infty} \tag{2.1}$$

where G_∞ is the shear modulus with a value of $\log_{10}(Pa) = 10 \pm 5$ (Dingwell and Webb, 1990) and η_N is the Newtonian shear viscosity. The cooling of a silicate liquid can be viewed as a series of temperature steps ΔT followed by isothermal holds with a duration of Δt. In the liquid field (equilibrium conditions) the value of τ for enthalpy is orders of magnitude smaller than Δt resulting in instantaneous re-equilibration of the property upon cooling. As the temperature decreases during further cooling the viscosity increases and as a result τ increases until at a given temperature τ exceeds Δt. At this point enthalpic relaxation is unable to run to completion in the time available and the system deviates away from the equilibrium conditions and enters into the glass transition temperature interval (Figure 2.1). As the temperature decreases further τ becomes increasingly greater than Δt until a temperature is

reached where the configuration of the enthalpy is frozen into the glass state. The temperature at which the enthalpy is frozen into the glass state is known as the limiting fictive temperature and it defines the low temperature end of the glass transition (Figure 2.1.).
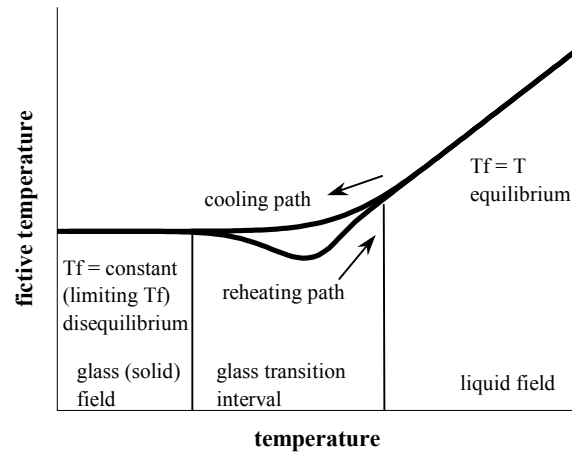
FIGURE. 2.1. The evolution of T_f of a silicate melt upon cooling from equilibrium (the liquid state where T_f = T) to disequilibrium (the glass or solid state where T_f = constant). This constant temperature is frozen into the glass structure and is known as the limiting T_f. The deviation from equilibrium is dependent on the cooling rate. Upon reheating across the glass transition the evolution of T_f displays a hysterisis whose path is dependent on the heating rate, the cooling rate, the temperature-dependent structure and its temperature dependent relaxation time.

The fictive temperature (T_f) concept was introduced by Tool (1946) in order to describe the evolution of a property that depends on the structural configuration during the heating or cooling of a glass or a liquid. In the liquid field at high temperatures, above the glass transition, the system is at equilibrium, so $T_f = T$. As the system is cooled into the glass transition interval T_f gradually evolves away from equilibrium until it becomes constant (T_f = constant) and is at disequilibrium in the glass field (Figure 2.2). It is this constant T_f that is frozen into the glass state and is known as the limiting T_f. The temperature at which T_f evolves away from equilibrium depends on the rate of cooling (Narayanaswamy, 1971; 1988; DeBolt et al., 1976; Scherer, 1986). If the cooling rate is rapid the departure from equilibrium occurs at higher temperatures and as a result a higher limiting T_f is frozen into the glass state. At slower cooling rates the system remains in equilibrium to a lower temperature and thus a lower limiting T_f results.

In principle, there are two cooling scenarios of the silicate liquid. The property of silicate liquid is at equilibrium during slow cooling until it reaches its melting temperature. At this temperature liquid starts to crystallize which corresponds to the discontinuities in first (enthalpy, volume, entropy) and second order (heat capacity, thermal expansion coefficient) thermodynamics properties (Figure 2.1). If cooled rapidly the liquid may not crystallize, even at tens or hundreds degrees below the melting temperature. Instead the properties reach a supercooled liquid just above the glass transition temperature. On entering the glass transition interva the cooling path shows a sudden change in first and second order properties. The glass property Φ (e.g., volume, enthalpy) strongly depends on the thermal history (Figure 2.2).
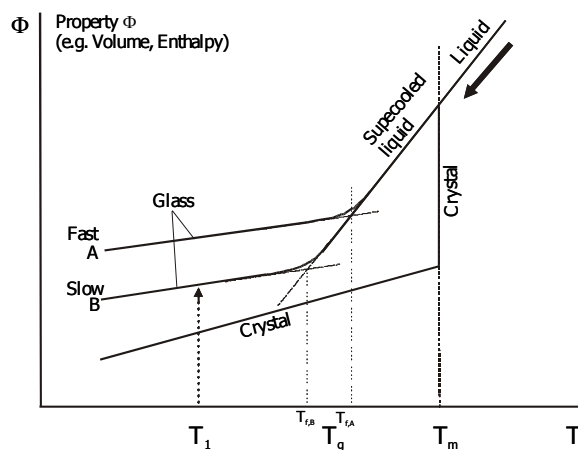
FIGURE 2.2. Schematic diagram showing the path of first order properties path with temperature. Cooling a liquid "rapidly" below the melting temperature T_m may results in the formation of a supercooled (metastable) or even disequilibrium glass conditions. The first order phase transition corresponding to the passage from a liquid to crystalline phase is also shown. The transition from metastable liquid to glassy state is marked by the glass transition that can be characterized by a glass transition temperature T_g. The vertical arrow in the picture shows the first order property variation accompanying the structural relaxation if the glass temperature is hold a T_1.

Now we can consider the evolution of T_f as the glass is reheated across the glass transition and then apply it to the process of enthalpic relaxation. Upon reheating of the glass T_f deviates away from the limiting T_f at the low-temperature onset of the glass transition and evolves back to equilibrium ($T_f = T$) in the liquid field. However, there is a hysteresis between the cooling and heating curves (Figure 2.1). The heating curve is dependent on the reheating rate, the cooling rate, the temperature-dependent structure and its temperature dependent characteristic relaxation time (DeBolt et al., 1976; Moynihan et al., 1976). The changes in fictive temperature as a function of temperature ($\Delta T_f/\Delta T$) can be monitored through measuring the first derivative of enthalpy ($\Delta H/\Delta T$), which is the heat capacity at

30

constant pressure (c_p). The c_p of a material can be measured using a calorimeter and the method is outlined in Chapter 2.2.2.
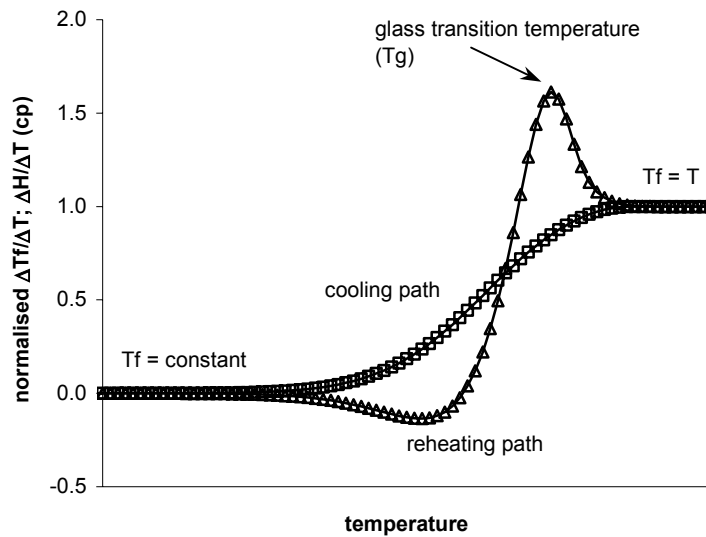
FIGURE 2.3. The variation of the temperature derivative of fictive temperature $\Delta T_f/\Delta T$ through the glass transition interval. $\Delta T_f/\Delta T$ can be directly correlated to the temperature derivative of enthalpy $\Delta H/\Delta T$; c_p. The geometry of the reheating path depends on the prior cooling rate and it is this path that it is modelled in order to determine this curve. The temperature at which the peak of this path occurs is used to define the glass transition temperature (T_g).

2.2. Structure of silicate melts

The main building block in a silicate melt is SiO_4^{4-} tetrahedra where Si^{4+} is in four-fold coordination. If the SiO_4^{4-} tetrahedra are linked to each other by Si-O-Si linkages where one oxygen connects two neighbouring SiO_4^{4-} tetrahedra, than the oxygen is defined as bridging (BO). A bridging oxygen can also bridge to tetrahedrally coordinated cations such as Al^{3+}, Fe^{3+}, B^{3+}, Ti^{4+}, Ge^{4+} or P^{5+} which are called a network forming cations. However Al^{3+}, Fe^{3+} and B^{3+} must be charge-balanced by either alkali or alkaline earth elements when they act as network formers. When an oxygen connects with a cation that is not tetrahedrally coordinated, then it is called a non-bridging oxygen (NBO). In addition to network forming, cations are also network modifiers or act to charge-balance in silicate melts. Network modifiers are K^+, Na^+, Ca^{2+}, Mg^{2+} and Fe^{2+}, which are octahedrally coordinated except when they charge-balance for either Al^{3+}, Fe^{3+} or B^{3+}. When these cations charge-balance, they should not be viewed as a network modifier (Mysen, 1988). Furthermore, Al^{3+}, Fe^{3+} and B^{3+} can also act as network modifiers. This occurs in the structure of the melts or glasses when there is an excess of Al^{3+}, Fe^{3+} or B^{3+} to the amount of charge-balancing cations. These charge-balancing cations are in higher coordination and they are known as network intermediates.

The results from the spectroscopic studies (e.g., NMR, Mössbauer, FTIR, RAMAN) show us that the structure of the melts and glasses is more or less polymerised. The degree of polymerisation is a function of the ratio of bridging to non-bridging oxygen. The number of NBO per tetrahedrally coordinated cation (NBO/T) can quantify the degree of polymerisation:

$$\frac{NBO}{T} \propto polymerization\ degree \tag{2.2}$$

A melt is fully polymerised when NBO/T = 0, and with increasing NBO/T the melts become gradually more depolymerised. The degree of polymerisation is calculated as:

$$\frac{NBO}{T} = \frac{1}{T} \sum_{i=1}^{i} nM_i^{n+} \tag{2.3}$$

where T is the total atomic abundance of tetrahedrally coordinated cation, M_i is the proportion of metal cation, after the proportion required for charge-balancing is subtracted, and n is the electrical charge of this cation (Mysen, 1988).

As the SiO_4^{4-} tetrahedra are treated as a near rigid units, the properties and structural changes in silicate melts are mainly controlled by the changes of the angle in the T - O - T and by changes in the bond length and the bond strength between tetrahedral and polyhedral units. Therefore, the properties of silicate materials vary with these parameters. The knowledge of these parameters is essential in order to understand silicate melt and glass structure.
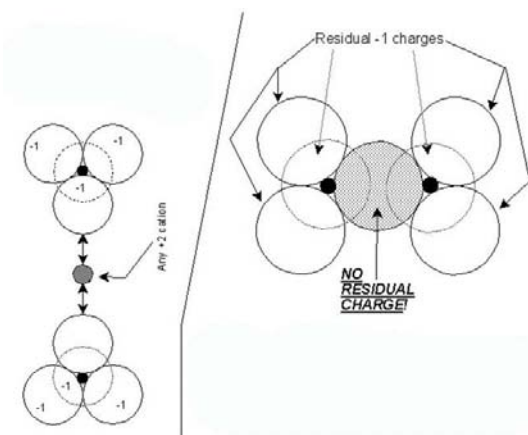
FIGURE 2.4. Schematic figure showing how to deal with residual charges of oxygen. a) Two tetrahedra are ionically bonded to a 2^+ cation between them. b) The second way of dealing with the negative charge on an oxygen is to covalently bond it to a second silicon, thereby using the oxygen at the corner of two different tetrahedra. The dotted oxygen atom in diagram is thereby shared between two adjacent tetrahedra. One of the extra electrons of the shared oxygen is used by one silicon, the other electron is used by the other.

2.3. Viscosity

Viscosity (η) is defined by Newton as the internal resistance to flow and assumed to be the proportionality between shear stress (τ) and strain rate (γ) ($\tau = \eta\gamma$). A silicate melt behaves Newtonian when the viscosity at a certain temperature is independent of changes in shear stress or strain rate. If the viscosity depends on the shear stress or strain rate, the melt behaves non-Newtonian. Silicate melts behaves non-Newtonian, only when the shear rate approches the relaxation rate. The viscosity is a function of temperature, pressure and bulk composition. For certain compositions it can also depend on the oxygen fugacity (Dingwell and Virgo, 1987 and Mysen, 1988). At a fixed temperature it varies by orders of magnitude as a function of composition (Richet, 1984). An increase in temperature decreases the viscosity since the structural rearrangements in the melt are easier because both the free volume and the configurational entropy increases (Richet, 1984). Most silicate melts show a non-Arrhenian behaviour, reflecting a non-linear relation between the $\log\eta$ vs. $1/T$. In general the viscosity at the glass transition is approximately equal to 10^{12} Pa s .

Many attempts have been made to predict the viscosity as a function of both composition and temperature (e.g., Vogel, 1921; Tammann and Hesse, 1926; Fulcher, 1925; Bottinga and Weill 1972; Adam and Gibbs, 1965; Angell, 1985; Neuville et al., 1992; Richet and Bottinga, 1995; Richet et al., 1996; Dingwell et al., 1996; Hess et al., 1995; Hess et al., 1996; Giordano and Dingwell, 2000). However, the mechanism for viscous flow of silicate melts is not fully understood.

This study provides new viscosity measurements for melts spanning a wide range of anhydrous compositions, viscosities (10^{-1} to 10^{12} Pas) and temperatures (973 to 1923 K). These new measurements, combined with other published data, provide a high-quality database comprising ~ 800 experimental data on 44 well-characterized melt compositions. This database is used to recalibrate the Giordano and Dingwell (2003a) model for predicting the temperature-dependent viscosity of natural silicate melts over a much wider range of temperatures (949 - 2653 K) and melt compositions (e.g., strong to fragile behaviour). Micropenetration and concentric cylinder viscometry were used in this study. A detailed description of both techniques follow in the next chapter. The results and application of the new model proposed in this study are described in Chapter 7.

2.4. Experimental methods and analytical hardware

2.4.1. Low temperature viscometry

Micropenetration viscometry was applied to determine the low-viscosities of the lavas. The technique and hardware are described in detail by Hess et al. (1995) and Hess (1996). The quantification of the penetration of an iridium hemisphere into the sample allows the viscosity to be calculated in the range $10^{8.5}$ to 10^{12} Pa s via

(2.4)

$$\eta = \frac{0.1875 Pt}{r^{0.5} l^{1.5}}$$

where 0.1875 is a geometric constant, r the radius of the hemisphere, P the applied force, a the penetration depth and t the experimental run time. The viscometer is calibrated against a lead-silica glass of the National Bureau of Standards (NBS 711) and a sodium-calcium-silica glass of the Deutsche Glastechnische Gesellschaft (DGG 1). 3 mm thick double polished glass disks were used for viscosity determinations. The accuracy of micropenetration viscosimetry is $\pm\log_{10}$ 0.23 Pa s, the precision of the measurements lies within $\pm \log_{10}$ 0.06 Pa s.
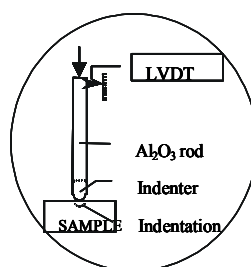
FIGURE 2.5. An altered vertical dilatometer (Bähr® DIL 802V and sketch of iridium indenter is shown on left.

2.4.2. High-temperature viscometry

High-temperature viscosity determinations were performed in a DelTech® DT-31-RS box furnace heated by $MoSi_2$ elements at air atmosphere. The sample was housed in a crucible, which was inserted into an alumina-silicium ceramic pedestal that ensured the sample was in the "hot zone" of the furnace. The height of the pedestal or the depth of the hole in which the crucible sat could be adjusted. The temperature profile of the final configuration was determined using a S-TYPE (Pt/Pt_{90}-Rh_{10}) thermocouple (shielded with platinum pipe-lid sheath), which was inserted directly into the melt sample. Stable, vertical and radial temperature gradient of 1.8 °C.cm^{-1} were recorded.

Viscosity was measured at a pressure of 1 bar in air with the concentric cylinder method. The samples were contained in cylindrical $Pt_{80}Rh_{20}$ crucible, 5.1 cm in height, with a 2.56 cm inner diameter and 0.1 cm wall thickness. The viscometer head, with which the viscosities

were measured, was a Brookfield model RVDT (Rotary Variable Displacement Transducer) with a full range torque of 7.2×10^{-2} N.m. In this study two types of spindles were used. Both were made from $Pt_{80}Rh_{20}$ with a circular cross-section and a 0.24 cm diameter stem. For more viscous melts the spindle had a diameter of 1.44 cm, a length of 3.32 cm and 45° conical ends to reduce end effects. For less viscous melts the spindle was 0.24 cm in diameter, 4.63 cm in length and did not have conical ends. The viscometer head drives the spindle at the range of constant angular velocity (0.5 to 100 rpm) and digitally records the torque exerted on the spindle by the sample.

The spindle and head were calibrated for viscosity measurements using NSB SRM 711 lead-silica glass for which the viscosity-temperature relationship is very well known. The precision of viscosity determination for this apparatus (±3% at the 2σ level, Dingwell, 1986) was derived from replication of viscosity determination of NSB SRM 711 involving successive immersions of the spindle and reoccupation of the temperature settings. The sample-bearing crucible was loaded through the bottom of the box furnace into the ceramic pedestal, such that one third of the crucible was within the pedestal. The viscosity spindle was connected to the reading head and lowered by a rack and pinion mechanism into the sample.

The viscometry determinations were initiated by equilibrating the melt sample with air. The rotation speeds of the spindle required to reach equilibration for each sample were 20 or 40 rpm depending on initial viscosity. The equilibration of melt sample was continuously monitored with a chart recorder that recorded the torque measured by the viscometer head as a function of time. For each sample, viscosity determination were initiated at the highest temperature and then made at successively lower temperatures. One hour was sufficient for equilibration of the sample over each 25-50 °C temperature decrease. During the decreasing temperature steps the thermal equilibrium was monitored with the chart recording of the sample viscosity. At the end of each step, when thermal equilibrium was reached, the melt glass were sampled using the "*dip*" technique (~150 mg). The samples were quenched in water for further iron oxidation and structural state and compositional investigation.

Torque measurements were made over a range of angular velocities for each sample. The obtained viscosities were independent of angular velocity in all cases. The measurements were continued with decreasing temperatures in steps until crystallization occurred or the limit of the apparatus was achieved. Crystallization during the final cooling step for each sample resulted in erratic viscosity readings and was easily confirmed by inspection of samples recovered at those times.

The last measurement of viscosity was always a redetermination of the highest temperature determination to test for experimental drift as a consequence of possible movement of pedestal, crucible or spindle, chemical change (loss of water, volatiles) and, last but not least, the decrease of surface inside the crucible by dip technique. No difference was observed between first and last high-temperature determinations. That indicates that no compositional or instrumental drift occurred during the viscosity measurement.

After all measurements the investigated sample was either poured out and quenched on an iron plate or the whole crucible, containing the analysed sample, was rapidly quenched in water. From this glass material cylinders 8 mm in diameter were cored for container based dilatometry or low temperature viscometry (micropenetration).
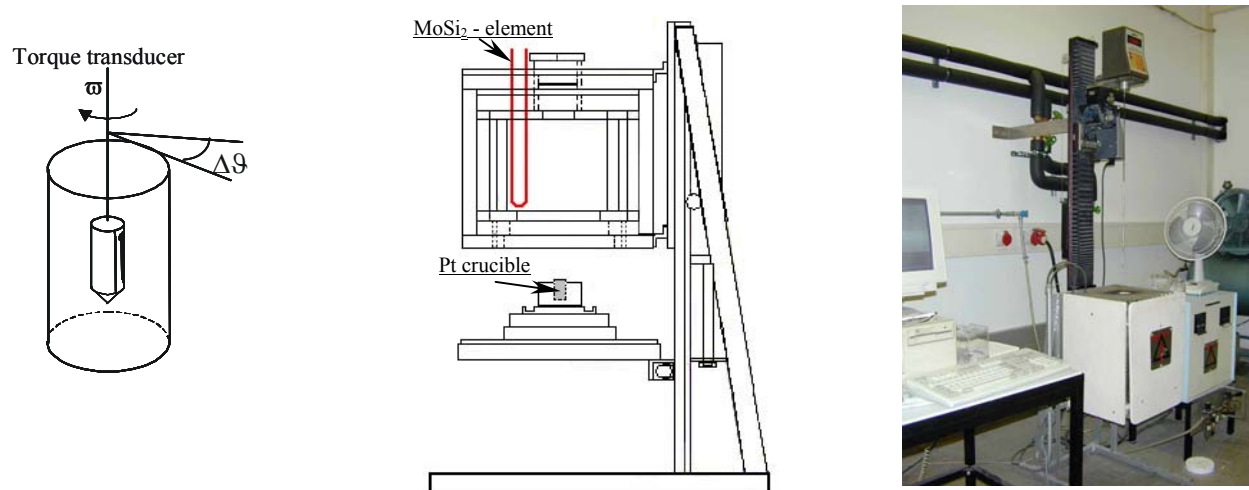
FIGURE 2.6. Schematic diagram of the concentric cylinder apparatus. The heating system Deltech furnace, position and shape of one of the 6 $MoSi_2$ heating elements is illustrated in the figure. Details of the $Pt_{80}Rh_{20}$ crucible and the spindle shape are shown on the left. The viscometer Brookfield RVTD stirring head is coupled to the spindle through a hinged connection which can be seen on the photograpf on the left.

2.4.3. Low temperature densitometry

The room temperature densities of the glass samples were obtained by employing an Archimedean-based technique using a SARTORIUS® MC-210P microbalance and density determination kit with ethanol as the immersion liquid. The measurements were performed on the samples after the second run of dilatometry. All the samples had the same thermal history, matching cooling and heating rates. The weight of each sample was measured in air and then entirely submersed in ethanol. Densities of glass samples (ρ_{glass}) were calculated using the relationship:

$$\rho_{glass} = \frac{[\rho_{ethanol}(T) * m_{air}]}{[m_{air} - m_{ethanol}]} \tag{2.5}$$

where m_{air} and $m_{ethanol}$ are the weights of the glass sample in air and submersed in ethanol, respectively. To account for the temperature-dependence of the density of ethanol $\rho_{ethanol}(T)$ the temperature of the immersion liquid was monitored carefully during the measurements. At least three individual measurements were conducted on the same piece of sample used to derive a standard error. The accuracy (< 0.3 %) of the room temperature densitometry was

FIGURE 2.7. Photograph and illustration of the microbalance SARTORIUS® MC-210P together with density determination kit.

established by replicate measurements of commercially available standard crystals (i.e. enstatite, diopside, periclase, quartz and sapphire) and comparing them to the density data published in the literature (Cameron et al., 1973; Haermon, 1979; Hazen, 1976; Lepage et al., 1980 ; Sasaki et al., 1982).

2.4.4. High temperature densitometry

The melt densities were determined using the double-bob Archimedean technique. The apparatus used is based on the concept of (Bockris et al., 1956). The technique used here has

been outlined previously (Dingwell and Brearley, 1988; Dingwell et al., 1988). The previously fused starting materials were re-melted into rigid, cylindrical, $Pt_{80}Rh_{20}$ crucibles (5.1 cm height, 2.56 cm inner diameter with 0.2 cm wall thickness) and bottom-loaded into a vertical alumina muffle tube furnace. The samples were supported in the hot zone of the furnace by an alumina-silica ceramic pedestal with a centred drilled hole for setting an S-type ($Pt-Pt_{90}Rh_{10}$) thermocouple. Hot zone temperature was maintained with an electronic set-point controller and a B-type ($Pt_{94}Rh_{06}-Pt_{70}Rh_{30}$) control thermocouple and monitored with a S-type thermocouple. The measuring alumina thermocouple was additionally sheathed in a Pt sleeve and immersed in the melt sample before and after each density determination. A 75 kg weighing table above the tube furnace supports an X-Y stage designed to position the weighing balance over the furnace. The balance employed is digital model METTLER$^{®}$ AE100. The automatic tare feature of this balance was used to obtain direct buoyancy readings. Dingwell et al. (1988) tested the precision of this technique, which they estimated to be better than 0.2%, by determining the density of molten NaCl. The protocol of the present measurements is described in detail by Courtial et al. (1999) and briefly outlined here. The experiments were conducted in a set of three immersions for two bobs of different volumes, in order to compute a mean and the standard deviation of the replicate buoyancy determinations. The liquid density was calculated from the buoyancy data via:

$$\rho_{liq} = \frac{(B_1 - B_2)}{(V_1 - V_2)}$$

(2.6)

where B_1 and B_2 are the buoyancies, and V_1 and V_2 are the submerged volumes of the large and small bobs, respectively. For each composition, the temperature of the melt was measured after the last buoyancy determination by dipping a Pt-sheathed thermocouple (S-type) into the crucible containing the melt. A second thermocouple (B-type) recorded the temperature during the calibration phase as well as during the buoyancy measurements. A calibration temperature curve (i.e., temperature of the melt vs. temperature of the crucible at the bottom) was determined for the temperatures of the melt during the buoyancy measurements, where direct temperature measurements of the melt are not possible. Temperature homogeneity was within ± 1 K during the buoyancy measurements or between the different immersions of the bobs at the same temperature. Temperature uncertainties, including contributions from thermal gradients and time fluctuations, are estimated to contribute an imprecision of less than 0.1% to the experimental density data, since the thermal expansivities of the samples are rather small (Courtial et al., 1999). The densities were determined in individual runs of decreasing temperature steps. The samples were held at each measurement temperature for at

38

least 30 min to allow the melt equilibrate with the atmosphere inside the furnace. After this isothermal hold the buoyancy was measured over 15 min at the given temperature. At the end of each isothermal hold, the liquid was sampled by inserting an alumina rod into the melt and withdrawing approximately 150 mg, which was then quenched in water. In the case of Fe-bearing samples, glasses obtained in this way were than used to determine the oxidation state of iron, using the wet chemistry method, and in all cases to measure the chemical composition, using electron microprobe. The density was determined three times for each Pt-bob in the same manner. At the end of the last cycle the crucible containing the sample was removed from the furnace and quenched in water. A cylinder of glass 6 mm in diameter was drilled from this final product of the high temperature densitometry. Parts of this cylinder were then used for calorimetric and dilatometric measurements.

FIGURE 2.8. Photograph of the alumina tube furnace with digital balance METTLER® AE100 above.

2.4.5. Calorimetry

The specific heat capacities of the investigated samples were determined using a differential scanning calorimeter (DCS Netzsch® 404C, STA Netzsch® 449C). The measurements involve a baseline measurement (two empty Pt-Rh crucibles, 6 mm in diameter, 0.1 mm wall thickness covered with a lid), sapphire standard measurement (with one crucible containing the standard and the other empty) and sample measurement (with one crucible containing the sample and the other empty). The glass sample was polished to within 1μm to ensure an accurate fit with the bottom of the Pt-crucible and to reach a mass comparable to that of the sapphire standard (55.85 mg). Calorimetry was performed under a constant argon flow. The calorimeter was calibrated within the temperature range from 293 K to 1263 K. The heat capacity (c_p) data were calculated using all the heat flow data (i.e., baseline, standard and sample) sample and standard weight and the known heat capacity of sapphire standard was taken from Robie et al. (1979). The precision of the heat capacities was ±0.7 % for the glassy values and ±2% for the supercooled liquid values. The accuracy of the heat capacity of the glassy values was ±1%, and for the supercooled liquid values ±3%.

Measured heat capacity of the glasses (in J g^{-1} K^{-1}) were fitted using a third order Maier - Kelley (1932) equation (c_p=a+bT+cT^{-2}). Two calorimetric measurements were made for each composition using a heating rate of 10 K.min^{-1}, in case of Fe-bearing samples using a heating rate of 5 K.min^{-1}. The first run was performed in order to relax the sample, 65 to 80 K above the glass transition temperature (T_g), and then cool the sample at a known rate. The second run was made to determine T_g and the heat capacity where both cooling and heating rates were identical. T_g values, obtained during the second run, were taken as the peak of the specific heat capacity curve.

FIGURE 2.9. Photographs of the differential scanning calorimeters (i.e., STA Netzsch® 449C Jupiter and DCS Netzsch® 404C Pegasus) used during this study.
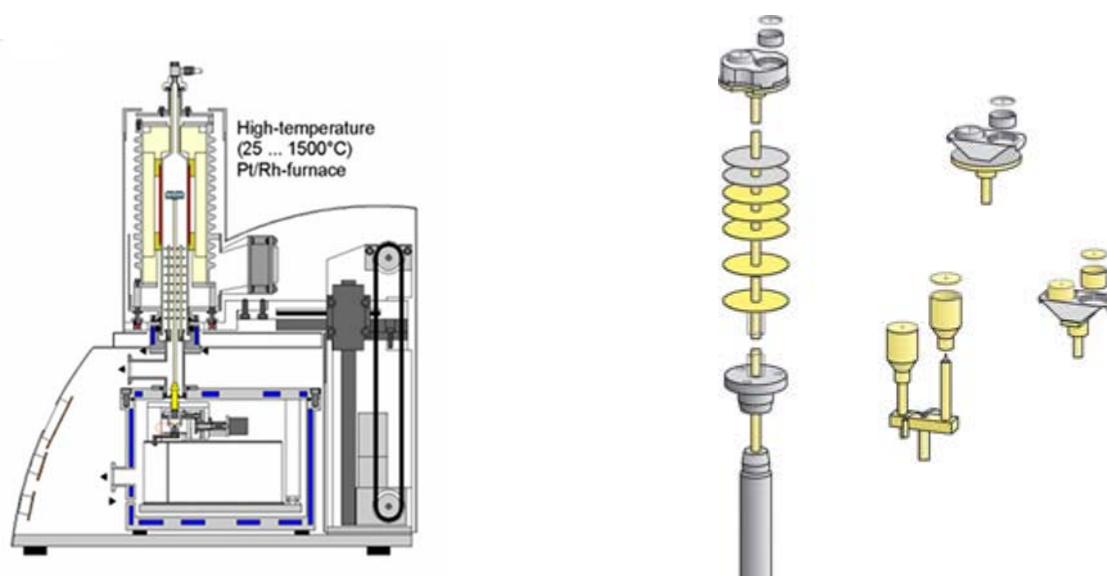
FIGURE 2.10. Schematic cross-section of the differential scanning calorimeter STA Netzsch® 449C Jupiter with microbalance together with details of the sample holder and four different crucible types. Two Pt crucible with Pt shielded sample holder was used during this study.

2.4.6. Dilatometry

Cylindrical, bubble-free glass samples (6 mm in diameter and 17 mm in length) were used for dilatometric investigations, the ends of which were grounded and polished to within 1 μm to ensure plane parallel surfaces. The measurements were performed using a Netzsch[®] DIL 402C dilatometer with a horizontal alumina-push rod.

The sample assembly is supported on an alumina base connected to a measuring head. The push rod sits horizontally and is in contact with the side of the sample assembly and is also manufactured from alumina. The relative length change of the sample and alumina rod is monitored by a linear variable displacement transducer (LVDT), which is calibrated against a standard single crystal of sapphire. The reference expansivity data are taken from the National Bureau of Standards. The precision of the expansivity is $<\pm0.1\%$, the accuracy is $<\pm0.2\%$ for temperatures up to 1263 K. All experiments were conducted under an inert gas (Ar, the purity of Ar gas was 5.0, i.e. 99.99999 %) atmosphere using a constant argon flow.

For each composition, two runs were made using identical heating and cooling rates as for previously conducted calorimetrical measurements. The sample was heated to tens of Kelvin above T_g, which corresponds to the dilatometric softening point. As with the DSC measurement the role of the first run was to relax the sample and then cool it at a known rate (e.g., 10 K min^{-1}). T_g and the molar thermal expansion were found based on the results of the second run where both the cooling and heating rates were known. T_g was taken as the inflection point of the relative length change ($\partial L/L_0$) curve during the second run. The inflection point corresponds to the peak point of the linear thermal expansion coefficient alpha (α_{linear}) curve as well as to the peak point of the $\partial V/\partial T$ curve. The α_{linear} is defined as the fractional increase in length (linear dimension) per unit rise in temperature. Horizontal
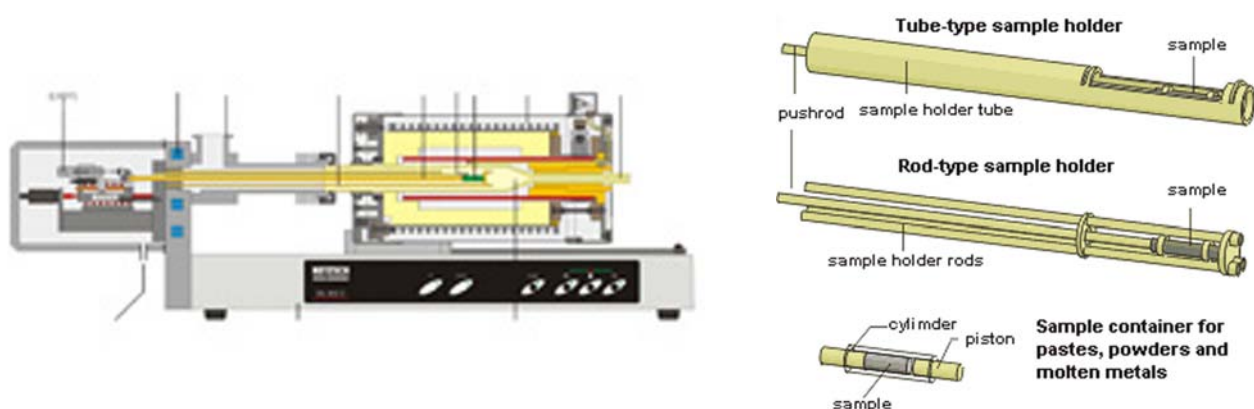
FIGURE 2.11. Schematic illustration of the horizontal dilatometer Netzsch® DIL 402C together with tube-type sample holder with alumina push rod was used during this study.

dilatometry provides $\partial L/L_0$ (where ∂L is the increment of the change in length at a given temperature, T, and L_0 is an initial length, in cm, of the sample), as a function of temperature. The linear thermal expansion coefficient can be calculated from these dilatometric data as the relative length change of the sample per Kelvin. It is difficult to measure the relative volume expansion, therefore the linear thermal expansion coefficient is calculated as the relative change in the length across temperature interval (∂T):

$$\alpha_{linear} = \frac{1}{L_0}\frac{\partial L}{\partial T} \tag{2.7}$$

The volume thermal expansion coefficient (α_{volume}) is 3 times α_{linear} ($=1/L_0(\partial L/\partial T)$) as glasses are isotropic, the linear and volume thermal expansion coefficients can be determined from one thermal expansion measurement. The thermal expansion coefficient strongly depends on the composition and temperature. The thermal expansion coefficient above the glass transition is 3 to 5 times larger than the one below the glass transition. The initial length and radius (r) of each sample was measured, in cm, using a micrometer, together with their mass (m) after the first dilatometric measurement (i.e., after heating and cooling at known rate, 10 K min^{-1}) at room temperature (T_{room}). Using this data the length of the sample ($L(T)$) at temperature T can then be calculated by:

$$L(T) = \partial L + L_0 \tag{2.8}$$

and the volume ($V(T)$, cm^3) of the sample at temperature, T, by:

$$V(T) = L(T)A(T) \tag{2.9}$$

where $A(T) = \pi r^2$ (cross-section area of the cylindrical sample with radius, r, at temperature, T). Density (ρ, g cm^{-3}) of the sample at temperature, T, is then calculated by:

$$\rho = \frac{m}{V(T)} \tag{2.10}$$

where m is the initial mass of sample (g).

Molar volume ($V_{mol}^{(T)}$, cm^3 mol^{-1}) at temperature, T, can be expressed as:

$$V_{mol}^{(T)} = V(T)\frac{gfw}{m} \tag{2.11}$$

where gfw is gram formula weight calculated from the composition.

The change in the molar volume of the glass with temperature is calculated at constant pressure using the molar thermal expansion coefficient ($\alpha_{mol}^{(T)}$), which can be determined using:

$$\alpha_{mol}^{(T)} = \frac{1}{V_{mol\_glass}^{(T)}} \frac{\partial V_{glass}}{\partial T} \qquad (2.12)$$

where $V_{mol\_glass}^{(T)}$ is the molar volume of the glass at temperature, T, and $\dfrac{\partial V_{glass}}{\partial T}$ is the molar

thermal expansivity of the glass. The temperature dependence of the $\alpha_{mol}^{(T)}$ can be expressed empirically:

$$\alpha_{mol}^{(T)} = \alpha_0 + \alpha_1 T \qquad (2.13)$$

where α_0 and α_1 are the empirical parameters. Equation 2.13 assumes a linear dependency and is only a first approximation and not intended as a perfect description of the data. To obtain the temperature dependence of the molar volume of the glass, Equation 2.12 is integrated between temperature, T, and 298 K using Equation 2.13, one obtains Equation 2.14:

$$V_{mol\_glass}^{(T)} = V_{mol\_glass}^{(298)} \exp\left[\alpha_0 (T - 298) + \frac{1}{2}\alpha_1 (T^2 - 298^2) \right] \qquad (2.14)$$

where $V_{glass}^{(298)}$ is the molar volume of the glass at room-temperature.

2.4.7. Electron microprobe

The composition of the samples that had been used in this study were measured by electron microprobe (CAMECA® SX 50) operating under following conditions: 15 kV acceleration voltage, 10nA beam current, 20 µm defocused beam diameter, counting time 20 s on the peak and 10 s on the background. A ZAF correction was undertaken. The calibration was based on mineral standards including albite (Na), wollastonite (Ca, Si), cordierite (Al), orthoclase (K), illmenite (Mn and Ti), hematite (Fe), periclase (Mg), apatite (P), sphalerite (Zn). The reason for using a defocused beam was to ensure a non-destructive analytical procedure especially concerning the volatilization of sodium and potassium-rich glasses. During microprobe analyses no loss of volatile elements was detected.

2.4.8. Potassium dichromate titration

Potassium dichromate titration was used to determine Fe(II) for all Fe-bearing samples. This method requires the use of concentrated sulphuric (H_2SO_4) and hydrofluoric acids (HF). A $\sim75.00 \pm 0.01$ mg of powder was placed in a Teflon crucible and covered with a Teflon lid. The lid has two holes, one for the inflow of CO_2 protective gas and the second

for the outlet of vapour and excess CO_2. Initially a geochemical rock standard was analyzed (BHVO-1 standard from US Geological Survey, which is a Hawaiian lava of known FeO concentration - 8.58 wt%).

Approximately 3 ml of deionised H_2O was added to the sample powder, than 10 ml of a solution of concentrated H_2SO_4, HF and deionised H_2O, in proportion of 1:0.8:3. The covered crucibles were moved to hot plate and left to simmer for 30 minutes under CO_2 gas protection, which was bubbled through the solution. Then the crucibles were placed in a water bath to cool, during which time they were continuously under CO_2 gas. After approximately 10 minutes, the crucible walls were washed down with deionised H_2O and 10 ml of boric acid (H_3BO_3) was added. All samples disintegration was conducted in a fume cupboard. Each crucible was transported to potentiometric titration with potassium dichromate ($K_2Cr_2O_7$).

The $K_2Cr_2O_7$ titrant with concentration of abut 0.01N was prepared and place in a 500 ml volumetric flask. One of the most important types of analytical titrations involves oxidation-reduction reactions. In this experiment we titrated Fe(II) solutions with a standard solution containing potassium dichromate ion to determine the percentage of iron in the iron containing sample. The solution was then titrated with a standard potassium dichromate solution (0.01 $mol.dm^{-3}$) with titration rate 1.00 ml min^{-1}. Similarly, the potential values were recorded automatically when the potential change were within ±2 $mV.min^{-1}$ for each additional. All potentiometric titrations were performed at 20 °C using a Metrohm Dosimat 665 automatic titrator and E 649 Magnetic Swing-out Stirrer with electrode holder.

The overall reaction is:

$$6\ Fe^{2+} + Cr_2O_7^{2-} + 14\ H^+ <\!\!-\!\!> 2\ Cr^{3+} + 6\ Fe^{3+} + 7\ H_2O$$
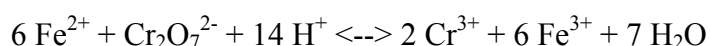
This reaction can be separated into two half-reactions. Dichromate ion acts as the oxidizing agent and its reduction can be written:

$$Cr_2O_7^{2-} + 14\ H^+ + 6\ e^- <\!\!-\!\!> 2\ Cr^{3+} + 7\ H_2O$$
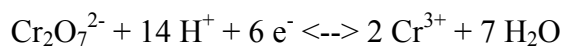
The iron(II) ion is oxidized to the iron(III) state by the dichromate ion:

$$Fe^{2+} <\!\!-\!\!> Fe^{3+} + e^-$$

As the titration proceeds the sample solution will turn green due to the presence of Cr^{3+}. The endpoint is reached when the very fine yellow colour (at the beginning of titration curve) of the Cr^{6+} titrant appears (at the end of titration curve). For a redox titration, one equivalent of an oxidizing agent ($Cr_2O_7^{2-}$) reacts with one equivalent of a reducing agent Fe(II). From the half reaction for dichromate it can be seen that one mole of dichromate ion requires six moles of electrons.

Calculation of ferric iron has been provided by following manner. To calculate the amount of Fe_2O_3 in own sample (not Fe_2O_{3Tot}), the computation is as follows: Weight % of Fe_2O_{3Tot} (from microprobe analysis) divided by 1.111348 is equal to weight % of $FeO_{Tot.}$ Total weight % FeO_{Tot} minus % FeO ($\pm$ titrated value) is equal to the amount of iron in the sample which really exists as Fe_2O_3 (ferric iron). This needs to be multiplied by 1.111348 to re-convert back to the ferric oxide state (Fe_2O_3).
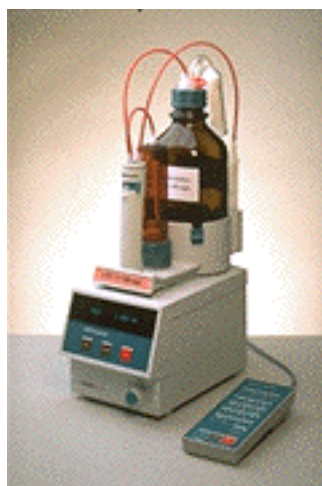
FIGURE 2.12. All potentiometric titrations were performed using a Dosimat 665, Metrohm automatic titrator, with a combination of the platinum electrode (reference electrode is a silver-silver chloride) and E 649 Magnetic Swing-out Stirrer.

2.4.9. X-Ray analysis

The possibility of crystallisation in the glassy samples has been evaluated in the samples prior to, and after, calorimetry and dilatometry measurements. Crystals have not been observed in any of the analyzed glasses. Peaks were not apparent within the spectra obtained using the DRON 2 X-ray diffractometer with Bragg Bertrand focusing and a Cu-K α as X-ray source with Ni filter. The measurements were performed in the range of 3 to 60º of the diffraction angle 2θ within step regime of 0.05 º and a measurement time of 3 sec at each step. The spectrum was interpreted using the program ZDS with data base PDF-2.

3. History of Density and Expansivity Determination at Supercooled Liquid Temperature

Knowledge of the thermal expansivity of silicate liquids is essential for the calculation of melt densities over the wide range of temperatures relevant for magmatic processes (Bottinga et al., 1983). Like other thermodynamic properties, the density of melts vary significantly with chemical composition as well as temperature and pressure. Thus, accurate data on the thermal expansivity of magmatic melts may play an important role in construction of PVT equations of state. Since Bottinga and Weill (1970) first suggested that the density of melts in two or three component systems could be used to determine partial molar volumes of oxide components in silicate liquids, several models based upon this approach have been proposed in the Earth science literature (Bottinga and Weill, 1970; Nelson and Carmichael, 1979; Bottinga et al., 1982; Lange and Carmichael, 1987; Courtial and Dingwell, 1995; Lange, 1997; Courtial and Dingwell, 1999).

Accurate determination of liquid densities and expansivities have proved difficult owing to experimental limitations. In high-temperature buoyancy-based density measurements only restricted ranges of temperature are accessible. This is variably due to the high liquidus temperature or high superliquidus viscosity of the melt. Restricted temperature ranges result in a large uncertainty in expansivity. An example is provided by the systems Na_2O-SiO_2 and $CaO-Al_2O_3-SiO_2$, where, with increasing silica content, the combination of decreasing accessible temperatures and decreasing expansivities, results in error of up to several hundred percent for expansivity (Bockris et al., 1956; Courtial and Dingwell, 1995; Courtial and Dingwell, 1999). The uncertainties associated with thermal expansion of silicate liquids have been emphasized in the last few decades by several authors (e.g., Bockris et al., 1956; Bottinga, 1985; Herzberg, 1987; Lange and Carmichael, 1987; Webb, 1992; Knoche et al., 1992; Knoche et al., 1994; Lange, 1996; Lange, 1997; Gottsmann et al., 1999; Toplis and Richet, 2000; Ghiorso and Kress, 2004, Gottsmann and Dingwell, 2000; Liu and Lange, 2001; Tangeman and Lange, 2001; Gottsmann and Dingwell, 2002).

Both in industry and in nature, several processes (e.g. crystallization, crystal-melt fractionation, fragmentation of magma) occur at temperatures where a melt phase persists in metastable equilibrium at subsolidus temperatures. Dilatometry is one of the techniques which can yield expansivity, and density data, at such temperatures. However, direct determination

of the expansivity of cylindrical samples just above the glass transition is difficult, since the sample will collapse under its own gravitational body forces at temperatures where the viscosity is less than 10^{11} Pa s. (e.g., Tool and Eichlin, 1931; Toplis and Richet, 2000). To predict supercooled liquid expansivites from dilatometric data on cylindrical samples requires a procedure, that removes the gravitational deformation effect from the dilatometric traces.

The first method was introduced by Webb et al., (1992). Supercooled liquid volumes and molar thermal expansivities are determined using scanning calorimetric and dilatometric measurements in the glassy region and at the glass transition. The extraction of supercooled liquid molar thermal expansivities from dilatometry/calorimetry is based on an assumed equivalence of the relaxation of volume and enthalpy at the glass transition. Using this technique, Knoche et al., (1992) first reported the temperature dependent expansivity of silicate melt. Recently, Sipp and Richet (2002) have provided compelling evidence in favour of the equivalence of enthalpy, volume and structural relaxation for a wide range of silicate liquid compositions. However, this procedure has met some scepticism, given that volume and enthalpy relaxation are not necessarily equivalent (Moynihan et al., 1976).

The existence of this problem led Lange (1996; 1997) to introduce an alternative method. In this method, the volume of the sample is determined at the limiting fictive temperature and combined with measurements made on the same material at superliquidus temperature. However, the calculation of molar thermal expansivity and molar volume in this way is critically dependent on precise determination of the limiting fictive temperature of the glass. In addition, Lange´s method is based on indirect measurement of expansivity in the glass transition range and the values were derived from just a single V-T coordinate.

More recently, Gottsmann et al. (1999) developed a direct method to observe the thermal expansivity of a silicate melt in the relaxed liquid state. A sample is inserted within a metal container composed of a hollow cylinder and two solid circular end pieces, which is then placed inside a dilatometer. The change in length of the assembly during the dilatometric measurement includes contributions from the liquid volume expansion, as well as two correction terms, one each for the expansion of the enclosing hollow cylinder and the end pieces. The reported precision of this method is about 3.5%.

Most recently, Toplis and Richet (2000) used a dilatometry technique, which was previously developed and described by (Sipp, 1998; Sipp and Richet 2002), to determine the melt expansivity. In their study the cylindrical glassy samples were annealed isothermally until relaxation occurred with time at constant temperature. The annealing temperatures were the temperatures at which the viscosity of the samples was high enough to support the rod

with which expansivity is measured. The lower part of the SiO_2 rod was in contact with the surface of the measured sample. A second SiO_2 rod was placed on a reference SiO_2 standard and the principle of differential dilatometry was applied. Despite the narrow temperature range (about 40 K), the melt expansivities were determined with a precision to within 3% and their results point to temperature dependent thermal expansivities of silicate liquids.

The results of the methods of Webb et al., (1992), Gottsmann et al. (1999) and Toplis and Richet (2000) are all in excellent agreement.

3.1. Combining dilatometric/calorimetric methods - Webb et al., (1992) method

Direct observation of thermal expansivity in supercooled liquids is impossible because of viscous deformation (the sharp drop in the dilatometric trace above the peak value shown in Figure 3.1b. In this study, the molar volume of the supercooled liquid and the molar thermal expansion of each sample across the glass transition region were calculated based on an assumed equivalence of the relaxation of volume and enthalpy at the glass transition region (i.e., Webb et al., 1992). The derivative properties (e.g., heat capacity, molar thermal expansivity) are used to reconstruct the temperature derivative of fictive temperature (T_f). T_f is defined as the contribution of the structural relaxation process to the property of interest (H or V) expressed in temperature units and may be considered as a measure of the order parameter associated with the structural relaxation process (Moynihan et al., 1976). To reconstruct the temperature derivative of T_f of any property in the glass transition interval (e.g., enthalpy, volume) the properties are normalized with respect to the temperature derivative of the liquid and glass. This normalized temperature derivative (equal to dT_f/dT) has a value of zero for the glass (i.e. T_f is constant) and 1 for the equilibrium liquid (i.e. T_f equals T). The normalized calorimetric trace is used to extend the dilatometric data of the glass into the supercooled liquid temperature range and to determine the molar thermal expansivity of the supercooled liquid across the glass transition region. An assumption of equivalent relaxation behaviour and relaxation times for different properties has been employed and is validated by the consistency between my results and results obtained using the methods of Gottsmann and Dingwell (2000) and Toplis and Richet (2000). The observation that the peak temperature values from the calorimetric data coincide with the molar thermal expansivity calculated from dilatometric measurements dictates that insignificant viscous deformation is recorded by the dilatometer at the temperature up to the peak temperature value (Figure 3.1b). The derivative

properties, P, (e.g., heat capacity, molar expansivity) are used to reconstruct the temperature derivative of T_f by:

$$\left.\frac{dT_f}{dT}\right|_T = \frac{\left[\left(\frac{\partial P}{\partial T}\right) - \left(\frac{\partial P}{\partial T}\right)_g\right]_T}{\left[\left(\frac{\partial P}{\partial T}\right)_e - \left(\frac{\partial P}{\partial T}\right)_g\right]_{T_f}} \tag{3.1}$$

where the subscripts e and g represent the liquid (equilibrium) and the glassy values of the property, respectively (Moynihan et al., 1976). In the present study, the enthalpy H and volume V are used as the macroscopic properties. Given the equality of the relaxation times of volume and enthalpy, Equation 3.1 can be rewritten as

$$\left.\frac{dT_f}{dT}\right|_T = \frac{c_p^{(T)} - c_{pg}^{(T)}}{c_{pe}^{(T_f)} - c_{pg}^{(T_f)}} = \frac{\left.\frac{\partial V^{(T)}}{\partial T} - \frac{\partial V_g^{(T)}}{\partial T}\right|_T}{\left.\frac{\partial V_e^{(T)}}{\partial T} - \frac{\partial V_g^{(T)}}{\partial T}\right|_{T_f}} \tag{3.2}$$

for heat capacity, c_p, and molar thermal expansivity, $\partial V/\partial T$. The behaviour of T_f in the glass transition region can be generalized to all properties with identical relaxation times for which sufficient glassy and liquid data exist. The relaxed value of the molar thermal expansivity can now be calculated from Equation 3.2.

The molar volume at the supercooled liquid temperature (V_{mol}^{Tsc}) just above the glass transition temperature was calculated using:

$$V_{mol}^{Tsc} = V_{glass}^{(298)} + \int_{Troom}^{Tsc} \frac{\partial V}{\partial T} \partial T \tag{3.3}$$

where $V_{glass}^{(298)}$ is molar volume of the sample at T_{room}. T_{sc} is the supercooled liquid temperature obtained by calorimetry and is the temperature at which stable c_p was first achieved, indicating the liquid was relaxed (Figure 3.1a). The molar volume at the supercooled liquid temperature (V_{mol}^{Tsc}) is equal to the molar volume of the glass at T_{room} ($V_{glass}^{(298)}$) and the area between the $\partial V/\partial T$ curve and inserted zero line at temperature range between T_{room} and T_{sc}. This volume increase was calculated in a step-by-step manner (i.e. 0.2 K).

An example comparing normalized relaxation in the dilatometric and calorimetric traces is illustrated in Figure. 3.1.
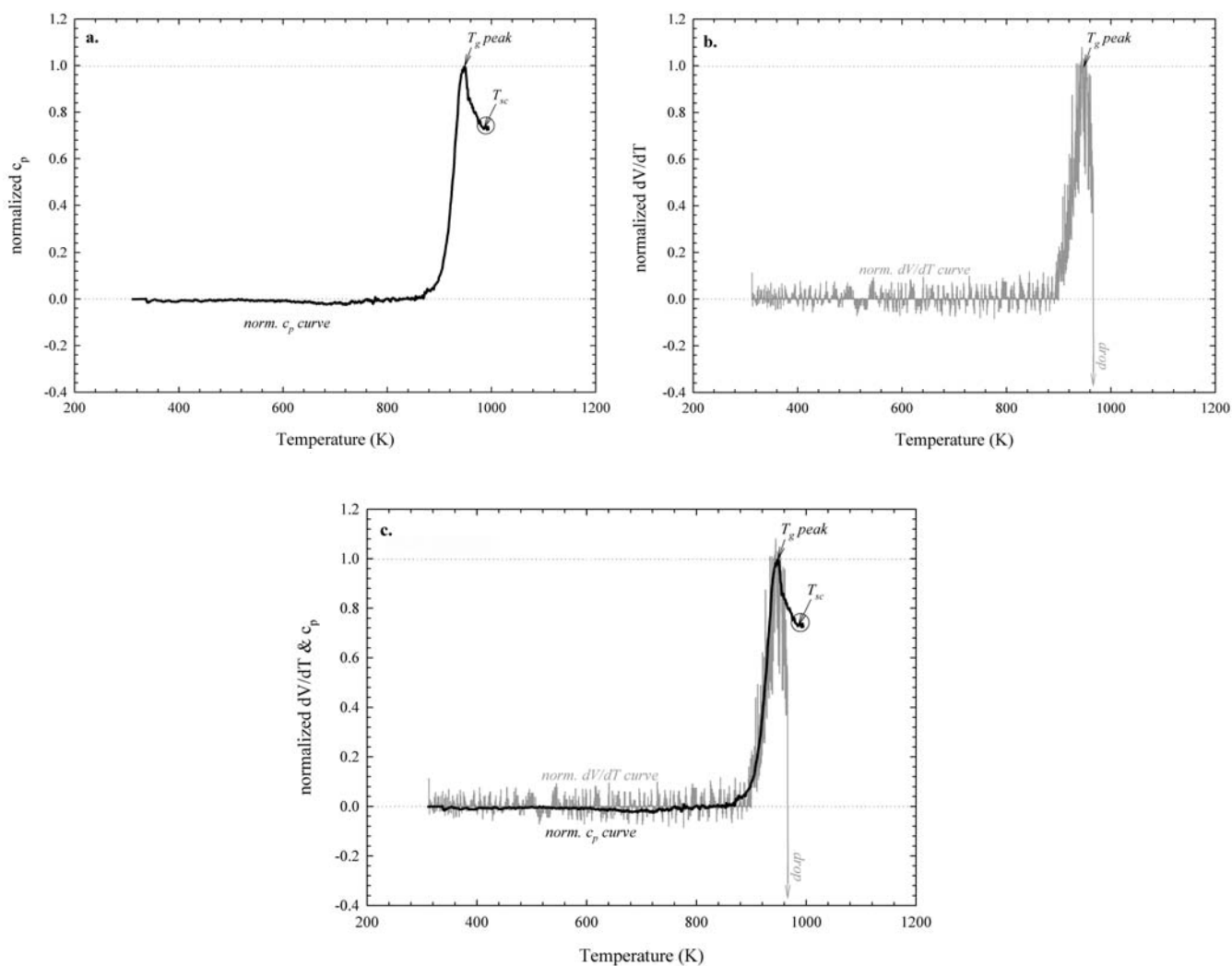
FIGURES 3.1. The normalization procedure to derive supercooled liquid expansivity using the Webb et al. (1992) method. The normalized specific heat capacity (**a**) where supercooled liquid (T_{sc}) is directly observable and the normalized thermal expansivity (**b**) data where T_{sc} is not observable due to viscose deformation of the sample (i.e., drop). Both traces were derived upon reheating the sample at matching heating rate. Specific heat capacity and thermal expansivity measurements were provided on the samples which exhibit the same thermal history. The glass data are normalized to zero and the peak values (T_g) are normalized to 1. T_{sc} is the temperature of the supercooled liquid where its expansivity can thus be predicted from the calorimetric trace (**c**).

4.   A Partial Molar Volume for ZnO in Silicate Melts

Trace elements in igneous petrology have, in comparison with major elements, a relevance in the petrogenetic modelling of magmatic differentiation that far outweighs their relative abundance. Optimal use of the information contained in trace element variations within igneous phases requires an accurate description of their partitioning behaviour as a function of phase composition and structure, as well as temperature and pressure. In this manner, the partial molar thermodynamic properties of trace elements in silicate melts may contribute to the petrogenetic modelling of such systems. With this in mind, a series of investigations into the partial molar properties of trace elements in silicate melts was carried out in recent years (Courtial et al., 1999; Holzapfel et al., 2001; Courtial and Dingwell, 2004). The volumetric properties of silicate liquids influence a wide range of processes which result in igneous differentiation in nature. Need for the quantification of such processes has spurred research into the density of silicate melts which has, as a result, been the subject of repeated experimental investigations in the second half of the last century (Bockris et al., 1956; Lange and Carmichael, 1987; Dingwell and Brearley, 1988; Dingwell et al., 1988; Knoche et al., 1992a; Knoche et al., 1992b; Knoche et al., 1994; Toplis et al., 1994; Lange, 1996; Lange, 1997; Toplis and Richet, 2000). The general approach to the volumetric description of silicate melts has involved the construction of multicomponent models whose compositional dependence of melt volume is cast as a set of partial molar volumes of individual oxide components, together with, where necessary, excess volumes of mixing (Bottinga and Weill, 1970; Lange and Carmichael, 1987; Knoche et al., 1995). These models have generally been restricted to the major and minor oxide components present in naturally-occurring igneous rocks.

This chapter extend this work to the analysis of the volumetric properties of ZnO in silicate melts. The densities of 8 Zn-bearing silicate melts were determined, in equilibrium with air, in the temperature range of 1363 to 1850 K. The compositional joins investigated (sodium disilicate (NS2) - ZnO; anorthite-diopside 1 bar eutectic (AnDi) - ZnO; and diopside - petedunnite) were chosen based on the pre-existing experimental density data set, on their petrological relevance and in order to provide a test for significant compositionally-induced variations in the structural role of ZnO. The ZnO concentrations investigated range up to 25 mol% for sodium disilicate, 20 mol% for the anorthite-diopside 1 atm eutectic and 25 mol% for petedunnite.

4.1. Background

Zinc containing glasses have been intensively studied using X-ray absorption spectroscopic methods in the last three decades. EXAFS, XANES and WAXS data exist for alkali silicate, alkali borate and borosilicate melts (e.g. Hurt and Phillips, 1971; Dumas and Petiau, 1986; Rosenthal and Garofalini, 1987; Calas et al., 2002; Galoisy et al., 2001). In Zn-poor alkali silicate glasses (<5 wt% ZnO) zinc improves mechanical properties, as well as chemical durability (Della Mea et al., 1986). In addition, zinc has a nucleating role in alkaline-earth silicate and aluminosilicate glasses (Dumas and Petiau, 1986). In alkali silicate glasses, zinc has been proposed to occur in tetrahedral and octahedral coordination (referred to as [4]Zn and [6]Zn, respectively), with a marked preference for tetrahedral coordination. The [4]Zn/[6]Zn ratio derived from molecular dynamics computer simulations increases as the Zn/Na or alkali ratio decreases, the sodium ions or alkalis compensating the charge deficit of the ZnO_4 tetrahedra (Hurt and Phillips, 1971; Rosenthal and Garofalini, 1987). The EXAFS data of Le Grand et al. (2000), obtained for aluminoborosilicate glasses, yield average Zn–O distances of ~1.96 Å and Zn coordination numbers of 3.8 to 4.7, consistent with a four-fold coordination of zinc. These data illustrate that the Zn-Si distance of 3.20 ± 0.03 Å is consistent with corner-sharing ZnO_4 and SiO_4 tetrahedra. The same samples later investigated by Calas et al. (2002), reveal two distinct local structures of the zinc K-edge EXAFS spectra for a Zn-containing glass (see Figure 3. in Calas et al., 2002). This local configuration satisfies one of Pauling´s rules: A coordination polyhedron of anions is formed around each cation, with the cation-anion distance being determined by the radius sum and the coordination number of the cation, and the cation by the radius ratio. In this case, zinc is in a network-forming position and oxygen triclusters are also present. Calas et al. (2002) used a visual bond-balance model which reveals that ZnO_4 tetrahedra are copolymerised with the silicate network. The visual bond-valence model shows that the Zn-O distances derived from EXAFS data are close to the equilibrium value when considering that, for example, two Na^+ ions charge compensating each oxygen are bound to both Zn and Si (Calas et al., 2002). The network-forming position of zinc can explain the improvement of the mechanical properties, durability and glass thermal stability induced by the presence of low zinc contents in borosilicate glasses containing low-field strength cations (Na, K, Cs, Rb etc.). The presence of zinc may contribute to the decrease of the effective network modifier concentration, as more alkalis are involved in charge compensation (Della Mea et al., 1986; Calas et al., 2002). In addition, similar Zn-Si distances have been found in cordierite glasses and in mixed alkali

borosilicate glasses, by EXAFS (Dumas and Petiau, 1986) and WAXS (Ennas et al., 1990), respectively. Finally, similar Zn-O distances (values of about 1.99 Å), have been found in low Zn-bearing magnesium aluminosilicate glasses (Dumas and Petiau, 1986).

Zinc, as a network-forming divalent cation, has been studied widely from a mineralogical point of view. The stability and chemographic relations of phases within the system $CaO-ZnO-SiO_2$ are relevant to the genesis of Zn-rich skarns and calc-silicate rocks. These rock types are present in the old cratons of current continental shield crust and are economically important sources of metal ores. Furthermore, zinc-bearing crystalline phases are also present in blast furnace slags in the refining of Pb ores. Experiments at variable P-T conditions to obtain stability fields of crystalline phases within the above mentioned ternary system have been provided by (e.g., Segnit, 1954; Doroshev et al., 1983; Essene and Peacor, 1987; Fehr and Hobelsberger, 1997). At low to intermediate pressures Zn^{2+} enters tetrahedral sites in crystalline silicate structures such as those of hardystonite, hemimorphite Zn-feldspar, willemite, and staurolite. Hendricksite is the only mineral that exhibits Zn^{2+} in octahedral sites at low pressures, but this site is strongly distorted. High pressures are required to force Zn^{2+} into large octahedral sites like the M1 site in petedunnite (P > 1GPa) or the M2 site in Zn clinopyroxene (P > 3 GPa). Zn-feldspar is restricted not only to low pressure but also to low temperatures, as indicated by its stability field (Fehr and Huber, 2001).

4.2. Experimental methods

4.2.1. Sample preparation

The synthetic materials investigated in this study were series of liquids synthesized by the addition of ZnO to base melt compositions corresponding to sodium disilicate (NS2) and to the anorthite-diopside 1 atm eutectic composition (AnDi), respectively. Additionally, the diopside composition has been modified via the exchange operator $ZnMg_{-1}$ to generate $CaZnSi_2O_6$ (petedunnite glass). Starting sodium disilicate was synthesized from SiO_2 (Alfa Aesar, 99.9% -Ign. loss < 0.3%) and Na_2CO_3 (Merck, 99.9%) mixes. Starting anorthite-diopside 1 atm eutectic was synthesized from SiO_2 (Alfa Aesar, 99.9% -Ign. loss < 0.3%), $CaCO_3$ (Merck, 98.5%), MgO (Riedel-de Haen, 97%) and Al_2O_3 (Merck, 99.9%). All these powders were dried at 120 ºC at least for 24 hours prior to weighing. They were ground, mixed and then fused in a platinum crucible for 3 hours in a $MoSi_2$ box furnace at 1000 ºC and 1500 ºC in the case of NS2 and AnDi, respectively. The melts were poured from high temperature onto a stainless steel plate for cooling. A comparison between the weight of the samples before and after the melting serves as a check for the complete volatilization of CO_2

from Na_2CO_3 and $CaCO_3$ powders. A cycle of grinding and fusion was repeated three times to ensure homogeneous starting Na-disilicate and AnDi glasses. ZnO (Merck, 99.99%) which was previously dried overnight at 120 ºC, was added in various proportions to finely ground fractions of the starting NS2 and AnDi glasses. These newly synthesised NS2-based, Zn-bearing liquids were then melted in air for ca. 2 hours between 1050 and 1300 ºC in platinum crucibles and the AnDi-based, Zn-bearing liquids were melted in air for ca. 2 hours between 1550 and 1600 ºC in platinum crucibles, in order to obtain the melts investigated volumetrically in this study. About 75 g were used for each high-temperature densitometry experiment. The quenched glasses were analysed by electron microprobe in order to check their composition and their homogeneity. The electron microprobe analyses of the materials prior to the experiments are presented in Table 4.1. In addition, the analyses of the samples after the high-temperature density experiments are also included in Table 1. (Note that NS2-based samples are hygroscopic and they have been kept in a desiccator prior to their analyses). The analyses of the starting material after the syntheses as well as after the high-temperature experiments differ only slightly from the nominal compositions. During the different high-temperature stages of this study, the glasses were kept in air. No change in the colour of these materials has been observed between the starting and the final glasses. All Zn-containing glasses exhibit the same light yellow colour. Zinc is present under these conditions in a 2^+ oxidation state.

4.2.2. Room temperature densitometry

The room temperature (T_{room}) densities of three glassy chips of each composition were obtained employing an Archimedean based technique a SARTORIUS® MC-210P microbalance and density determination kit with ethanol as the immersion liquid. The chips were previously heated and cooled at 5 K.min^{-1} from approximately 80 K above the glass transition temperature (i.e., from the relaxed liquid state). The glass transition temperature (T_g) was defined as the temperature where the viscosity of my sample (unpublished data) equals to $10^{11.22}$ Pa.s (Webb and Knoche, 1995). The sample weight was measured in air and subsequently in ethanol. Densities of glass samples at T_{room} were calculated using the Equation 2.5 For a detailed description of the room temperature densitometry and the accuracy of this method see also Chapter 2.4.3.

4.2.3. High temperature densitometry

The melt densities were determined using the double-bob Archimedean technique above the superliquidus temperatures. The protocol of the present measurements is described in detail in Chapter 2.4.4. The liquid density was calculated using the Equation 2.6.

4.3. Results

4.3.1. Room temperature densitometry

The room-temperature densities of the present Zn-containing Na-disilicate, AnDi and petedunnite glasses were measured on the glassy samples that experienced a 5 K/min heating/cooling thermal history. The individual errors were obtained from three replicate measurements performed on each chip and range from 0.004 to 0.09% and the mean error is about 0.025%. The room-temperature density of these glasses, (listed in Tables 2 and 3) varies from 2.516 to 3.024 $g.cm^{-3}$ and from 2.796 to 3.219 $g.cm^{-3}$ for the NS2-ZnO and for the AnDi-ZnO glasses, respectively. In addition, the room-temperature density of petedunnite glass is 3.303 $g.cm^{-3}$.

4.3.2. High temperature densitometry

The results of the high-temperature density measurements are listed in Tables 2 and 3 and are plotted as functions of temperature in Figures 4.1a, 4.1b and 4.1c. Within the uncertainties, the experimental density data can be described as a linear function of temperature (Figs. 1a - 1c). The parameters and the correlation coefficients which return from these linear fits are reported for each composition in Table 4. Within the temperature range investigated, the density varies from 2.26 to 2.99 $g.cm^{-3}$ and from 2.62 to 3.06 $g.cm^{-3}$ for the Zn-bearing NS2 and for the AnDi melts, respectively, where it increases with increasing ZnO contents (Figures 4.1a and 4.1c).

The high temperature densities within the investigated temperature range for petedunnite vary from 3.04 to 3.13 $g.cm^{-3}$. The Zn-bearing AnDi melts exhibit a greater density than the Zn-bearing NS2 melts at equivalent molar concentrations of Zn, which is resulting from their different base compositions (NS2 vs. AnDi). Furthermore, the addition of ZnO to both base compositions results in a nearly parallel shift of the density vs. temperature lines in each system (NS2 and/or AnDi). This result suggests that the thermal expansion does not change with the addition of ZnO within the temperature range investigated. The individual errors (calculated based on the standard deviation of the three replicate buoyancy measurements for each bob) range from 0.1 to 0.5% and are reported in Tables 4.2 and 4.3

and plotted in Figures 4.1a - 4.1c for each temperature and composition. The largest errors, generally in AnDi and NS2 melts, are for the most viscous melts. NS2-ZnO melt determinations yield higher precision, half that of the AnDi-ZnO melts. The mean error, which derives from the replicate buoyancies determinations of all the measurements conducted in this study is ca. 0.3%.
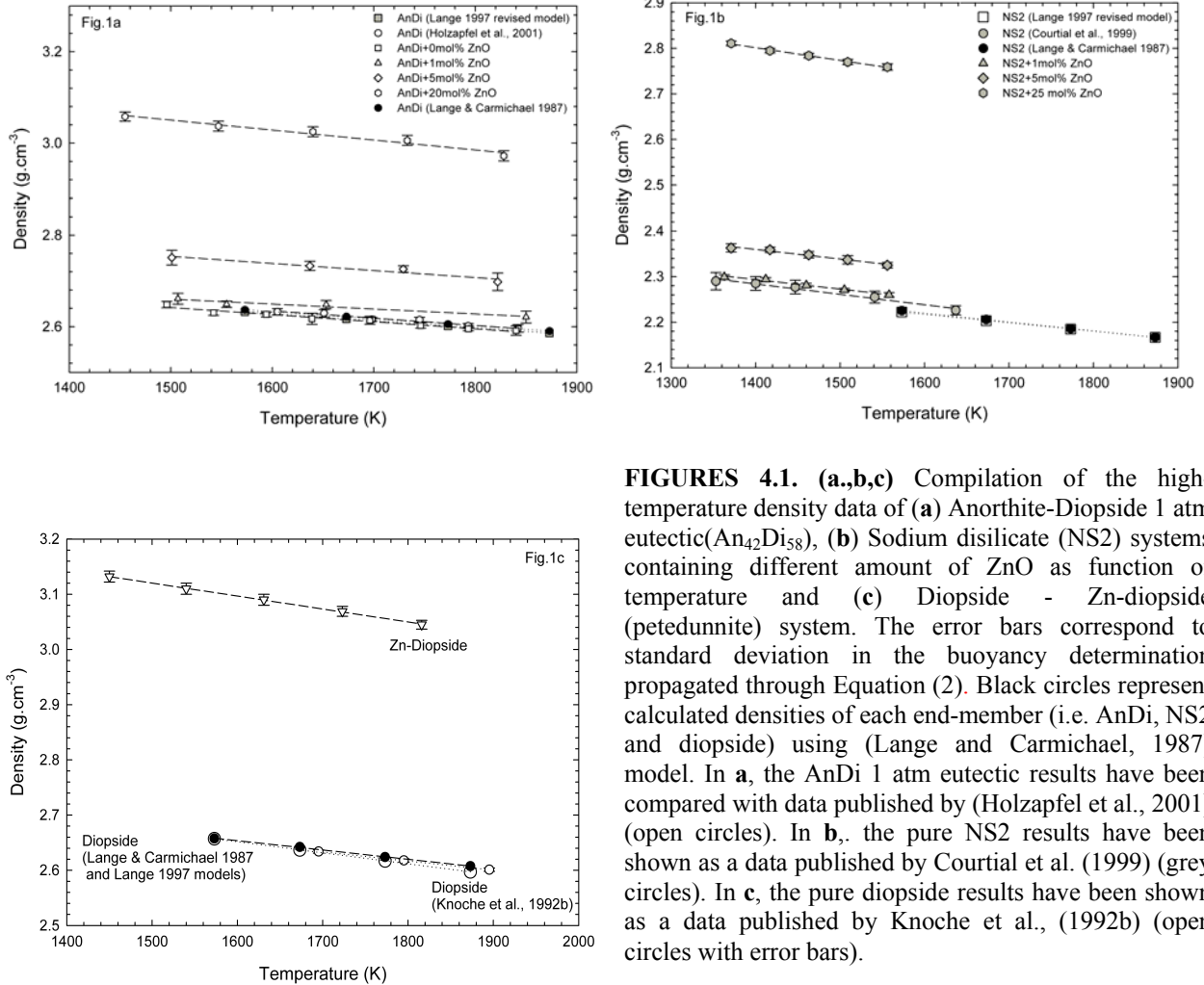
FIGURES 4.1. (a.,b,c) Compilation of the high-temperature density data of (**a**) Anorthite-Diopside 1 atm eutectic(An$_{42}$Di$_{58}$), (**b**) Sodium disilicate (NS2) systems containing different amount of ZnO as function of temperature and (**c**) Diopside - Zn-diopside (petedunnite) system. The error bars correspond to standard deviation in the buoyancy determination propagated through Equation (2). Black circles represent calculated densities of each end-member (i.e. AnDi, NS2 and diopside) using (Lange and Carmichael, 1987) model. In **a**, the AnDi 1 atm eutectic results have been compared with data published by (Holzapfel et al., 2001) (open circles). In **b**,. the pure NS2 results have been shown as a data published by Courtial et al. (1999) (grey circles). In **c**, the pure diopside results have been shown as a data published by Knoche et al., (1992b) (open circles with error bars).

4.3.3. Molar volumes of liquids

The molar volume can be calculated using Equation 4.1:

$$\rho(T) = \frac{gfw}{V(T)}$$

(4.1)

where ρ is the measured density of the liquid at a temperature (T), gfw is gram formula weight and V is molar volume at T. The molar volumes for all investigated samples are plotted as functions of temperature in Figures 4.2a - 4.2 c.

The temperature dependence of liquid density can be expressed empirically using Equation 4.2:

$$\rho_{liquid}(T) = A^{density} + B^{density} T(K) \tag{4.2}$$

The least square fit parameters $A^{density}$ and $B^{density}$ of Equation 4 are listed in Table 4.4.

The change with temperature of the molar volume of the liquid is expressed at constant pressure by Equation 4.3:

$$V_{liquid}(T) = a_{vol} + b_{vol} T(K) \tag{4.3}$$

The least square fit parameters a_{vol} and b_{vol} within the investigated temperature range ΔT are listed in Table 4.5. The mean error for the high-temperature density determination is 0.3%. Here, it should be noted slightly different analysed composition results (AS and HT in Table 4.1). These differences in composition will contribute, however, to an error less than 0.1 % on the molar volume. We can thus estimate that the mean error in the precision of the experimental measurements and additional analytical errors originate in minor deviation of the compositions propagate into a combined error of less than 0.5% in the molar volumes of the present liquids.

4.3.4. Compositional dependence of the molar volume of the present liquids

The influence of ZnO on the volumetric properties of both AnDi and NS2 base composition is plotted in Figures 4.3 and 4.4 as function of transition metal oxide content. In these figures, it can be seen that the molar volume of these liquids diminishes gradually from the base composition (i.e. AnDi and NS2) down to the most ZnO-rich compositions (i.e., 20 and 25 mol% of ZnO, respectively). The influence of ZnO on the molar volumes of measured samples can be expressed linearly and this trend remains valid within the volume uncertainties. Therefore, from the data plotted in Figures 4.3 and 4.4 it can thus be concluded that, within the experimental uncertainties, the molar volume of the Zn-containing liquids behaves ideally within the composition and temperature ranges investigated. In addition, molar volumes at 1450 K and 1800 K for diopside and petedunnite are plotted in Figure 4.5 as a function of $ZnMg_{-1}$ content, respectively. Petedunnite exhibits a larger molar volume than diopside at 1800 K.

4.3.5. Partial molar volume of ZnO

The compositional dependence of the liquid molar volume can be, in general, expressed by Equation 4.4.

$$V_{liquid}(T) = \sum X_i V_i(T) \qquad (4.4)$$

where V_{liquid} is measured liquid molar volume, X_i the mole fraction of the oxide (i), and V_i the partial molar volume of the oxide (i). The molar volumes of the present ZnO-bearing liquids were independently analysed using Equation 4.5:

$$V_{liquid}(T) = \sum X_i \left[V_{i(1500)} + \left(\frac{\partial V_i}{\partial T} \right)(T - 1500) \right] \qquad (4.5)$$

where V_{liquid} is the measured liquid molar volume, X_i the average of the mole fraction analysed of the end-member (i), $V_{i(1500)}$ the partial molar volume of the pure end-member (i) and ($\partial V_i/\partial T$) the thermal molar expansivity of the pure end-member (i) at 1500 K. From Equation 7, the partial molar volume of each end-member component was obtained (i.e., NS2
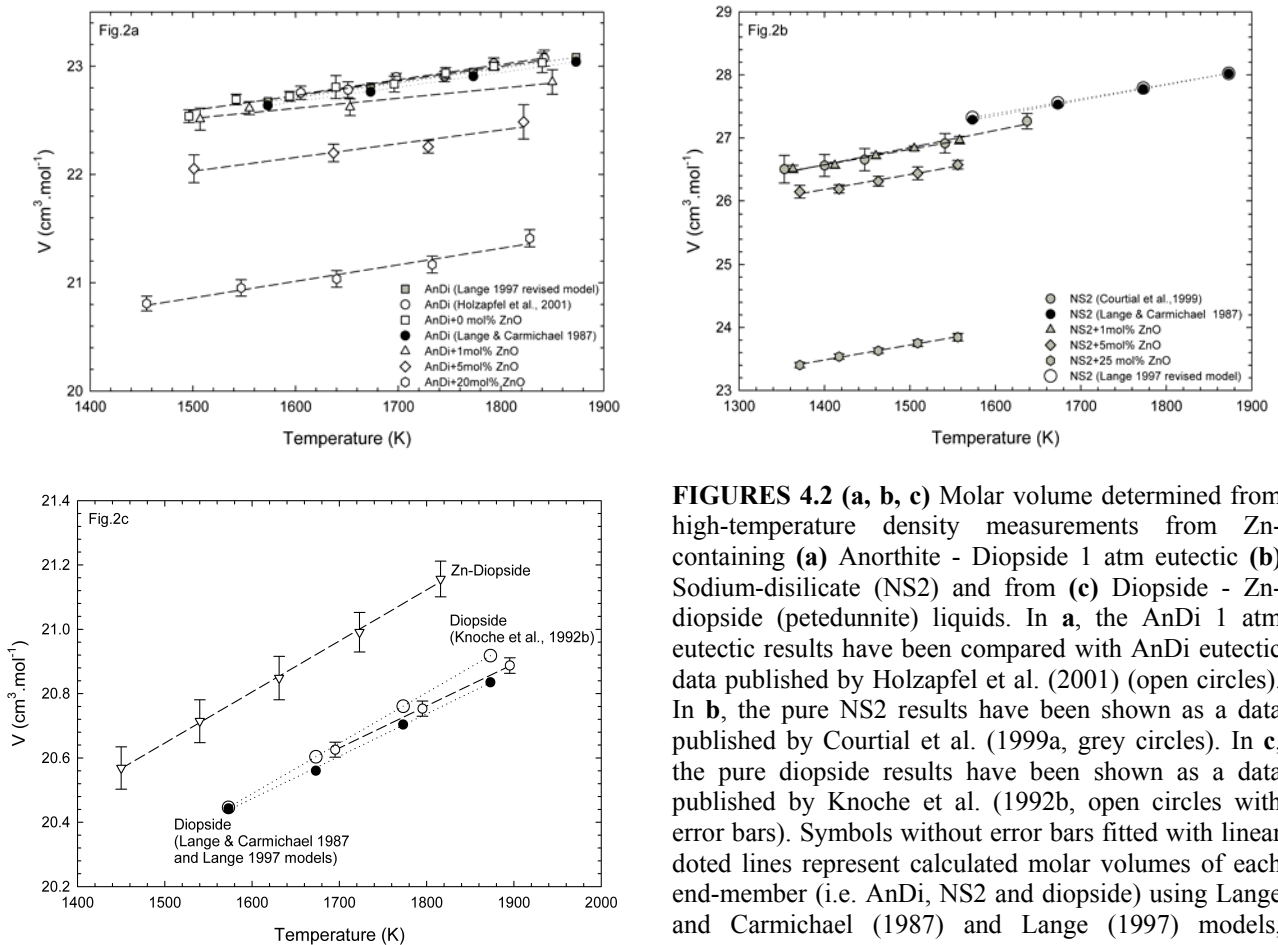
FIGURES 4.2 (a, b, c) Molar volume determined from high-temperature density measurements from Zn-containing **(a)** Anorthite - Diopside 1 atm eutectic **(b)** Sodium-disilicate (NS2) and from **(c)** Diopside - Zn-diopside (petedunnite) liquids. In **a**, the AnDi 1 atm eutectic results have been compared with AnDi eutectic data published by Holzapfel et al. (2001) (open circles). In **b**, the pure NS2 results have been shown as a data published by Courtial et al. (1999a, grey circles). In **c**, the pure diopside results have been shown as a data published by Knoche et al. (1992b, open circles with error bars). Symbols without error bars fitted with linear doted lines represent calculated molar volumes of each end-member (i.e. AnDi, NS2 and diopside) using Lange and Carmichael (1987) and Lange (1997) models, respectively.

and ZnO for the first regression, AnDi and ZnO for the second one). The Equation 4.4 can be used if the molar volume has a linear variation with the temperature. Courtial and Dingwell (1995) demonstrated that the molar volume does not behave ideally in the $CaO-Al_2O_3-SiO_2$ system, implying at least one excess term. Equation 4.4 thus needs to be rewritten in form:

$$V_{liquid}(T) = \sum X_i V_i(T) + XS \qquad (4.6)$$

where XS is the excess volume term corresponding to the possible interactions between SiO_2 and CaO; SiO_2 and Al_2O_3; CaO and Al_2O_3. Courtial and Dingwell (1995) identify an excess volume term between SiO_2 and CaO ($XS_{SiO2\ CaO}$) within the compositional range investigated which was defined as:

$$XS_{SiO_2CaO} = X_{SiO_2} . X_{CaO} . V_{SiO_2CaO} \qquad (4.7)$$

where X_{SiO_2} and X_{CaO} are the molar fraction of SiO_2 and CaO respectively, and V_{SiO_2CaO} the corresponding excess volume term. These authors tested several alternative regression equations involving an ideal model, an excess term between one of each pair of oxides, two excess terms between two of each pair of oxides and three excess terms for each pair of oxides. Based on statistical criteria, Courtial and Dingwell (1995) recommended use of a model including an excess term between SiO_2 and CaO:

$$V_{liquid}(T) = \sum X_i \left[V_{i(1500)} + \left(\frac{\partial V_i}{\partial T}\right)(T - 1500) \right] + X_{SiO_2} X_{CaO} \left[V_{SiO_2CaO(1500)} + \left(\frac{\partial V_{SiO_2CaO(1500)}}{\partial T}\right)(T - 1500) \right]$$

(4.8)

Here, the molar volumes of the present ZnO-bearing liquids were independently analysed using a regression of Equation 4.8 to obtain partial molar volumes of individual oxides and ZnO (i.e., a multicomponent model for the third regression). Note that the partial molar volumes (Vi) and thermal molar expansivities ($\partial V_i/\partial T$) for the multi-component system were calculated using all my high-temperature density data (i.e., NS2-ZnO, AnDi-ZnO and petedunnite) and the high-temperature density data from Lange and Carmichael, 1987 (i.e., samples LC2-15) and all high-temperature density data from Courtial and Dingwell 1995, 1999a. In doing so, the partial molar volumes for SiO_2, Al_2O_3, MgO, CaO and Na_2O were better constrained. Nevertheless, we obtained the same V_{ZnO} and $\partial V_{ZnO}/\partial T$ as the V_{ZnO} and $\partial V_{ZnO}/\partial T$ as those obtained by applying the end-member regression to all my data (within uncertainty of the regression). Only the molar expansivity of ZnO obtained from AnDi-ZnO

regression appears to be larger.

The reference temperature 1500 K was chosen to be within the temperature range where high-temperature densitometry was performed. The regressions as a function of composition and temperature were made simultaneously on the ZnO-bearing liquids over the temperature range from 1350 to 1550 K in the NS2 system, and from 1500 to 1850 K in the AnDi and in the multicomponent systems, respectively. The results of these regressions following the model of Equation 4.5 and 4.8 are reported in Table 4.6. In Table 4.6, the fit parameters for NS2 and AnDi obtained for both fits are also listed since I used this composition as an end-member for my fits. The difference between the calculated molar volumes of NS2 using the parameters listed in Table 4.6 and the molar volume determined from the parameters given in Table 4.5 is less than 0.64 % for temperatures ranging from 1350 to 1550 K. In addition, the difference between the calculated molar volumes of AnDi using the parameters listed in Table 4.6 and the molar volume determined from the parameters
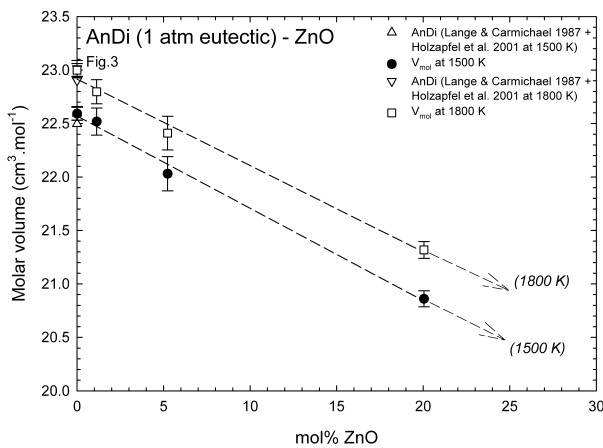
FIGURE 4.3. Molar volume calculated at 1500 and 1800 K from the individual fits of Table 5 plotted as a function of ZnO content in the anorthite - diopside (AnDi) 1 atm eutectic system.
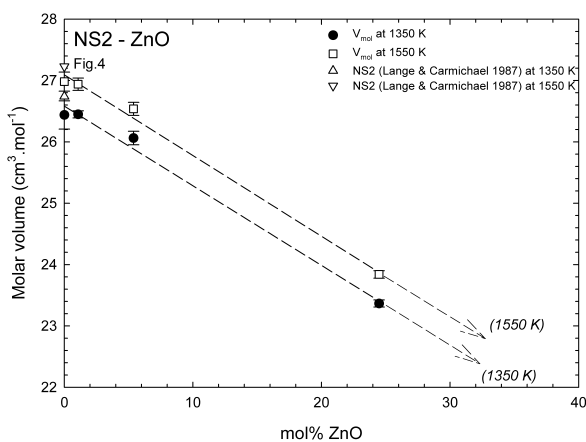
FIGURE 4.4. Molar volume calculated at 1350 and 1550 K from the individual fits of Table 5 plotted as a function of ZnO content in the sodium disilicate (NS2) system.
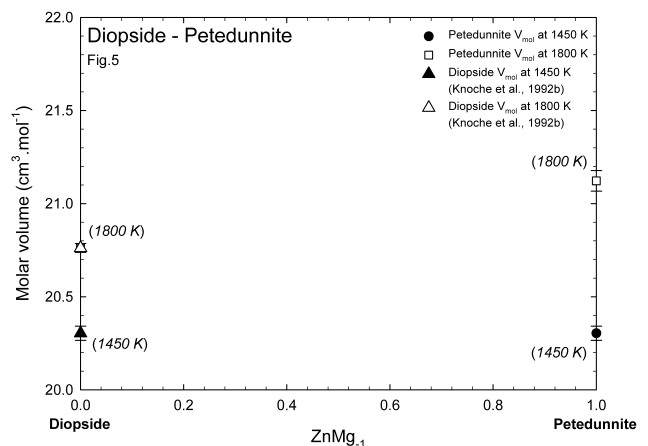
FIGURE 4.5. Molar volume calculated at 1450 and 1800 K from the individual fits of Table 5 plotted as a function of the diopside - petedunnite binary system.

given in Table 4.5 is less than 0.45% for temperatures ranging from 1500 to 1850 K. The uncertainties in and the quality of these fits are indicated by the standard error of each fit coefficient (in parentheses in Table 4.6). The relative standard error of the fit, when compared with the experimental uncertainties, indicates whether the fit can adequately reproduce the data within the best estimate of experimental uncertainties. The coefficient of determination (R^2), the adjusted R^2 statistic (the adjusted R^2 is most often used in multiple regressions because it accounts for the number of variables in the regression equation), the relative standard error of the fit (*S*) are also included in Table 4.6.

4.4. Discussion

4.4.1. Comparison with the previous literature data

To the best of the authors knowledge, volumetric data on Zn-containing silicate liquids are absent from the literature to date. High temperature density data from (Toyoda et al., 2003) have been obtained on $50ZnO-50P_2O_5$ glass melts. Na-silicate melts have been more widely investigated (Stein et al., 1986; Knoche et al., 1994). Here, I will compare my results to those of (Bockris et al., 1956), who have measured the molar volume of melts at 1673 K along the Na_2O-SiO_2 binary join. Interpolation of (Bockris et al., 1956) results to Na-disilicate composition obtained by (Courtial et.al., 1999) exhibits an excellent agreement at 1673 K (i.e., 0.6%). In addition, the molar volumes of Na-disilicate and AnDi melts were calculated using the revised model of (Lange, 1997), which reproduces (Courtial et. al., 1999) measurements on Na-disilicate and my measurements on AnDi within errors estimated from the standard deviation of three replicate mass determination using buoyancy measurements.

Partial molar volumes of transition metals, metals and metalloids in silicate melts of fourth row of the periodic table of elements have been studied by several authors (i.e. Lange and Carmichael, 1987; Dingwell and Brearley, 1988; Dingwell et al., 1988; Dingwell, 1991; Dingwell, 1992; Lange, 1997; Courtial et al., 1999; Holzapfel et al., 2001). Inspection of the partial molar volumes of the transition metals obtained from silicate melts at 1500 K (1 atm) yields: (TiO_2 (~25 in Na_2SiO_3 and $CaSiO_3$ melts), FeO (12-23 a large compositional variation), CoO (~15.89), NiO (~13.39), ZnO (~13.59-this study) and for Ga_2O_3 (~35.87 in AnDi melt and ~50.92 in NS2 melt). In addition, the partial molar volume of GeO_2 , has been proposed by Holzapfel et al. (2001) to be ~29.46 in NS2 melt and ~29.69 in AnDi melt at 1400 K They calculated the partial molar volume of GeO_2 from 1800 to 1400 K and showed that across the whole range it varied less than their stated uncertainties. We extrapolated their

data to 1500 K to permit comparison with the partial molar volumes of other transition metals, which gives an average partial molar volume for GeO_2 of ~ 29.64 for NS2 and AnDi melts.

Partial molar volume of the transition metal oxides likely depends, amongst other factors, on the number of oxygens which are bound with each element. If the basic molecule has a form XO, where X is a transition metal and O is oxygen, then partial molar volume should follow the general trend of bond radii or atomic radii observed within the transition metals. The atomic radii and the bond radii in (Å) for the transition metals are as follows (Element (atomic radius; bond radius): Ti(2;1.32) > Fe(1.72;1.17) > Co(1.67;1.16); Ni(1.62;1.15) > Zn(1.52;1.25) > Ga(1.81;1.26) > and Ge(1.52;1.22). The general trend of the atomic radius (bond radius) within transition elements is Sc > Ti > V > Cr > Mn > Fe > Co > Ni> Cu > Zn. Although there is a slight contraction at the beginning of the series, the atoms are all near the same size. The size is determined by the 4s electrons. The attraction of the increasing number of protons in the nucleus is approximately offset by the extra screening due to the increasing number of 3d electrons. Today, the valence bond model has largely been supplanted by the molecular orbital model. In this model, as atoms are brought together, the atomic orbitals interact so as to form a set of molecular orbitals, which extend over the entire molecule. Half of these orbitals tend to be bonding orbitals, while the other half are anti-bonding orbitals. Electrons in bonding orbitals result in the formation of a chemical bond, while those in anti-bonding orbitals prevent bonding. Electrons may also occupy non-bonding orbitals, which are neither bonding nor anti-bonding. The formation of a chemical bond is only possible when more electrons occupy bonding orbitals than anti-bonding orbitals.

Unfortunately, few data are available in the literature on the molar volume of silicate melts at temperatures in the glass transformation range. Across the results and the temperature range examined in this study, we cannot exclude that there is a possibility that the thermal expansivity is temperature dependent, particularly when extrapolating down to T_g. However, low temperature density data (i.e., above T_g) would be necessary to test for temperature dependency.

Based on the unpublished viscosity data, where crossovers have been observed between high temperature viscosity and viscosity measured above the glass transition temperature, I cannot rule out that changes in coordination number of ZnO occur over this wide temperature range. The possible evidence for two or more coordination states of zinc in silicate melts, whose proportions might vary as a function of temperature, pressure and composition, remains to be investigated.

Amongst other possible causes, such the detailed coordination number of each element, uncertainties of high temperature densitometry, error from chemical analyses, variable valence state we cannot rule out the possibility that there may be some nonideal volumetric behaviour for transition metal-bearing silicate melts as a possible explanation of why the partial molar volumes of the transition metals do not follow the sequence FeO - CoO - NiO - ZnO.

5. Temperature Independent Thermal Expansivities of Calcium Aluminosilicate Melts between 1150 and 1973 K in the System Anorthite-Wollastonite-Gehlenite (An-Wo-Geh): A density model

This chapter concentrates on the quantification of expansivities and molar volumes of supercooled silicate melts. The Webb et al. (1992) method was adopted to determine expansivity and volume of the calcium aluminosilicates just above the glass transition temperature. This study has focussed on this system because these oxides are present in all natural volcanic melts and glasses and the CAS system serves as a model for experimental petrology. Horizontal dilatometry has been used to determine the density and expansivity of glassy samples, which have the same thermal history (10 K min^{-1} cooling/heating rate). Archimedean-based densitometry on separate aliquots of the samples was used to determine sample density at room-temperature. The Lange and Carmichael (1987), Lange (1997) and Courtial and Dingwell (1995) models have been used to calculate the densities of the investigated samples at superliquidus temperatures. Combining all these methods allows us to cover a wide temperature range in order to predict the molar thermal expansivity of the investigated calcium aluminosilicates.

Previous investigations of the compositional dependence of melt properties in the $CaO-Al_2O_3-SiO_2$ (CAS) system have been focused primarily on the metaluminous join SiO_2-$CaAl_2O_4$ which is highly polymerised with a nominal number of non-bridging oxygen equal to zero. In addition, recent work by Solvang et al. (2004; 2005) and Toplis and Dingwell (2004) all concentrate on the "peralkaline" field. The calcium aluminosilicate melts are important for the glass fibre industry, especially the stone wool industry (they make up to 80% of both stone wool fibres and E-glass). Understanding the physico-chemical properties and thermodynamics of the calcium aluminosilicate is crucial for optimizing the production procedures as well as for predicting fiber quality, fiber drawing ability, bio-solubility, mechanical strength of fibers and other important parameters.

The density and expansivity of 10 calcium aluminosilicate melts included in the anorthite (An) - wollastonite (Wo) - gehlenite (Geh) ($CaAl_2Si_2O_8$-$CaSiO_3$-$Ca_2Al_2SiO_7$) compatibility triangle (Figure 5.1) have been investigated over a large temperature range. This

study focuses on the "peralkaline" field by studying the compositional dependence of melt properties along the lines with NBO/T=0.5 and 1. This allows us to study the effect of composition on the density and expansivity at a constant degree of polymerization and to explore the structural changes along and between the lines. So far the densities and expansivities of the melts with compositions in the An-Wo-Geh compatibility triangle have not been systematically studied.

5.1. Experimental methods

5.1.1. Sample preparation

Melts were synthesized from SiO_2 (Alfa Aesar, 99.9 % -Ign. loss < 0.3 %), $CaCO_3$ (Merck, 98.5 %), and Al_2O_3 (Merck, 99.9 %) mixes (Figure 5.1). The powders were dried at 393 K for at least 24 hours prior to weighing. They were ground, mixed and then fused in a platinum crucible for 3 hours in a $MoSi_2$ box furnace at 1898 K. The melts were poured from high temperature onto a stainless steel plate for cooling. A comparison between the weight of the samples before and after the melting serves as a check for the complete volatilization of CO_2 from $CaCO_3$ powder. The high temperature viscosity was measured on the samples from
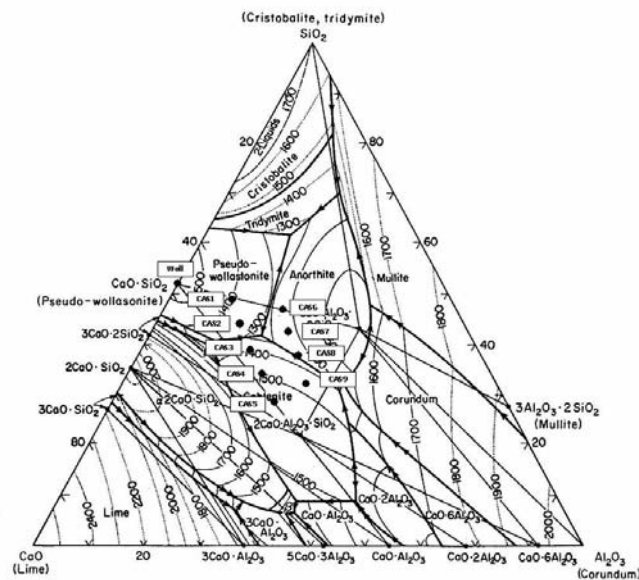
FIGIRE 5.1. Phase diagram of the $CaO-Al_2O_3-SiO_2$ (CAS) system (after Ehlers, 1972; Gentile and Foster, 1963; Osborn and Muan, 1960). The investigation deals with compositions in the anorthite-wollastonite-gehlenite (An-Wo-Ge) compatibility triangle. The compositions are in wt %. The line between CAS1 and CAS5 are the samples with NBO/T = 1 and the line between CAS6-CAS9 are the samples with NBO/T = 0.5.

1316 to 1849 K at ambient pressure (Solvang et al., 2004). Then cylindrical bubble free glassy samples, 6 mm in diameter were drilled out from the viscometer crucible. From these cylinders glass samples for differential scanning calorimetry (DSC), dilatometry and X-ray fluorescence spectroscopy measurements were prepared and stored in a desiccator until use (Solvang et al., 2004). The compositions determined by XRF (Philips 1404) are presented in Table 5.1. In addition, the composition of the samples that had been used in the calorimetry and dilatometry were measured by electron microprobe (CAMECA$^{®}$ SX 50). There were no significant differences between the composition obtained by XRF and electron microprobe analyses, both with no change from the nominal compositions (Table 5.1). During the various high-temperature stages of study (Solvang et al., 2004), the melts were kept in air, whereas during the low temperature experiments (i.e., DSC, dilatometry) the samples were held in a protective Ar atmosphere. There was no observable difference between the colour of the starting and the final products.

5.1.2. Low temperature dilatometric/calorimetric method

Both dilatometric and calorimetric measurements were conducted applying matching thermal cycles; i.e., the glasses heated at rates of 10 K/min were previously cooled at 10 K/min. The dilatometric measurements were performed using a Netzsch$^{®}$ DIL 402C dilatometer with a horizontal alumina-push rod on cylinders carefully drilled from the synthesized glassy block (see Chapter 2.4.6). T_g and the molar thermal expansion were found based on the results of the second run where both the cooling and heating rates were known. T_g was taken as the inflection point of the relative length change ($\partial L/L_0$) curve during the second run (Figure 5.2). The inflection point corresponds to the peak point of the linear thermal expansion
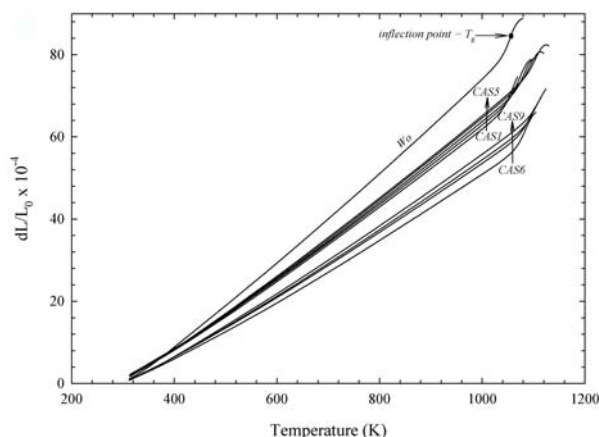
FIGURE 5.2. dL/L_0 curves of investigated samples obtained from scanning dilatometry.

coefficient alpha (α_{linear}) curve as well as to the peak point of the $\partial V/\partial T$ curve as shown in Figure 5.3a., 5.3b and 5.5. The specific heat capacities of the investigated samples were determined using a differential scanning calorimeter (STA Netzsch® 449C) using a procedure described by Chapter 2.4.5. in detail. Measured heat capacity of the glasses (in J g^{-1} K^{-1}) were fitted using a third order Maier - Kelley (1932) equation ($c_p=a+bT+cT^{-2}$) (Table 5.3) and were compared with existing model of Richet (1987). The calculated values are consistent with measured c_p values (within uncertainty of DSC). The calculated c_p of glasses are higher of about 1% (absolute) for all samples except the temperature interval slightly below (~300K) the onset temperature, where rapid increases of c_p trace can occur. The predicted c_p values are lower (~2-5%) than the measured c_p in that temperature range. An example of the predicted and measured c_p of the glass is shown on pseudo-wollastonite, CAS6 and CAS9 samples in (Figure 5.4). The horizontal line in Figure 5.4, at a value of 3R, is a theoretical upper limit to glassy heat capacity at constant volume (c_v), where R is the ideal gas constant. This line represents theoretical limit for a mole of isolated simple harmonic oscillators that have only vibrational degree of freedom (i..e., in the solid state). Silicate glasses have relatively small thermal expansivity, thus c_p and c_v differ by less then 1%, so this harmonic limit should also apply to c_p (i.e., heat capacities of the glasses).

Supercooled liquid density, molar volume and molar thermal expansivities were indirectly determined by combining differential scanning calorimetric and dilatometric measurements assuming that the kinetics of enthalpy and shear relaxation are equivalent. The applied Webb et al. (1992) method is described in Chapter 3.1.
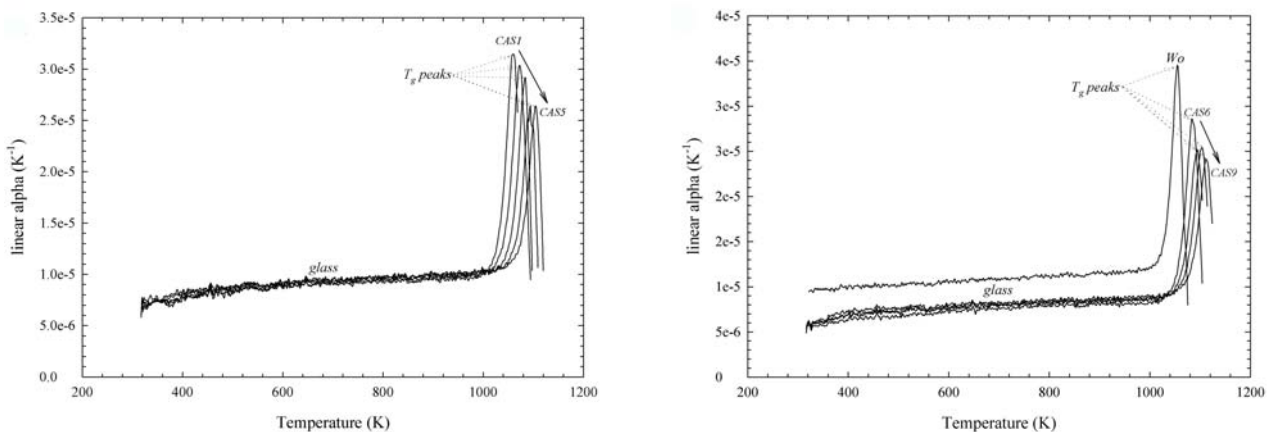
FIGURE 5.3. (a, b) Comparison of the variation of linear thermal expansion alpha coefficient curves as a function of temperature obtained using scanning dilatometry during the second run at a heating rate of 10 K min^{-1} for (**a**) samples with NBO/T = 1 (CAS1-CAS5) and (**b**) samples with NBO/T = 0.5 (CAS6-CAS9 and pseudo-wollastonite.
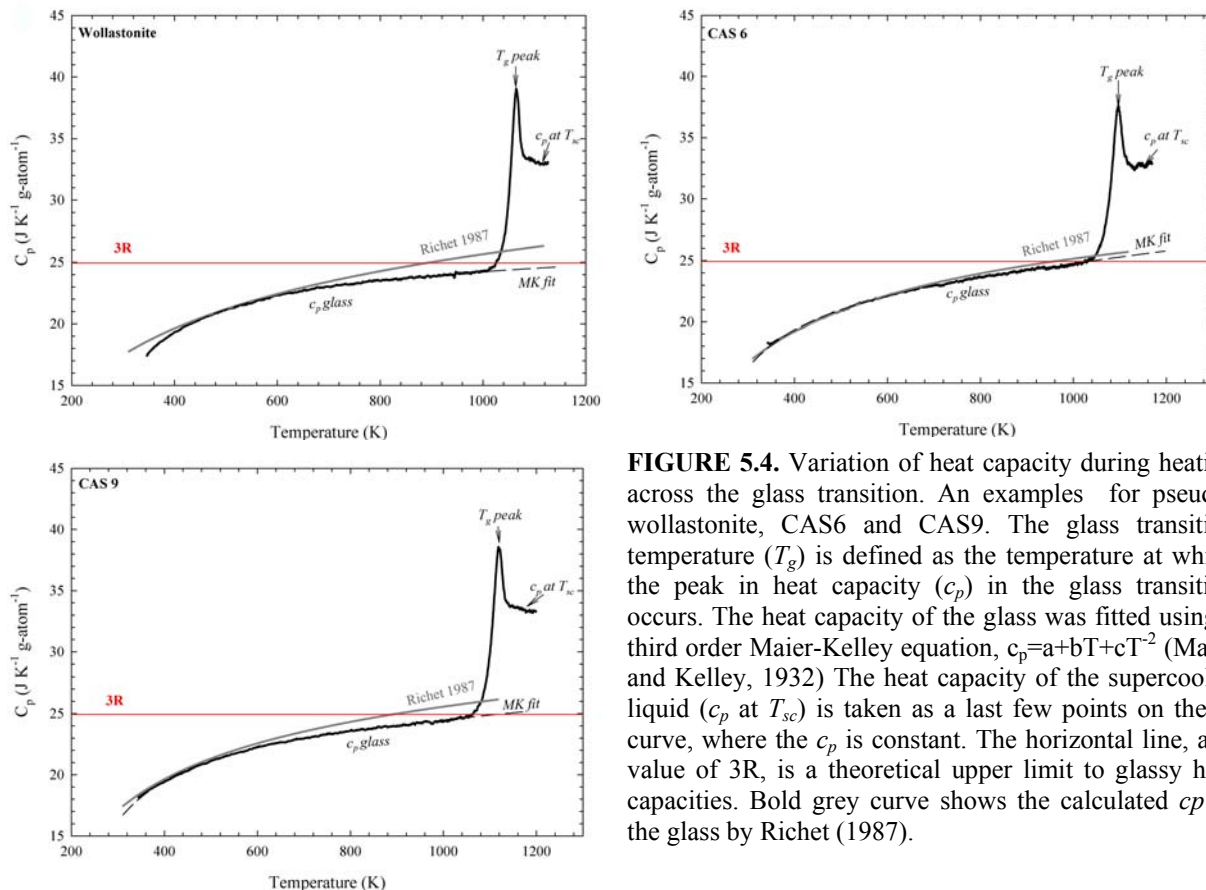
FIGURE 5.4. Variation of heat capacity during heating across the glass transition. An examples for pseudo-wollastonite, CAS6 and CAS9. The glass transition temperature (T_g) is defined as the temperature at which the peak in heat capacity (c_p) in the glass transition occurs. The heat capacity of the glass was fitted using a third order Maier-Kelley equation, $c_p=a+bT+cT^{-2}$ (Maier and Kelley, 1932) The heat capacity of the supercooled liquid (c_p at T_{sc}) is taken as a last few points on the c_p curve, where the c_p is constant. The horizontal line, at a value of 3R, is a theoretical upper limit to glassy heat capacities. Bold grey curve shows the calculated cp of the glass by Richet (1987).

5.1.3. Room temperature densitometry

The densities at T_{room} of the CAS glasses from this study were measured after the dilatometric measurements. As a results, all the samples had the same cooling history (10 K.min^{-1}). The room temperature densities of the glass samples were obtained by employing an Archimedean-based technique using a SARTORIUS® MC-210P microbalance with density determination kit. A detailed description of the room temperature densitometry was already given in Chapter 2.4.3.

5.1.4. Partial molar volumes

The compositional dependence of the liquid molar volume is, in general, expressed by:

$$V_{liquid}(T) = \sum X_i V_i(T) \tag{5.1}$$

where V_{liquid} is the measured liquid molar volume, X_i the mole fraction of oxide, i, and V_i the partial molar volume of the oxide, i. This equation is valid if the molar volume has a linear variation with temperature. Courtial and Dingwell (1995) demonstrate that the molar
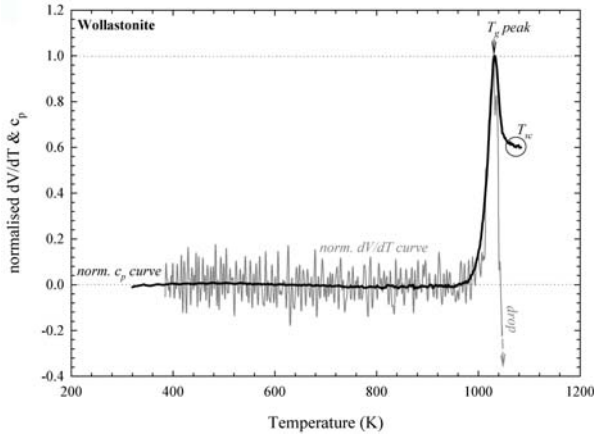
FIGURE 5.5. The method of normalization of calorimetric and dilatometric traces illustrated for the pseudo-wollastonite sample. T_g is the glass transition temperature and T_{sc} is the temperature of the supercooled liquid.

volume exhibits non-ideal behaviour in the CaO-Al$_2$O$_3$-SiO$_2$ system, implying at least one excess term. Equation 5.1 thus needs to be rewritten:

$$(5.2)$$

$$V_{liquid}(T) = \sum X_i V_i(T) + XS$$

where *XS* is the excess volume term corresponding to the possible interactions between SiO$_2$ and CaO, SiO$_2$ and Al$_2$O$_3$, CaO and Al$_2$O$_3$. An excess volume term between SiO$_2$ and CaO (*XS$_{SiO2\ CaO}$*) was identified and defined as:

$$(5.3)$$

$$XS_{SiO_2CaO} = X_{SiO_2} X_{CaO} V_{SiO_2CaO}$$

where X_{SiO_2} and X_{CaO} are the molar fraction of SiO$_2$ and CaO respectively, and V_{SiO_2CaO} is an excess term of these two oxides. Courtial and Dingwell, (1995) tested several regression equations on the dependence of the molar volume in the CaO-Al$_2$O$_3$-SiO$_2$ system on temperature. These included an ideal model and one with one, two and three binary excess terms. The authors recommended use of the following model, which includes an excess term between SiO$_2$ and CaO:

$$V_{liquid}(T) = \sum X_i \left[V_{i(1200)} + \left(\frac{\partial V_i}{\partial T}\right)(T-1200) \right] + X_{SiO_2} X_{CaO} \left[V_{SiO_2CaO(1200)} + \left(\frac{\partial V_{SiO_2CaO(1200)}}{\partial T}\right)(T-1200) \right]$$

$$(5.4)$$

The molar volumes of the liquids in this study were independently analysed using this equation.

The partial molar volume, molar thermal expansivity of each individual oxide and an excess term between SiO$_2$-CaO were obtained from two independent regressions following the model of Equation 16. The reference temperature (1200 K) was chosen with respect to the temperature range investigated in this study. The first regression was performed on the samples used in this study. The second regression covered all the samples used in this study, together with all the CAS samples from Courtial and Dingwell (1995) and those samples with compositions relevant to the CAS system from Lange and Carmichael (1987) (samples LC3-

LC8). All the samples used in the second regression contain only CaO, Al_2O_3 and SiO_2.

5.2. Results

5.2.1. Room temperature densitometry

The density at T_{room} of samples with NBO/ T = 1 (CAS1-CAS5) range from 2.8325 to 2.9062 g cm^{-3} and for samples with NBO/T = 0.5 (CAS6-CAS9) range from 2.7627 to 2.8395 g cm^{-3}. In addition, the density of pseudo-wollastonite at T_{room} was determined to be 2.9128 g cm^{-3}. Results from room temperature densitometry are presented in Table 5.2, showing that the density decreases greatly with increasing SiO_2 content for each of the NBO/T lines. The individual errors derived from those replicate measurements on each sample range from 0.08 to 0.19%, with the mean error being 0.12%.

5.2.2. Molar volume of glasses (low temperature densitometry)

The dilatometric technique allows the expansivity of the glassy samples to be measured up to the glass transition temperature.

Figure 5.2 shows the second run of the dilatometric measurements as $\partial L/L_0$ for the investigated sample. The linear thermal expansion coefficient curves for all samples were obtained from the data collected during the second run of dilatometric measurements and are shown in Figures 5.3a and 5.3b. The dilatometric and calorimetric glass transition temperatures, and the linear fit parameters a^{dila} and b^{dila}, which were obtained across the temperature interval ΔT, are reported in Table 5.4. Importantly both dilatometry and calorimetry give the same glass transition temperatures within experimental error ($\pm$ 3 K).

In addition, the variation of the molar volume of the glass may be approximated as a linear function of temperature, providing an average value of the molar thermal expansivity of the glass, $\overline{\partial V_{glass}/\partial T}$ (Table 5.5). The variable $\overline{\partial V_{glass}/\partial T}$ is equal to the regression parameter corresponding to the slope of the molar volume of the glass as a function of absolute temperature. The molar volume of the glass at T_{room} ($V_{glass}^{(298)}$) was calculated using Equation 2.11. In addition, the molar volume of the glass at the given temperature T ($V_{mol\_glass}^{(T)}$) up to onset of the glass transition area is described by Equation 2.14. The parameters α_0 and α_1 were obtained as the regression parameters of Equation 2.14 by fitting the molar volume of the investigated glasses as a function of absolute temperature. Values of $V_{glass}^{(298)}$, $\overline{\partial V_{glass}/\partial T}$, α_0 and α_1 are listed in Table 5.5 for all the glasses.

The molar volume at T_{room} of samples with NBO/ T = 1 (CAS1-CAS5) range from 21.833 to 22.347 cm^3 mol^{-1} and for samples with NBO/T = 0.5 (CAS6-CAS9) range from 23.532 to 23.881 cm^3 mol^{-1} (Table 5.5). A systematic increase in molar thermal expansivity with decreasing SiO$_2$ content was observed for all samples irrespective of their NBO/T. Molar thermal expansivity range from 5.268 x 10^{-4} to 6.346 x 10^{-4} cm^3 mol^{-1} K^{-1} for all CAS samples (Table 5.5). Additionally, pseudo-wollastonite, which does not contain Al$_2$O$_3$ in the structure, has the lowest molar volume at T_{room} (19.953 cm^3 mol^{-1}) but the highest molar thermal expansivity (6.472 x 10^{-4} cm^3 mol^{-1} K^{-1}), relative to the other investigated compositions.

5.2.3. Molar volume of liquids

The molar volume of the fully relaxed supercooled liquid just above the glass transition range was obtained for all investigated samples. The results derived from the normalization procedure of Webb et al. (1992) are reported in Table 5.6 for the T_{sc} temperature slightly higher (65 - 80 K) than T_g. A systematic increase in T_g with decreasing SiO$_2$ content is observed for both NBO/T-sets of samples. The molar volumes of the samples with the NBO/T = 1 at T_{sc} range from 22.485 cm^3 mol^{-1} to 23.010 cm^3 mol^{-1} for CAS1 and CAS5, respectively. The same trend of systematic increase in T_g with decreasing SiO$_2$ was also observed for samples with NBO/T = 0.5, with their molar volume ranging from 24.12 cm^3 mol^{-1} to 24.50 cm^3 mol^{-1} for CAS6 and CAS9, respectively. In addition, pseudo-wollastonite has the lowest molar volume at T_{sc}. The molar thermal expansivities of the samples with NBO/T =1 are identical to within error. They have an average value of 17.30 cm^3 mol^{-1} K^{-1}. The samples with NBO/T =0.5 have a slightly lower average value of 14.20 cm^3 mol^{-1} K^{-1}. In contrast, the molar thermal expansivity of pseudo-wollastonite is higher (20.62 cm^3 mol^{-1} K^{-1}). The molar thermal expansion coefficients ($\alpha_{mol}^{(Tsc)}$) of all the samples with NBO/T=1 are roughly the same (within 0.32%) at T_{sc}, with an average of 75.954 K^{-1}. The $\alpha_{mol}^{(Tsc)}$ for samples with NBO/T=0.5, similarly do not vary greatly, but are slightly smaller, with an average of 58.436 K^{-1}. The individual errors of the V_{mol}^{Tsc} and $\alpha_{mol}^{(Tsc)}$ determinations range from 0.04 to 0.05% and from 0.79 to 4.44%, respectively for all samples used in this study, with mean errors of 0.04 and 2.9%, respectively.

The high temperature (HT) molar volume of the investigated samples were calculated using the Lange and Carmichael (1987), Lange (1997), Courtial and Dingwell (1995) and Toplis and Richet (2000) models across the valid temperature range. The low- and high-temperature datasets were combined in order to determine the molar volumes of the samples

over a very large temperature range (i.e., from the supercooled liquid up to the superliquidus liquid). The combination of the measured molar volumes at T_{sc} and the calculated molar volumes at superliquidus liquids is shown in Figure 5.6. Linear predictions of the molar volumes at T_{sc} have been provided for all presented liquids using these three models. The molar volume predicted by the Courtial and Dingwell (1995) model at T_{sc} are in excellent agreement with the data derived for all samples from combining dilatometry and calorimetry. The molar volumes can be expressed empirically using a linear equation ($V_{mol\_liq} = a + bT(K)$) within the temperature interval ΔT. The fit parameters a and b, together with ΔT are listed in Table 5.7.
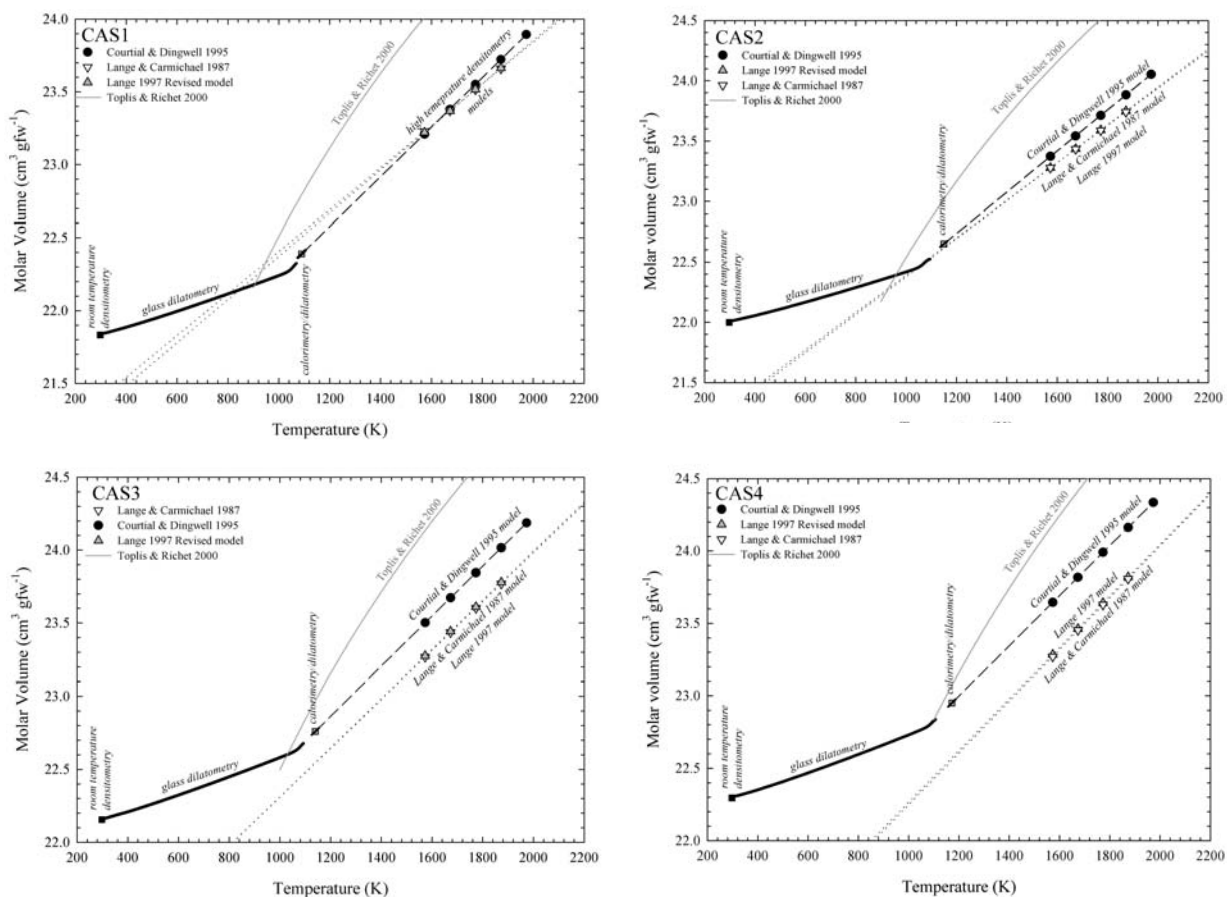
FIGURE 5.6. Molar volume as a function of temperature for all investigated samples over the wide temperature range.
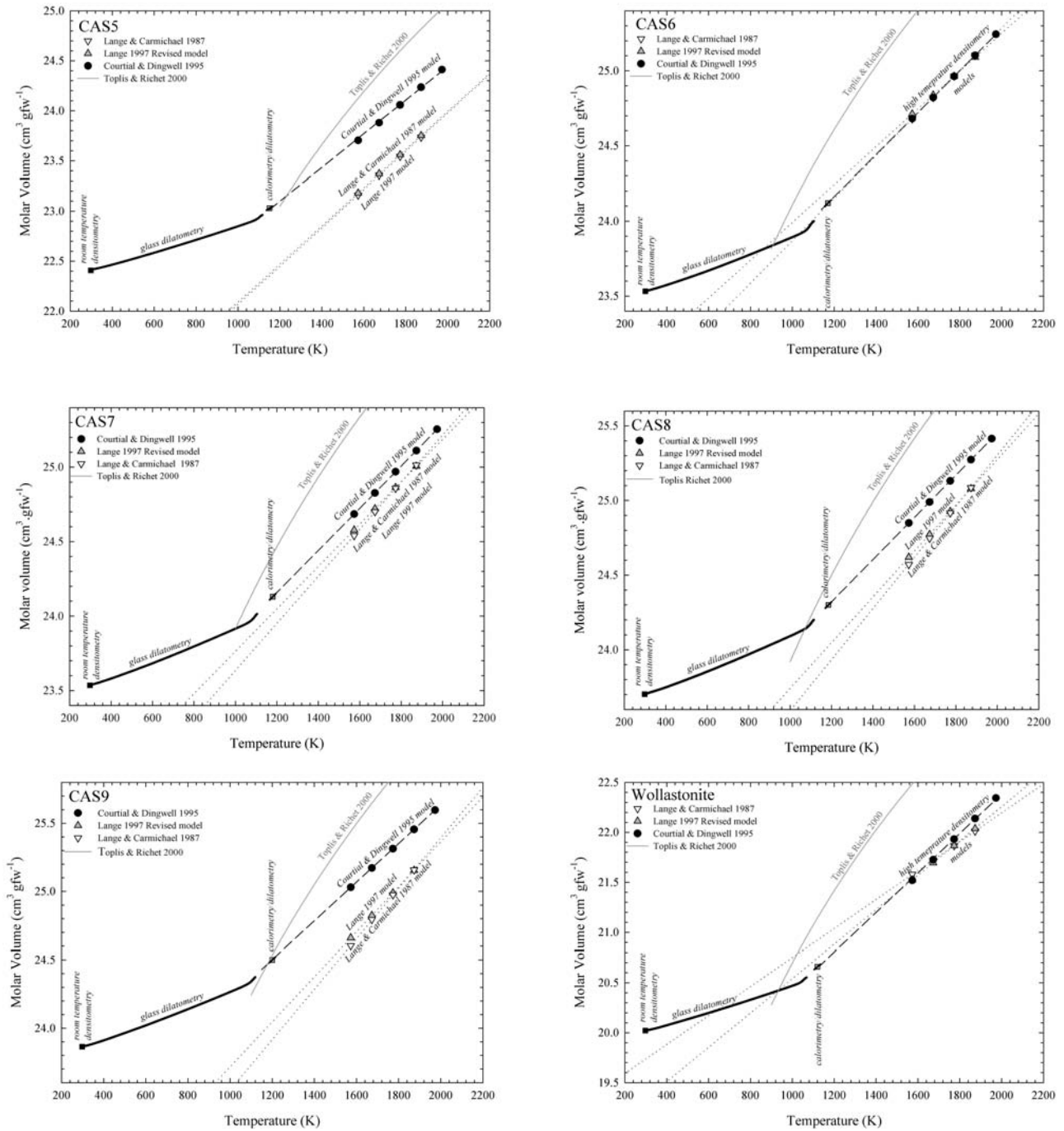
FIGURE 5.6. (continued)

The Courtial and Dingwell (1995) model is based on ten measurements of liquids which cover almost the entire CAS compositional range. The accessible range was controlled by the temperature of the liquidus surface and by the area of immiscibility. Their four liquid measurements are within the An-Wo-Geh system and the other three lie just outside of the

system. In practice, partial molar properties are difficult to determine, especially in systems containing many components. The other models (i.e., Lange and Carmichael, 1987 and Lange, 1997) underestimate the molar volumes at T_{sc}. This results in these models overestimating the densities at T_{sc}. Only for the three compositions CAS2, CAS6 and pseudo-wollastonite does the Lange (1997) model predict the molar volume at T_{sc} to within the uncertainty of the measurements. The Toplis and Richet (2000) model is based on two liquids (i.e., anorthite and diopside) where the authors have enough volumetric data to describe them as a linear function of the logarithm of absolute temperature. The authors make the assumption that, to a first approximation, this form of temperature dependence is valid for a volumes of all liquids in the system K_2O-Na_2O-CaO-MgO-Al_2O_3-SiO_2. This model does not take into account compositional and temperature dependency of T_f . The molar volumes of samples were calculated using the Toplis and Richet (2000) model (Figure 5.6). This model overestimates the molar volumes of An-Wo-Geh melts at superliquidus temperatures. Only for the two compositions CAS4, CAS9 does the Toplis and Richet (2000) model predict the molar volume at T_{sc} or T_f within the uncertainty of the measurements. The individual errors of the molar volume predictions at T_{sc} range from 0.04 to 2.44% and from 0.03 to 2.59%, for the Lange and Carmichael (1987) model and for the Lange (1997) model, respectively.

5.2.4. Partial molar volumes and molar thermal expansivities

The partial molar volume (V_i) and molar thermal expansivity ($\partial V_i / \partial T$) of each individual oxide were calculated using Equation 5.4. The results of two regressions following the model of Equation 5.4 are reported in Table 5.8. Both these regressions were performed as a function of composition and temperature on all liquids over the temperature range from 1200 to 1873 K. The difference between the molar volumes of the samples calculated using the parameters listed in Table 5.7 and these calculated using the parameters in Table 5.8 is less than 0.05% for temperatures ranging from 1200 to 1873 K. The uncertainties and the quality of these regressions are indicated by the standard error of each fit coefficient (in parentheses in Table 5.8). The relative standard error of the regression, when compared with the experimental uncertainties, indicates whether the regression can adequately reproduce the data within the best estimate of experimental uncertainties.

The V_i and $\partial V_i / \partial T$ calculated using these regressions are directly compared with V_i and $\partial V_i / \partial T$ obtained by Lange and Carmichael (1987), Lange (1997) and Courtial and Dingwell (1995) at the reference temperature (T_{ref}) of 1873 K in Table 5.9. Fitted partial molar volumes and thermal expansivities at $T_{ref.}$ are listed in Table 5.9. The molar thermal expansivities of

SiO_2 and Al_2O_3 are equal to zero in both provided regressions. This is in agreement with results given by Lange 1997 model but in contrast to the results of the Lange and Carmichael (1987) and Courtial and Dingwell (1995) models. The obtained partial molar volumes of CaO are in good agreement with results of the Courtial and Dingwell (1995) model, but higher from the Lange and Carmichael (1987) and Lange (1997) models. In addition, the molar thermal expansivities of CaO obtained in both regressions are the lowest, in comparison with the other models. An excess volume term between SiO_2 and CaO can only be compared with the Courtial and Dingwell (1995) model (see Table 5.9).

5.3. Discussion

The rheological and thermodynamic properties of aluminosilicate melts are determined by the arrangement of the tetrahedral structural units in the melt, which relates to the chemical bonding situation within a structural unit and between units. Aluminum differs from silicon, since tetrahedrally coordinated aluminium is charge-balanced by either one alkali cation or half of earth alkaline cation. The charge-balancing cations for the Al^{+3} tetrahedra play a large role in the melt structure. The structural role of the alkali or earth alkaline cations commonly depends on the Al^{+3} content of the melt (Richet et al., 1993). The short range ordering in the aluminosilicate network depends on the composition and the charge-balancing or network modifying cations. For aluminosilicates it is assumed that an energetically favourably case is a random occurrence of the network forming linkages Si–O–Si, Si–O–Al and Al–O–Al. Loewenstein (1954) introduced the principle of Al-avoidance based upon consideration of mineral structures. It was postulated that the Al-O-Al linkages are energetically unfavourable. This means that the short range ordering is not random (e.g., not totally disordered). A tendency towards Al-avoidance would also appear to be the case for silicate liquids as may be inferred from thermochemical investigations (Roy and Navrotsky, 1984), NMR spectroscopy (Murdoch et al., 1985; Lee and Stebbins, 1999a; 1999b) and variations of configurational entropy (Toplis et al.,1997). However, the presence of a small amount of Si–O–Si in glasses of anorthite compositions observed by triple quantum MAS NMR spectroscopy (Stebbins and Xu, 1997) suggests some Al–O–Al linkages (Lee and Stebbins, 1999a; 1999b).

The investigated melts are all characterised by an excess of Ca^{2+} over the ions that act as charge-balancing for Al^{3+}. The excess of Ca^{2+} acts as a network modifier (Mysen, 1988; Sato et al., 1991; Stebbins and Xu, 1997; Cormier et al., 2000). Toplis and Dingwell (2004) discuss in detail the validity of the idea that all aluminium is associated with charge-balancing cation in peraluminous melts $(M^{n+}/nAl) \geq 1$. However, although Toplis and Dingwell (2004) infer

that aluminosilicate melts may contain a larger number of NBO than that predicted assuming that all Al is charge balanced (resulting in erroneous values of NBO/T). They also show that for calcium aluminosilicates this is only a major concern close to the metaluminous join where nominal NBO/T is close to zero. For the relatively depolymerised liquids considered here we have therefore calculated NBO/T using the standard calculation procedure of Mysen (1988). The deviation of NBO/T from nominal values is a complex function of the liquid composition, in particular the nature of the monovalent and divalent cations.

Solvang et al. (2004) documented a difference between the structural arrangement along the NBO/T lines = 0.5 and 1 for the identical composition as discussed in this study. The difference in structural arrangement can explain the crossover reported between the low (just above T_g) and the high viscosity data along the NBO/T = 0.5 and 1 lines. The charge-balancing cation (Ca^{2+}) have a tendency to attract the neighbouring tetrahedra of the network former, namely at the low temperature range, where the viscosity range from 10^8 to 10^{12} Pa s. Poggemann et al. (2003) confirmed that Ca^{2+} ions contract the channels in the glass network. Hence, the structural network become stronger with increasing substitution of Al^{3+} + $1/2Ca^{2+}$ for Si^{4+}. The apparent linear dependency of the T_{room} density, molar volume of glasses (V_{glass}^{298}) and molar volume at T_{sc} ($V_{mol}^{T_{sc}}$) and T_g with increasing substitution of Al^{3+} + $1/2Ca^{2+}$ for Si^{4+} for both NBO/T lines is a direct consequence of this structural arrangement at the low temperature range. An increase in the molar volume at both T_{room} and T_{sc} as a function of the increased substitution of Al^{3+} + $1/2Ca^{2+}$ for Si^{4+} reflects that the structural units besides becoming stronger also favour larger clusters and hence the volume of the structural units become larger (Figures 5.7a and 5.7b).

A linear temperature dependence of the molar volume between T_{sc} and the superliquidus temperature at 1 atmosphere was found for each melt. The slight increase in molar volume at T_{sc} with increasing substitution of Al^{3+} + $1/2Ca^{2+}$ for Si^{4+} for the NBO/T = 0.5 and 1 lines, reflects increasing size of the structural units with increasing substitution, due to the role of Ca^{2+}. However, both the molar thermal expansivity and the molar thermal expansion coefficient alpha at T_{sc} are independent of the substitution. Both parameters (molar thermal expansivity and the molar thermal expansion coefficient at T_{sc}) decrease with decreasing NBO/T along the Wo-An binary join. This is a response to the change in degree of polymerisation. From Wo towards CAS6 the amount of network modifying cations decreases, and hence the liquid molar volume increases. The formation of Al-O-Si linkages in the melt decreases the amount of NBO, since the Si-NBO sites bonds are replaced by the cross-linked Al-O-Si bonds (Mysen, 1988). The most depolymerised melt (in this case Wo) has the highest

molar thermal expansivity and molar thermal expansion coefficient at T_{sc}, because the NBO sites are the weakest in the silicate network (Stebbins and Xu, 1997). With increasing polymerization the Al-O-Si bonds tend to strengthen the structure and the molar thermal expansivity decreases. The change from a temperature independent thermal expansivity for wollastonite to a temperature dependent thermal expansivity for diopside (Knoche et al. 1992), despite similarity in degree of polymerisation and silica content, seems to relate to Mg content. A confirmation of such theory requires further investigation.

I would like to emphasise, that the calculation of the molar volume in a binary, ternary or multicomponent system over a wide temperature range must be treated with caution. Furthermore, it should be appreciated that the thermal expansivity is a complex function of the composition of the liquid, in particular the nature of the cation valence. The measurements in this study have been performed at a pressure of one atmosphere. Several changes occur in the structure of silicate melts at higher pressure. For example, high coordination number of Al or hybrid structure in amorphous silicates are known to be favoured at higher pressure. These complications can cause non-ideal behaviour in the physical properties of silicate melts. As a results further spectroscopic studies, particularly at high temperature and pressure are essential. There is also lack of precise densitometry data provided on silicates with high viscosity and high melting point. This problem can be solved using a high temperature densitometry where the volume is measured on a levitated sample. Such measurements combined with in-situ spectroscopic measurements remain a challenge.
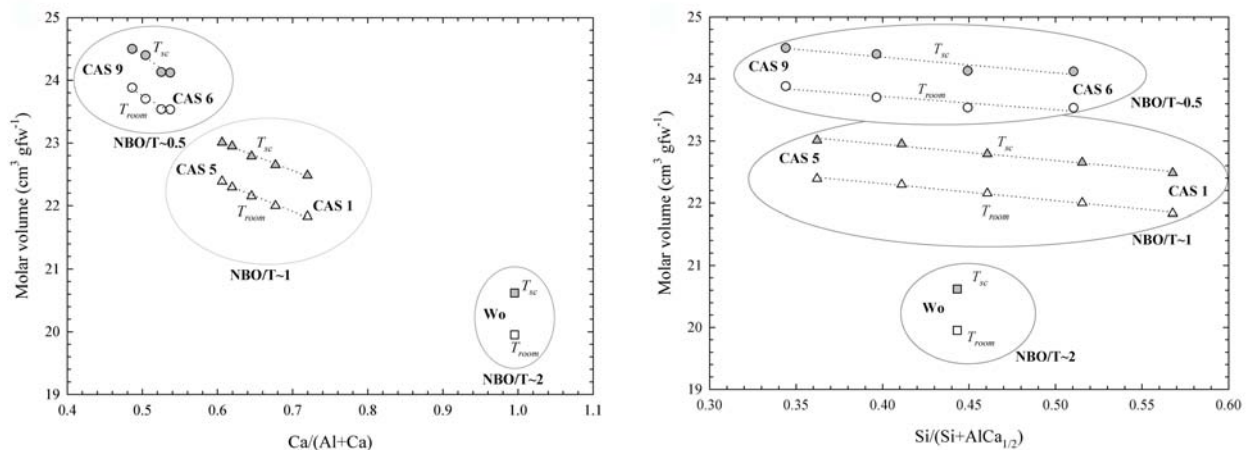
FIGURES 5.7 (a, b). Molar volume as a function of (**a**) Ca/(Al+Ca) ratio and (**b**) Si/(Si+AlCa$_{1/2}$) ratio for all investigated samples. A linear dependence is shown for each NBO/T line at supercooled liquid (T_{sc}) and room (T_{room}) temperature.

6. Temperature Dependent Thermal Expansivities of Multicomponent Natural Melts Between 993 and 1803 K

A high temperature densitometry and combined dilatometric/calorimetric methods were provided on three multicomponent natural lavas. The sample compositions investigated here represent natural lavas from Vesuvius 1631 eruption, Etna 1992 eruption and an Oligocene-Miocene lava flow from Slapany in the Bohemian massif. The combination of the results from high- and low-temperature measurements cover a large temperature interval (298-1803 K) where the thermal expansivities of the investigated natural glasses and melts were obtained. High temperature densities were measured using Pt double bob Archimedean densitometry. across the super-liquidus temperature interval. The density values of the glassy samples were derived from dilatometic measurements of each sample after cooling at 5 K min^{-1} at 298 K, followed by measurements of the glass thermal expansion coefficient from 298 K to the samples´ respective glass transition interval. Supercooled liquid volumes and thermal molar expansivities were determined by combining scanning calorimetric and dilatometric measurements, assuming that the kinetics of enthalpy and shear relaxation are equivalent (Webb, 1992). The resulting data for volumes near glass transition temperature (993 - 1010 K) and at super-liquidus temperature (1512 - 1803 K) are combined to yield temperature dependent thermal expansivities over the entire supercooled and stable liquid range.

6.1. Introduction

Information on the density and thermal expansivity of silicate liquids is a fundamental prerequisite in order to derive the buoyancy forces associated with melt transport in magmatic processes. Thus, accurate data on the thermal expansivity of magmatic melts should play an important role in the construction of PVT equations of state. Expansivity data are also required as thermodynamic input for the calculation of physical properties, such as melt compressibilities from fusion curves of minerals (Bottinga, 1985; Herzberg, 1987). Such data are also necessary for the reduction of adiabatic wave velocity data to isothermal conditions (Rivers and Carmichael, 1987). The uncertainties associated with the thermal expansion of silicate liquids have been emphasized in numerous studies (e.g., Bouhifd et al., 2001; Bottinga, 1985; Herzberg, 1987; Lange and Carmichael, 1987; Lange, 1997; Gottsmann and

Dingwell, 2000; Gottsmann and Dingwell, 2002; Gottsmann et al., 1999; Knoche et al., 1994; Knoche et al., 1992a; Lange, 1996; Lange, 1997; Liu and Lange, 2001; Tangeman and Lange, 2001; Toplis and Richet, 2000; Webb, 1992).

Simple dilatometric measurements of glassy expansivity can be performed directly on a free standing cylindrical glass sample. However, the viscous deformation obstructs the direct measurement of relaxed supercooled liquid thermal expansivity. In order to use dilatometric data to predict the supercooled liquid expansivities of silicate melts the Web et al. (1992) method for removing this deformation from the dilatometric trace, was used.

6.2. Experimental methods
6.2.1. Sample preparation

The samples investigated in this study are natural volcanic melts and glasses with high polymerized structure and relatively low activation energies above the superliquidus temperature (i.e., fragile melts). These samples have been chosen by virtue of their low viscosity values at superliquidus temperature ($<10^{2.5}$ Pa s), which allow the buoyancy-based high temperature densitometry to be applied.

- Slapany (basalt/basanite), collected from the Slapany deposit situated near Cheb in the western part of the Bohemian massif (Czech Republic). The Slapany deposit was formed by simple the effusion of basalt magma. It is from the first Oligocene-Miocene neovolcanic phase of the Czech massif (Pacltova and Žert, 1958) and serves as the source for cast basalt.

- Etna (trachybasalt), sample from lava flow of the 1992 eruption of Etna, Sicily, Italy.

- Vesuvius (tephriphonolite), white total rock. A sample from Vesuvius-Italy, which is representative of the 1631 plinian eruption.

Firstly, the natural samples were ground in an agate mortar. The resulting powders were melted and equilibrated in air at a temperature of 1873 K in a $MoSi_2$ box furnace for 24 hours. The melts were then quenched on a stainless steel plate and broken into chips. These were then melted stepwise in a $Pt_{80}Rh_{20}$ rigid cylindrical crucible (5 cm height; 2.5 cm inner diameter and 2 mm wall thickness) for a second time in order to obtain a homogenous sample. This $Pt_{80}Rh_{20}$ crucible was used several times before to melt iron bearing samples which contained approximately the same amount of iron as the samples investigated here. The propensity of iron to be lost to the crucible wall has been reduced by using this crucible.

6.2.2. High temperature densitometry

The high temperature melt densities were determined using the double-bob Archimedean technique. The apparatus used is based on the concept of Bockris et al. (1956). The technique and calculation of the densities used here has been outlined previously in Chapter 2.4.4. The densities were determined in total six individual runs of decreasing temperature steps. The samples was held at each measurement temperature for an one hour to achieve an equilibrium of the melt with the atmosphere inside the furnace. After this isothermal hold the buoyancy measurement follow which take usualy over 15 min at the given temperature. At the end of each isothermal hold, the liquid was sampled by inserting an alumina rod into the melt and withdrawing approximately 150 mg. This sample was then quenched in water. These glasses were than used to determine the oxidation state of iron, using the wet chemistry method (Wilson, 1960; Grillot et al., 1964), and to measure the chemical composition, using electron microprobe. At the end of the last cycle the crucible containing the sample was removed from the furnace and quenched in water. As a final product, a cylinder of glass 6mm in diameter was drilled from the Pt crucible. Parts of this cylinder were then used for calorimetric and dilatometric measurements. The authors would like to stress, that these cylinders, taken at the last point of the high temperature densitometry,
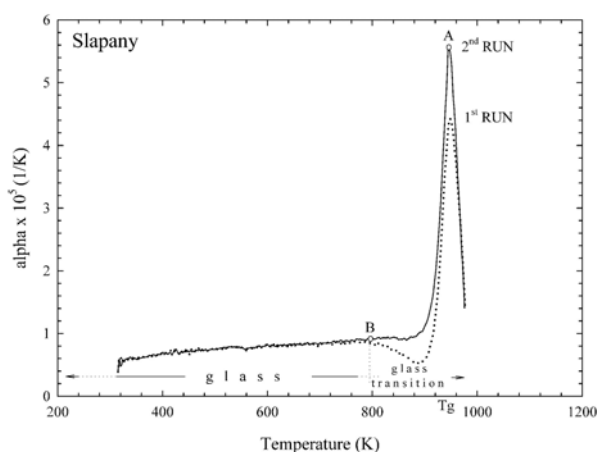
FIGURE 6.1. Comparison of two alpha dilatometric heating (5 K.min^{-1}) curves for Slapany sample. Alpha is defined as $\alpha = 1/L \, (\partial L/\partial T)$, where L is the length of sample at temperature T, and $\partial L/\partial T$ is an incremental change in length over a given small temperature interval (in this case 0.2 K). The initial drop in the 1st run curve (dotted line) followed by a rapid increase in alpha values is common for samples which have been rapidly cooled (X00 K.min^{-1}) from fully relaxed liquid state through the glass transition area to the un-relaxed glassy state. This drop appears in the next heating curve if the heating rate is about two orders of magnitude smaller than the previous rapid cooling rate. This point (**B**) can be defined as the point at which the glass transition is entered. The solid curve represents the 2nd experimental run on the sample carrying the thermal information frozen within its structure. This information has been saved into sample structure during the 1st cooling which started from the temperature where the structure was fully relaxed. Solid curve does not exhibit the drop at the beginning of the glass transition area because the previous cooling rate (5 K min^{-1}) is equal to heating rate (5 K min^{-1}) at which the measurement was performed. (**A**) is a peak point in the alpha curve where the maximum is reached. The temperature at this point is used to define the glass transition temperature (Tg) in this study. This peak point (Tg temperature) is easier to detect and directly corresponds to the temperature of the peak point of the specific heat capacity curve (c_p) or thermal expansivity curve ($\partial V/\partial T$), for any given sample with identical thermal history.

82

have isochemical compositions, which were determined by microprobe and wet chemistry analyses

6.2.3. Calorimetry

The specific heat capacities of the investigated samples were measured using a differential scanning calorimeter (DSC Netzsch® 404C). The detailed measurement procedure of the heat capacity is described in Chapter 4.4.5. Here, I just state that two heat capacity measurements were performed for each composition at 5 K min⁻¹ heating rate. The sample was heated to a temperature approximately 50 K above the glass transition temperature (*Tg*) and then cooled at 5 K min⁻¹. The *Tg* given was obtained during the second run (where both cooling and heating rates were known) and was defined as the peak of the specific heat capacity curve.

6.2.4. Dilatometry

The dilatometer used during this work was a Netzsch® DIL 402C dilatometer with alumina-push rod in horizontal geometry. The sample assembly was supported on a alumina base connected to a measuring head. For each composition two heating cycles were performed on the same sample. The first measurement of length change ($\partial L/L$) of the glass cylinders with temperature was measured with an heating rate of 5 K min⁻¹ on the samples of unknown thermal history (previous cooling rate) from room-temperature up to their respective glass transition temperature. The measurement was provided to temperatures approximately 40 K above T_g, which corresponds to the dilatometric softening point. The second measurement of length change ($\partial L/L$) of the glass cylinders follows after the first one (Figure 6.2).
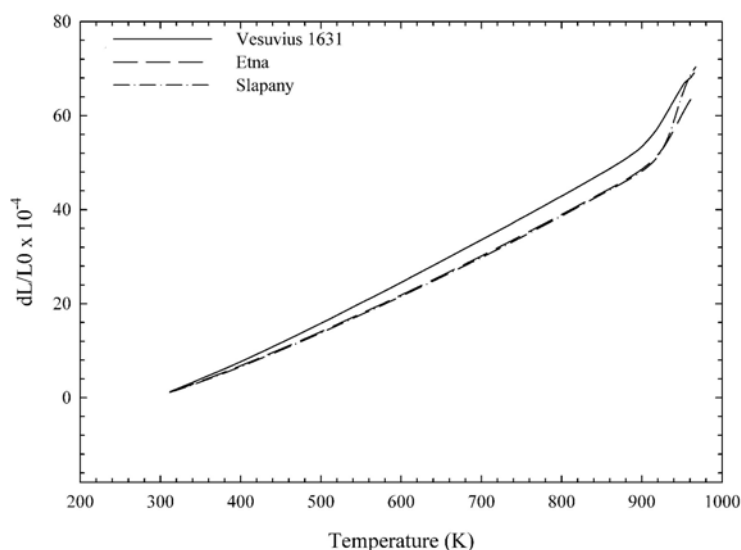
FIGURE 6.2. dL/L_0 curves of investigated samples obtained from scanning dilatometry.

The glass cylinders has then a known thermal history (5 K min^{-1}) and was heated by 5 K min^{-1} from room-temperature up to their respective glass transition temperature. All the measured ($\partial L/L$) lie within the uncertainties of the measurements so that we will only refer to the data of the glasses which were heated and cooled 5 K min^{-1} in the rest of this paper. A linear fit of their length change has been carried out as a function of temperature until the occurrence of the onset of the glass transition. As the glass approaches the glass transition, the slope of the length change vs. temperature changes, as the structure of the glass relaxes upon its approach to the glass transition. The molar volume of the glass at room temperature, linear thermal expansion coefficient and empirical parameters α_1 and α_0 were calculated using Equations 2.11, 2.13 and 2.14, described in Chapter 4.4.6, respectively. The thermal expansivity at supercooled liquids for all natural samples studied here were derived by combining dilatometric/calorimetric method (Webb et al., 1992) described in Chapter 3.1. An example of the normalization procedure of dilatometric and calorimetric traces obtained for Etna samples is shown in Figure 6.3.
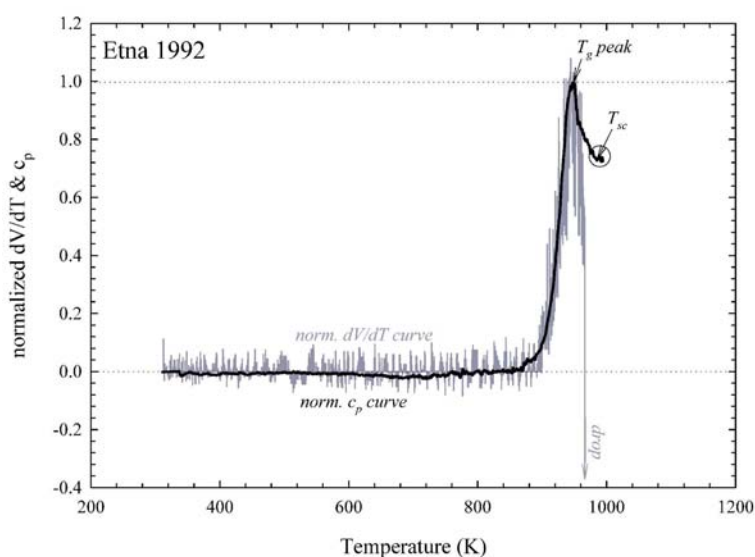
FIGURE 6.3. The method of normalization of calorimetric and dilatometric traces illustrated for Etna sample.

6.2.5. Room temperature densitometry

The room temperature density measurements were performed on the samples after the second run of dilatometry. All the samples have the same thermal history (5 K min^{-1} cooling/heating rate). Each sample weight was measured in air and then subsequently in

ethanol. Densities of glass samples (ρ_{glass}) were calculated using the relationship 2.5 described in Chapter 2.4.3.

6.3. Results

6.3.1. Sample composition and Fe oxidation state

The bulk composition of samples was determined by electron microprobe CAMECA® SX 50. Microprobe analyses are listed in Table 6.1. No change in bulk composition was observed at the beginning of each cycle of HT density experiment. However, as the temperature changed during HT-densitometry experiments in 50 K steps, the fO_2 inside of the furnace changed as well.

Potassium dichromate ($K_2Cr_2O_7$) titration has been applied to analyze iron, which is presented as Fe(II) in the withdrawn melts. As a standard has been used BHVO-1 standard from US Geological Survey, which is Hawaiian lava of known FeO concentration - 8.58 wt%. The dependence of ferric/ferrous ratio on temperature has been determined for all investigated samples. The parameters and the correlation coefficient derived from these linear fits are reported for each composition in Table 6.2. The knowledge of the sample composition at the given temperature is crucial for the calculation of the molar volume by using existing models (i.e., Lange and Carmichael, 1987, Lange, 1997).

In addition, the possibility of crystallisation in the glassy samples has been evaluated in the samples obtained prior to, and after, calorimetry and dilatometry measurements. Peaks were not apparent within the spectra obtained using the DRON 2 X-ray diffractometer with Bragg Bertrand focusing and a Cu-K α as X-ray source with Ni filter. The measurements were performed in the range of 3 to 60º of the diffraction angle 2θ within step regime of 0.05 º and a measurement time of 3 sec at each step. The spectrum was interpreted using the program ZDS with data base PDF-2. Crystals have not been observed in any of the analyzed glasses.

6.3.2. Room temperature densitometry

The density at room-temperature of basalt/basanite, trachybasalt and tephriphonolite glasses, which had all experienced the same cooling history (5 K min^{-1}), were 2.873±0.003, 2.768±0.003 and 2.621±0.002 g cm^{-3} respectively (Table 6.3). This shows that the density decreases greatly with increasing SiO_2 content. Replicate measurements give individual errors ranging from 0.06 to 0.09% with a mean error of about 0.07%.

6.3.3. Low temperature calorimetry and dilatometry

Heat capacity of the glasses were fitted using the Maier and Kelley (1932) equation (i.e., $Cp=a+bT+cT^{-2}+dT^{0.5}+eT^{2}$) where the first three parameters have been only used (i.e., *a*, *b* and *c*). These parameters are listed in Table 6.4. The fit parameters of the relative length change ($\partial L/L)$ as a function of temperature, together with the correlation coefficient (*R*), are listed in Table 6.5. The glass transition temperatures obtained from dilatometric and calorimetric measurements is reported in Table 6.5. Importantly both methods give the same glass transition temperatures within the errors involved (± 2 K).

The molar volume of the glass at the room temperature ($V_{mol\_glass}^{(298)}$) together with α_0 and α_1 is listed in Table 6.6 for all glasses. α_0 and α_1 have been obtained by fitting the dilatometric data with Equation 2.14 across the temperature interval, ΔT, reported in Table 6.6. In addition $\alpha_{Vmol}^{(T)}$ can also be determined by multiplying by three the term *1/L($\partial L/\partial T$)* or by multiplying by three the term α_{linear} measured by dilatometry or calculated from Equation 2.7 since glasses are isotropic materials. The linear relationship between the molar volume of the glass and absolute temperature provides an approximation of the thermal molar expansivity of the glass ($\partial V_{glass}/\partial T$). $\partial V_{glass}/\partial T$ is equal to the regression parameter which corresponds to the slope of the line. The dilatometry derived values of the glassy molar volume provide the molar expansivites, which are $5.39\pm0.57\times10^{-4}$ cm^3 mol^{-1} K^{-1} for basalt/basanite, $5.83\pm0.50\times10^{-4}$ cm^3 mol^{-1} K^{-1} for trachybasalt, and $6.90\pm0.53\times10^{-4}$ cm^3 mol^{-1} K^{-1} for tephriphonolite.

6.3.4. Molar volumes of liquids

High-temperature density measurements on natural melts are listed in Table 6.3 and are plotted as function of temperature in Figure 6.4a. Molar volume of the liquids have been calculated using Equation 2.11. Within the uncertainties, the experimental density, molar volume and specific volume data are linear as a function of temperature (Figures 6.4a - 6.4c). The parameters and the correlation coefficient derived from these linear fits are reported for each composition in Table 6.7. Across the temperature interval investigated, the densities range from 2.655±0.002 to 2.708±0.012 g cm^{-3} for basalt/basanite, from 2.578±0.003 to 2.601±0.002 g cm^{-3} for
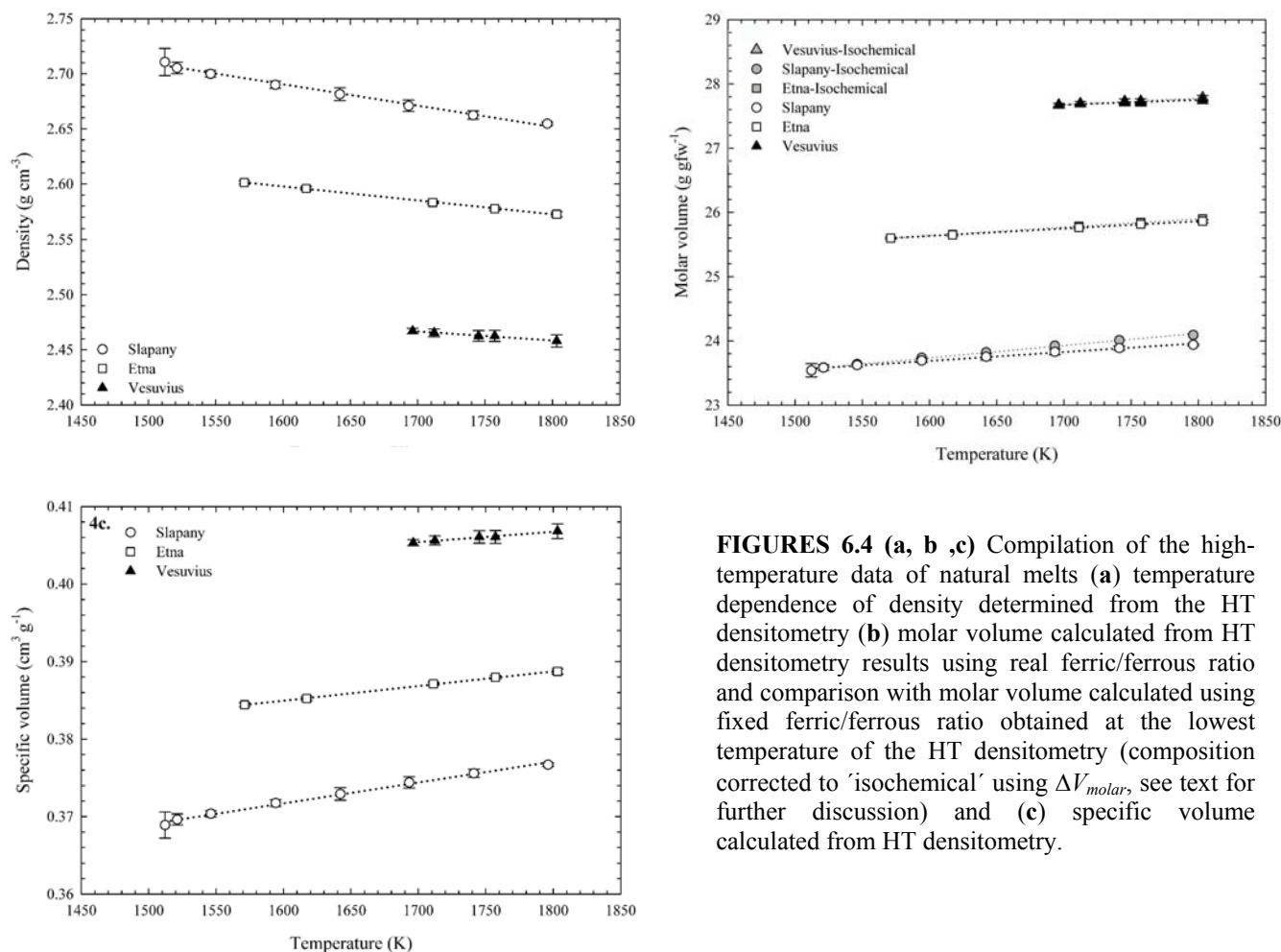
FIGURES 6.4 (a, b ,c) Compilation of the high-temperature data of natural melts (**a**) temperature dependence of density determined from the HT densitometry (**b**) molar volume calculated from HT densitometry results using real ferric/ferrous ratio and comparison with molar volume calculated using fixed ferric/ferrous ratio obtained at the lowest temperature of the HT densitometry (composition corrected to ´isochemical´ using ΔV_{molar}, see text for further discussion) and (**c**) specific volume calculated from HT densitometry.

trachybasalt and 2.458±0.006 from 2.467±0.002 g cm^{-3} to tephripholnolite. This indicates, that density at any given temperature decreases with increasing SiO$_2$ contents (Figure 6.4a). The linear relationships between density and temperature for each sample are not parallel, which suggests that the thermal expansion changes with composition within the temperature range investigated. This has been confirmed by a linear fit of calculated molar volume of the samples at high temperature. The gradient of such a linear fit represents the thermal molar expansivity ($\partial V/\partial T$) of the sample. Thermal molar expansivities decrease with increasing SiO$_2$ content for the samples investigated here. The individual errors, which are calculated based on the standard deviation of the three replicate buoyancy measurements for each bob, range from 0.06 to 0.24% and are reported in Table 6.3 and plotted in Figures 6.4a - 6.4c for each temperature and composition. The largest errors correspond generally to the most viscous melts, whereas the errors are smaller for the most fluid melts. The mean error, which is derived from the replicate buoyancies determinations of all the measurements conducted in this study, is about 0.19%. The high temperature densitometry derived value of liquid molar expansivity is 13.14±1.97x10^{-4} cm^3 mol^{-1} K^{-1} for basalt/basanite, 11.51±0.90x10^{-4} cm^3 mol^{-1}

K^{-1} for trachybasalt, and $7.54\pm1.73\text{x}10^{-4}$ cm^3 mol^{-1} K^{-1} for tephriphonolite.

For all the natural silicates investigated in this study, the molar volume of their supercooled liquid and their thermal molar expansion across the glass transition region were calculated based on an assumed equivalence of the relaxation of volume and enthalpy at the glass transition region (Webb et al., 1992).

Heat capacities (c_p) of the glass and supercooled liquid are obtained using differential scanning calorimetry (Figure 6.5). Thermal molar expansivities ($\partial V/\partial T$) of the glass were calculated from the length change of the sample measured by scanning dilatometry. As noted above, due to the effect of viscous deformation a direct observation of thermal expansivity in the supercooled liquid is impossible in this scanning regime. The normalized calorimetric trace is used to extend the dilatometric data of the glass into the supercooled liquid temperature range and to determine the thermal molar expansivity of the supercooled liquid across the glass transition region. The molar volume of the supercooled liquid just above the glass transition temperature was obtained from the glass density at room temperature and the glass thermal expansion coefficient up to the glass transition temperature. As an example, the normalized comparison of relaxation in the dilatometric and calorimetric traces is illustrated in Figure 6.3 for the Etna-trachybasaltic composition. In Figure 6.3, the effect of viscous deformation on the dilatometric trace in the supercooled liquid region is clearly shown by a sharp drop in the trace above the peak value. The results derived from the normalization procedure of Webb et al. (1992) have been reported in Table 6.8 for a temperature (Tsc)
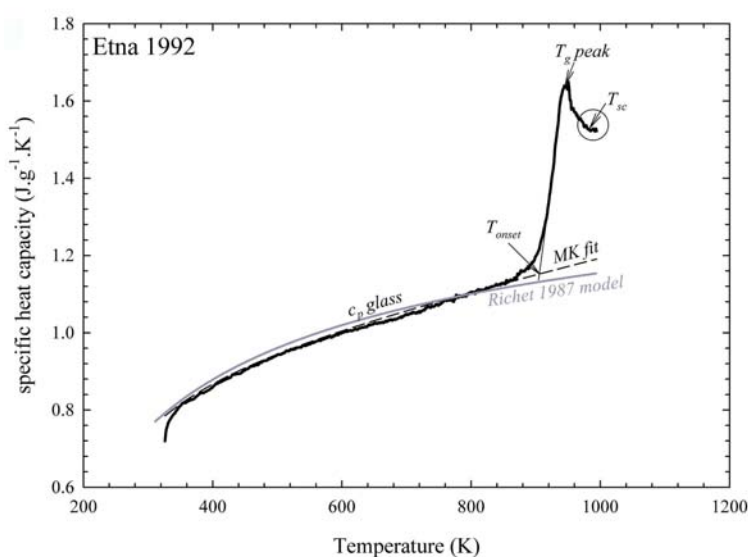
FIGURE 6.5. Scanning calorimetric determination of heat capacity of Etna sample across the glass transition. Bold gray curve shows the calculated c_p of the glass by Richet (1987). T_{sc}-temperature of supercooled liquid. T_{onset}-onset temperature of glass transition.

slightly higher than the glass transition temperature (i.e., 46, 49 or 50 K higher) for which the liquid was relaxed. Setting the peak values from the calorimetric and dilatometric measurements to be equal assumes that insignificant viscous deformation is recorded by the dilatometer at temperatures up to the peak temperature.

The molar expansivity of supercooled liquid derived from combined dilatometry / calorimetry varies from $16.86 \pm 0.48 \times 10^{-4}$ cm^3 mol^{-1} K^{-1} for basalt/basanite, to $18.99 \pm 0.48 \times 10^{-4}$ cm^3 mol^{-1} K^{-1} for trachybasalt, and $20.98 \pm 0.62 \times 10^{-4}$ cm^3 mol^{-1} K^{-1} for tephriphonolite. The molar thermal expansion coefficients of all the liquids are roughly for the same (within 3%) at Tsc. The individual errors for the thermal molar expansion coefficient of the different samples used in this study at Tsc range from 2.5 to 2.9%. Whereas, the mean error of the molar volume is about 0.1%. As shown in Figures 6.6a and 6.6b low- and high-temperature datasets were combined in order to determine the molar volumes of the liquids over a very large temperature range (i.e., from room temperature through the supercooled liquid up to the stable liquid, at temperatures at least 150 K higher than the melting point). Low- and high-temperature volumetric data were fitted together as a non-linear function of temperature for all the liquids. If the molar volume of silicate melts vary as a non-linear function of temperature, an appropriate mathematical form must be chosen to describe this variation. The equations such as $V=a+b/T$, $V=a+b/T^2$, or $V=a+bln(T)$ can describe the non-linear temperature dependence of volume, with only two adjustable parameters. These three equations have been tested by Toplis and Richet (2000). As they recommended we have used the equation $V=a+b$ $ln(T)$. The variation of molar volume as a function of the natural logarithm of absolute temperature for all samples is shown in Figure 6.7. The fit parameters, together with the correlation coefficient have been reported in Table 6.9. Note that the fits were made with the high- and low-temperature molar volumes. The values of $\partial V/\partial T$ calculated by derivation of this function ($=b/T$) are within 2% of the experimentally determined values from the supecooled temperature to superliquidus temperature. However, there are other equations which can describe the non-linear temperature dependency of the molar volume for the silicate melts. Polynomial or quadratic equations have been chosen by, for example, Gottsmann and Dingwell (2000) and Knoche et al. (1992b) to fit this non-linearity, but such equations have three or even more adjustable parameters. Another problem
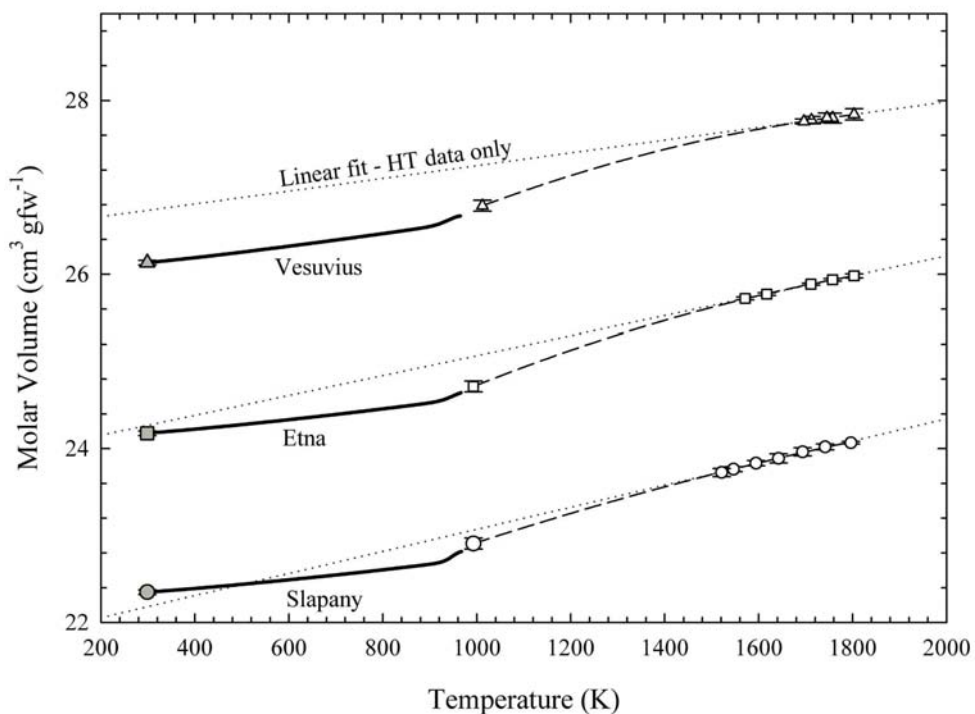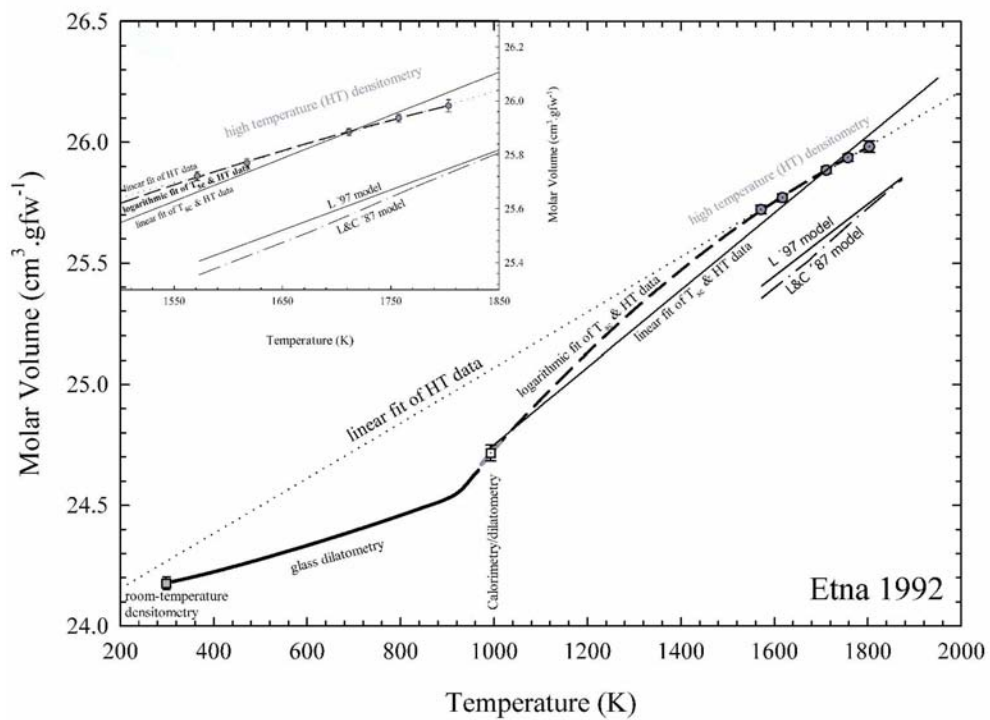
FIGURE 6.6 (a, b) Molar volume across the wide temperature range investigated (**a**) detail of the corrected to ´isochemical´ Etna molar volume with description of the used methods (**b**) comparison of the molar volume of all investigated ´isochemical´ samples plotted as a function of temperature.

associated with these equations is that they have innate inflection points, which increases the uncertainty of their extrapolation.

It is important to note that the treatment of the calorimetric and dilatometric data has been successful because for each sample the composition, thermal history, and as a result, the limiting fictive temperature were identical for the calorimetric and dilatometric measurements.
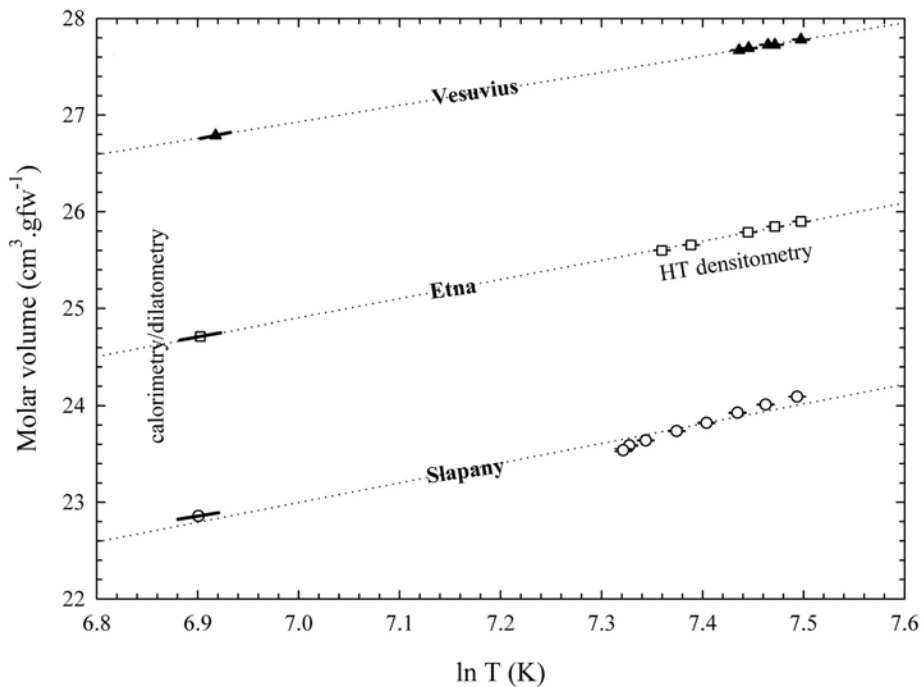
FIGURE 6.7. The variation of molar volume of the liquids as a function of the natural logarithm of absolute temperature for all samples.

6.4. Discussion

The two primary sources of thermal expansivity data are i) superliquidus liquid density determination by the double platinum bob Archimedean method and ii) expansivity data for the supercooled melt obtained by dilatometric method. The high-temperature density measurements are often limited by restricted ranges of temperature accessible using these more traditional techniques. This can result from high liquidus temperature or high superliquidus viscosity which result in a large uncertainty in expansivity. An example is provided by the systems Na_2O-SiO_2 and $CaO-Al_2O_3-SiO_2$, where, with increasing silica content, the combination of decreasing accessible temperatures and decreasing expansivities results in an error of up to several hundred percent (Bockris et al., 1956; Courtial and Dingwell, 1995). Multicomponent modelling of liquid densities yields thermal expansivities of partial molar volumes with uncertainties up to $\pm100\%$ (Lange and Carmichael, 1987).

During igneous petrogenesis, however, several magmatic processes (e.g., crystallization, crystal-melt fractionation, fragmentation of magma) occur at the temperatures below the solidus where the melt remains in local disequilibrium at subsolidus temperature. Dilatometry is one of the techniques which can yield expansivity data at such temperatures provided the nature of the glass transition is properly appreciated (Dingwell and Webb 1989; Dingwell and Webb 1990). Attempts to determine the expansivity of the molten silicates just above the glass transition have been challenging. The weight of the rod used to measure length changes results in dilatometry, causes it to penetrate into the sample surface when the viscosity becomes lower then about 10^{11} Pa s. Even if the rod was weightless, or the dilatometer was arranged horizontally, there would be an upper temperature limit where the viscosity becomes lower then about 10^7 Pa s. In such conditions the sample would collapse under its own gravitational body forces (e.g., Tool and Eichlin, 1931; Toplis and Richet, 2000). In this work we recover the supercooled liquid molar expansivities from combined dilatometry/calorimetry method proposed by Webb et. al. (1992).

The glassy cylinders, used for scanning dilatometry and room temperature densitometry, were obtained from the last temperature point of the high temperature densitometry and are isochemical. This was confirmed by microprobe and wet chemistry analyses. At higher temperatures during the superliquidus densitometry the samples have different compositions due to changes in fO_2. The ferric/ferrous ratio is controlled by the redox reactions occurring within samples at HT during the superliquidus densitometry experiments. The temperature dependence of Fe(II) content can be expressed linearly and the regression parameters of these fits are listed in Table 6.2. Grams per formula weight (*gfw*) is also a temperature dependent value due to the change in the ferric/ferrous ratio. To correct for the effect of change in ferric/ferrous ratio on the molar volume at the higher temperature points (i.e., at which HT densitometry was performed) I used the Lang and Carmichael (1987) and Lange (1997) models with fixed ferric/ferrous (that at the lowest superliquidus densitometry temperature). These molar volumes were compared with molar volumes calculated using the Lang and Carmichael (1987) and Lange (1997) models with the actual ferric/ferrous ratio measured by the wet chemistry method. The difference between these two molar volumes gives the ΔV_{molar}, which has been added to the values measured using superliquidus densitometry. This means that the superliquidus densitometry data are now ´isochemical´ along with the calorimetry, dilatometry and room temperature densitometry (e.g. in terms of ferric/ferrous ratio, gfw). The effect of this correction on the molar volume at higher temperature is negligible (Figure 6.4b). The change in curvature of the logarithmic fit

between supercooled liquid and corrected superliquidus liquid molar volume is minor and cannot be detected on the scale of Figures 6.6a and 6.6b. Furthermore, the Figure 6.6a and its close-up shows that the linear fit of molar volume at Tsc and superliquidus values is insufficient for all molar volume data at superliquidus temperature range. The error of such fit increase from basalt/basanite to tephriphonolite.

In addition, other structural parameters may change with temperature in part due to changes in the coordination number of Fe. The Lange and Carmichael (1987) and Lange (1997) models require an exact composition of the sample at temperature T. Changes in gfw have been taken into account and the composition of all samples (at temperature T) were recalculated and normalized to 100%. Molar volumes at superliquidus temperature were calculated by both models using recalculated and normalized compositions. Both the Lange and Carmichael (1987) and Lange (1997) models underestimate the molar volume of all samples across the HT range. Linear fits of calculated molar volumes using both models were extended to the supercooled liquid area. Values obtained in this way underestimate the molar volumes at Tsc by 1 to 2%. The error bars in Figures 6.4a - 6.4c correspond to standard deviation in the buoyancy determination propagated through Equation 2.6. However, both models are based on ideal mixing of oxide components. Furthermore, only four from total of twenty eight samples measured by Lange and Carmichael (1987) and Lange (1997) contain iron. The ferric/ferrous ratio is relatively restricted in their study. Nevertheless, authors claimed that the effect of iron redox state on density of variety of natural liquids are to most amount a variation of 1%. In addition, the Lange (1997) model did not take in to account the excess volume term corresponding to the possible interaction between SiO_2 and CaO, proposed by Courtial and Dingwell (1995). There is a lack of precise densitometry data provided on Fe-bearing silicates provided at different fO_2. This problem may be solved soon using new high temperature densitometry method where the volume is measured on a levitated sample. Such measurements may be combined with in-situ spectroscopic measurements.

The kinetics of redox reactions are slower at lower temperature (e.g., Bouhifd et al., 2004) so it is possible that some of my superliquidus densitometry steps, especially those at lower temperature, were not in equilibrium with air. This would not have any affect on the experimental results, because the HT densitometry was measured in three independent cycles for each Pt-bob. At the end of each cycle, when the lowest T (i.e., 1512 K for Slapany, 1571 K for Etna and 1696 K for Vesuvius) was reached, the sample was reheated again to the highest temperature (i.e., 1796 K for Slapany, 1803 K for Etna and 1803 K for Vesuvius)

where it was held for at least 8 hours. This allowed sufficient time for equilibrium in ferric/ferrous ratio to be reached. This has been confirmed using the Kress and Carmichael (1991) and Ottonello et al. (2001) models. Therefore the samples at the beginning of each cycle were in equilibrium with air. The intervals during which temperature changed, the isothermal holds and the measurement time and temperature were the same during all experiments (Figure 6.8) and the composition was checked by taking small amounts of sample (via the "dip" technique) for wet chemistry and microprobe analyses. Furthermore, the samples taken at the same temperature show no evidence of compositional change due either to gravitational separation or loss of iron through reaction with the platinum crucible.
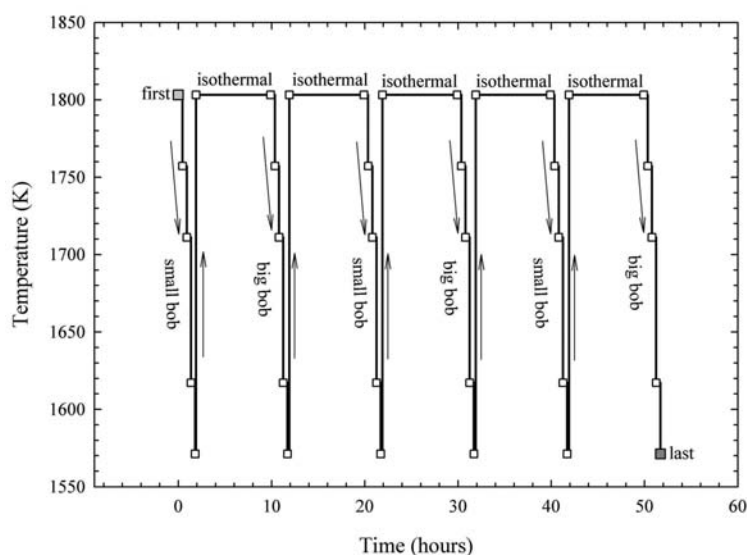
FIGURE 6.8. An example of the temperature profile of the high temperature densitometry as a function of time (Etna sample). Each temperature point has been measured three times using both small and big bob and sampled using "dip" technique for compositional investigation. At the end of each cycle, when the lowest temperature was reached, the sample was reheated again into the highest temperature where it remained for at least 8 hours (usually over night) to achieve an equilibrium. The last temperature point represents the temperature at which the sample was quenched. This glass was then drilled to provide samples for scanning dilatometry and calorimetry (isochemical composition).

The measured calorimetric results were compared with existing model of Richet (1987). The calculated values are consistent with measured c_p values (within uncertainty of DSC). The calculated c_p of glasses are higher of about 1% (absolute) for all samples except the temperature interval slightly below (~80K) the onset temperature, where rapid increases of c_p trace can occur. The predicted c_p values are lower (~1%) then the measured c_p in that temperature range. An example of the predicted and measured c_p of the glass is shown on Etna sample in Figure 6.5.

Some binary, ternary and quaternary systems seem to have temperature independent thermal expansivities from the supercooled liquid temperature to the superliquidus temperature. However, the AnDi system exhibits a temperature dependency of the $\partial V/\partial T$ (Gottsmann and Dingwell, 2000; Knoche et al., 1994; Knoche et al., 1992b; Toplis and Richet, 2000). Thus thermal molar expansivity of multicomponent natural melts appears to be, in general, temperature dependent and can be expressed by a logarithmic function.

7. An Expanded non-Arrhenian Model for Silicate Melt Viscosity: A Treatment for Metaluminous, Peraluminous and Peralkaline Liquids

7.1. Introduction

The prediction of the viscosity of silicate liquids, over the range of temperatures and compositions encountered in nature, remains one of the most challenging and elusive goals in Earth Sciences. Recent work (Giordano and Dingwell, 2003a, Russell et al., 2002, 2003; Russell and Giordano, 2005) suggests that there are now sufficient experimental melt viscosity data available to create new viscosity models to replace previous Arrhenian models (Shaw, 1972; Bottinga and Weill, 1972). As mentioned in these works, the Arrhenian assumption of early models was fully consistent with the available data; however, the current database of viscosity measurements covers a significantly wider interval of melt compositions and temperatures (e.g., Richet and Bottinga, 1995; Dingwell, 1995). The new data require that future viscosity models accommodate strong non-Arrhenian temperature dependencies (e.g., Richet, 1984; Hummel and Arndt, 1985; Angell, 1985) and extend the compositional range of more recent non-Arrhenian models (Hess and Dingwell, 1996).

Most recently, Giordano and Dingwell (2003 a, b) presented an empirical model for accurately predicting the non-Arrhenian temperature dependent viscosity and fragility of silicate melts over a wide range of anhydrous compositions (e.g., rhyolite to basanite). Their analyses covered the widest range of anhydrous natural silicate melt compositions so far investigated. The experimental database constitutes ~800 high quality measurements of viscosity on silicate melts that vary in character from strong to fragile (Angell, 1985). The purely empirical Vogel-Fulcher-Tamman (VFT) (Vogel, 1921, Fulcher, 1925; Tammann and Hesse, 1926) equation is used to accommodate the non-Arrhenian temperature dependence of melt viscosity (η) :

$$\log \eta = A + B/(T - C) \tag{7.1}$$

where η is the viscosity in Pa s and T is absolute temperature T (K). The variables A, B, C are adjustable parameters representing the pre-exponential factor, the pseudo-activation energy, and the VFT-temperature, respectively (e.g., Angell, 1985). In the recalibration that I have

performed of this viscosity model I have also assumed that all silicate melts converge to a common value at high-temperature which requires that the value of A is constant and independent of composition (e.g., Russell et al., 2003; Russell and Giordano, 2005).

The database of experimentally determined pairs of values of T(K) versus log η is substantially larger (about 800 data and 44 compositions) than originally available to Giordano and Dingwell (2003a) (about 800 data on 44 melt compositions vs. ~ 350 experiments on 20 different melt compositions). Also, the calibration provided here considers a temperature range from 613 to 2265°C, much wider than that used by Giordano and Dingwell (2003a) (i.e., 700 to 1600°C). Specifically, the new database comprises peralkaline (A.I. = Na_2O+K_2O/Al_2O_3 > 1), metaluminous and peraluminous (P.I. = $Al_2O_3/CaO+Na_2O+K_2O$ > 1) melt compositions. These data show that, compared to metaluminous liquids (Na_2O+K_2O < Al_2O_3 < $CaO+Na_2O+K_2O$), the peralkaline and peraluminous melts have lower and higher viscosities, respectively.

Past and recent models of silicate melt viscosity have demonstrated the drastically different rheological behaviours of peralkaline, metaluminous and peraluminous melts. Multicomponent models based on the Arrhenian temperature dependence of viscosity (Shaw, 1972; Bottinga and Weill, 1972, Persikov et al., 1990) have shown that metaluminous melts typically have viscosities between those of peraluminous (higher viscosity) and peralkaline (lower viscosity) melts. The early models adopted an Arrhenian temperature dependence, fully consistent with the available data at the time, which is now viewed as inadequate as silicate melts commonly show a pronounced non-Arrhenian temperature dependence of viscosity (e.g., Angell, 1985; Giordano and Dingwell, 2003b; Russell et al., 2003). The seminal work from Bottinga and Weill (1972) and more recent studies that have incorporated both dry and H_2O-bearing melts (e.g. Baker and Vaillancourt, 1995; Dingwell et al., 1998, 2000; Hess et al., 2001; Giordano et al., 2000; Witthington et al., 2000, 2001; Giordano and Dingwell, 2003; Bouhifd et al., 2004; Webb et al., 2004) recognized that the rheological behaviour of peralkaline and peraluminous melts is complicated relative to metaluminous melts.

A simple recalibration of the Giordano and Dingwell (2003a) model using the extended database reproduces the viscosity data on metaluminous liquids very well but it is less accurate when predicting the viscosities of peralkaline and peraluminous melts at temperatures lower than 1000 °C. I accommodate the discrepancies between the model predictions and the observed viscosities of peralkaline and peraluminous melts using an empirical factor based on the ratio of excess of alkalies over the alumina (AE = Na_2O+K_2O-

Al_2O_3) to SM, the sum of all the structure modifier oxides. SM as defined in Giordano and Dingwell, (2003a) is SM is the sum on a molar basis of ($Na_2O + K_2O + CaO + MgO + MnO + FeO_{tot}/2$), disregarding the contribution of charge-balancing cations. The temperature-dependent factor allows us to reproduce the complete database of melt viscosity to within a RMSE (Root Mean Square Error) of 0.45 logunits.

7.2. Experimental rationale

The quality, amount and distribution of experimental data strongly affect our ability to create new predictive models. With this in mind the gaps in the T-X spaces were reduced, as previously explained by Giordano and Dingwell (2003a), by measuring additional melt compositions (rhyolitic, trachytic, moldavitic, andesitic, latitic, pantelleritic, basaltic and basanitic) and incorporating them into the existing database of silicate melt viscosities (e.g., Giordano et al., 2005; Mangiacapra et al., 2005a,b; Bouhifd et al., 2004; ; Giordano and Dingwell, 2003a; Whittington et al., 2000, 2001; Dingwell et al., 2000, 1996; Alibidirov 1997; Richet et al., 1996; Neuville et al., 1993). It is thanks to these new viscosity determinations and recent advances in modelling the viscosity of silicate melts (e.g. Russell et al., 2002, 2003; Giordano and Dingwell, 2003a) that we are now able to generalize previous
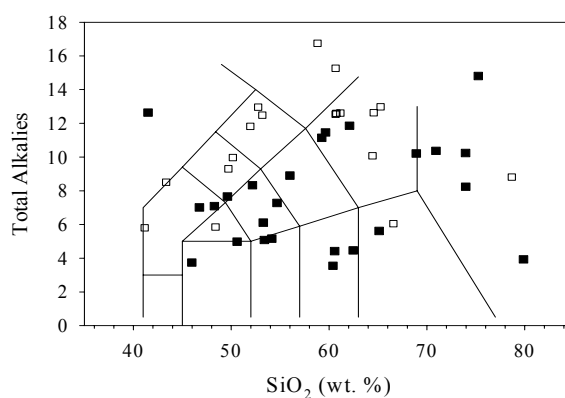
FIGURE 7.1. Chemical compositions of the (newly) investigated products (closed symbols) compared to compositions presented in Giordano and Dingwell (2003a) (G&D_'03) (open symbols). The chemical range of the samples investigated is given according to the T.A.S. (Total Alkali Silica) diagram (after Le Bas et al., 1986) reporting the values of the total alkali (Na_2O+K_2O) content vs. the SiO_2 (wt%)s. Table 7.1 reports the chemical compositions as determined by microprobe analysis.

observations to an extended database for multicomponent silicate systems.

The chemical composition and a description of the samples measured for this study are provided in Table 7.1 and Figure 7.1. The compositions of other natural and synthetic silicate melts for which viscosities have been measured by other research groups. The samples

measured in this study are derived from natural samples collected from the fallout deposits of the Fondo Riccio (Di Vito, 1999)(FRa) and the Campanian Ignimbrite (Civetta et al, 1988) (CI_OF*) plinian eruptions, at the Phlegrean Fields (PF, Italy). Other volcanic products were collected at Stromboli (STB*) (Italy), Monserrat (MST) (Martinique), Slapany (SLP) (Czech Republic) and Merapi (MRP) (Indonesia) during their last phases of activity (see Table 7.1). They include a range of compositions from foidite and basanite to basaltic-andesites, andesites, phonolite, dacite and rhyolites (Figure 7.1).

The starting materials used for the viscosity determinations were prepared by fusion of the total rocks of the selected samples. The experimental techniques used to measure the viscosity of the multicomponent liquid investigated include: (a) high-T (1050 to 1650 °C) concentric cylinder techniques for viscosity determinations in a range from about 10^{-1} to 10^5
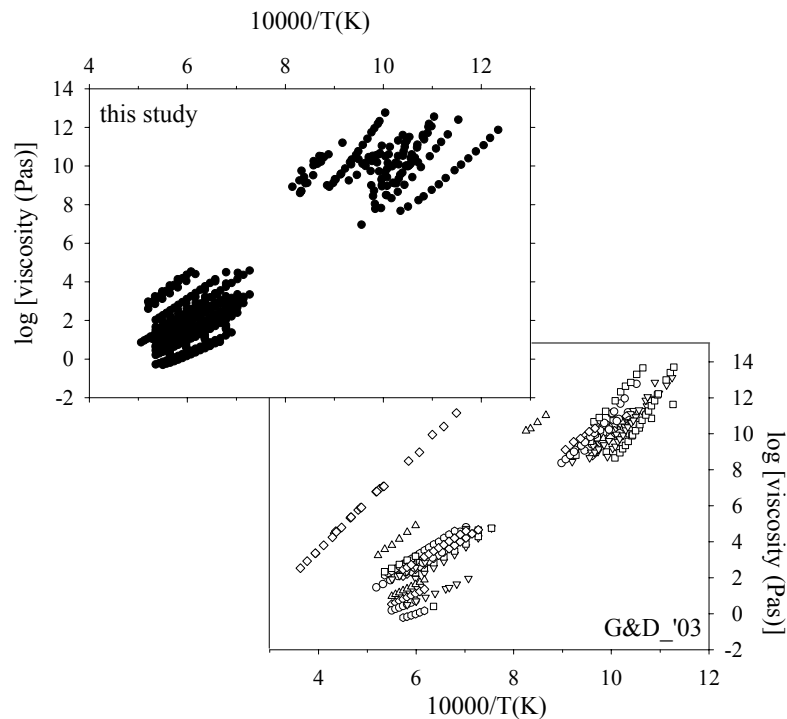
FIGURES 7.2. (a) Viscosity data measured and analysed in this study (closed symbols) and, **(b)** experimental data (open symbols) considered from Giordano and Dingwell (2003 a)(G&D_'03). Datasets are reported in the viscosity - reciprocal temperature diagram, where viscosity is in logarithmic scale. Tables 7.1 and 7.2 report data sources and measured viscosity data for the silicate melts investigated.

Pa s, and (b) low-T micropenetration viscometry (676 to 919 °C) on quenched glasses to measure melt viscosity in the interval from about 10^8 to 10^{12} Pa s and close to the glass transition temperature (Hess et al., 1995; Dingwell et al., 1996). Details of these experimental techniques have been described extensively in previous works (e.g. Dingwell and Virgo,

1988; Hess et al., 1995). The major element compositions of the glasses were determined using a CAMECA® SX 50 microprobe (Table 7.1).

The viscosity data for each sample are plotted in the Arrhenian diagram (Figure 7.2). The complete dataset presented here includes that used by Giordano and Dingwell (2003a), as well as, the 157 new viscosity measurements on 8 new melt compositions reported in Table 7.2.

The database also uses viscosity determined for multicomponent silicate melts by Neuville et al. (1993), Dingwell et al. (1996), Richet et al. (1996), Alibidirov (1997), Toplis et al. (1997), Dingwell et al. (2000), Bouhifd et al. (2004), Whittington et al. (2000, 2001); Giordano et al. (2005); Mangiacapra et al. (2005a, b). Over the temperature range of about 613 to 2265 °C, the measured compositions show a near Arrhenian to strongly non-Arrhenian behavior.

7.3. Results and numerical strategy

As mentioned above, the new calibration adopts a slightly different strategy from the Giordano and Dingwell (2003a) model for modeling the viscosity of silicate melts as a function of temperature and composition. Here, it is assumed that all silicate liquids converge to a common, high-temperature limiting value of viscosity (e.g., Russell et al., 2002; Russell et al., 2003; Russell and Giordano, 2005). This assumption requires the parameter A to be
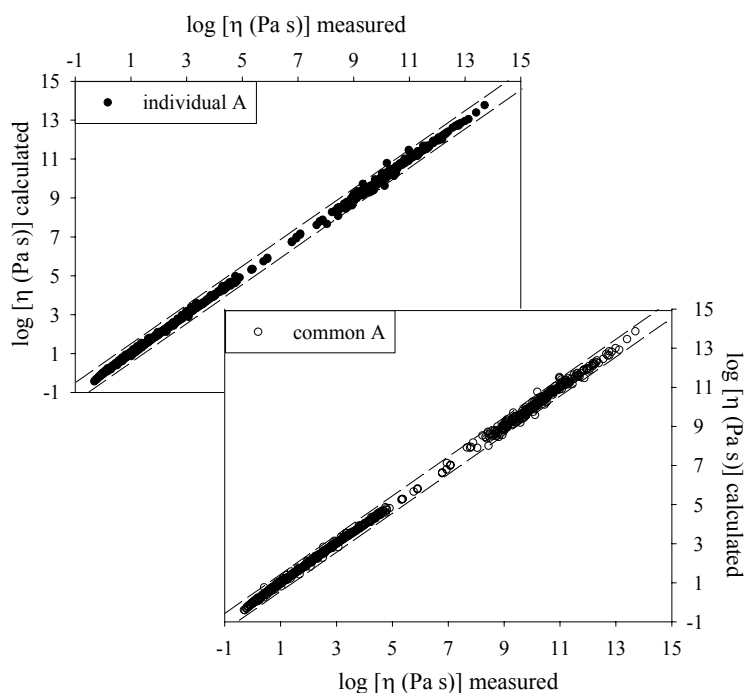
FIGURE 7.3. Comparison between the measured values of viscosity (x-axis) and the values of viscosity predicted by fitting the datasets for individual melts to: i) independent values of A, B and C (Equation 7.1), and ii) independent values of B and C coupled to a common value of A (=-4.07) for all the sets of data. VFT parameter and error analysis values are provided in Table 7.3. Parallel line indicate $\pm$ 0.25 logunits.

constant and independent of melt composition (e.g. Angell, 1995).

Consequently, all compositional controls must be accommodated by variations in the B and C terms (Russell and Giordano, 2005). This assumption is justified by theoretical studies (e.g. Glasstone, 1941; Myuller, 1955; Frenkel, 1959) and operationally by the fact that there is no statistical difference between the quality of fits of the VFT functions to individual data sets or to data sets coupled via a single optimized value of A (e.g. Russell et al., 2003; Russell and Giordano, 2005) (Figure 7.3). The main consequence of this assumption is that the number of variables (e.g., A, B and C) necessary to describe the T-dependence of viscosity for N individual melt compositions is reduced from 3N (where N is the number of data sets) to 2N+1.

For each melt composition the optimum VFT coefficients (e.g., A, B and C) have been calculated. The data for each composition have been fitted by first assuming unique values of A for each composition and then, assuming they share a common, but unknown, value of A. The parameters obtained in the two different circumstances are reported in Table 7.3 with their respective χ^2 and the RMSE values. The results of the optimization are summarized in Figure 7.3a and 7.3b where the misfits between the calculated and measured values of viscosity are compared. For the individual fits RMSE $\simeq$ 0.24 logunits which represents the ability of the VFT equation to reproduce the experimental measurements. In the case of a common value of the A parameter an optimal value of -4.07 (in logarithmic units) is found. This agrees well with the pre-exponential factor (A = $10^{-4.5\pm1}$ Pa s) predicted by theories based on kinetic rate processes (e.g., Frenkel 1959; Glasstone et al., 1941) and utilized by Myuller (1955) for the description of the Arrhenian T-dependence of viscosity. Furthermore, the resulting RMSE is 0.30 logunits, which is only slightly larger than the value of 0.24 logunits obtained for individual values of A (and N-1 extra parameters).

Given that A is constant and independent of composition, the compositional effects on melt viscosity must be completely accommodated by the values of B and C. The B and C parameters fitted with a constant value of A are strongly correlated and the covariation between the model values of B and C (Table 7.2) is illustrated in Figure 7.4. The values of B and C parameters describe 3 separate trends for the metaluminous, peralkaline, and peraluminous melt compositions, respectively. Peralkaline melts tend to have lower values of C at fixed values of B, peraluminous have higher values of C and metaluminous are intermediate.

In particular, B and C values appear to be correlated with the degree of melt polymerization expressed using the parameter SM (= Σ mole% (Na_2O + K_2O + CaO + MgO + MnO + FeO_{tot}/2) (Giordano and Dingwell, 2003a) (Figures 7.5a and 7.5b). In fact, the values of B, taken separately for each compositional suite, decrease with increasing SM parameter, whereas an opposite trend, albeit slightly more scattered, is observed for the C parameter (Giordano and Dingwell, 2003b; Russell et al., 2003). At higher values of SM and increasing degree of depolymerization (low B and high C values) the C values for the peralkaline and the metaluminous melts seem to merge. For peraluminous melt compositions the C parameter defines a different trend. In addition, at fixed values of SM the peralkaline "suite" typically exhibits lower C values with respect to both metaluminous and peraluminous melts. On the other hand, the peraluminous "suite" has the highest C and the lowest B values.

The SM parameter constitutes the dominant chemical control on B and C values. Nevertheless Figures 7.4, 7.5a and 7.5b illustrate that SM alone is not sufficient to describe
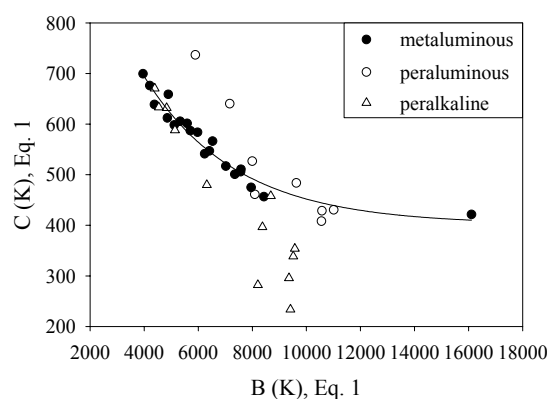
FIGURE 7.5. Variation of the Bvft and Cvft parameters with the SM parameter (SM = Na_2O+K_2O+CaO+MgO+MnO+FeO_{tot}/2 (mole%) - Giordano and Dingwell, 2003a). To a first approximation SM represents the "polymerization degree" of the silicate network. Symbols as in Figure 7.3.

the variations in B and C found for all melt compositions. In fact, the B and C parameters for melts ranging from peralkaline to peraluminous are poorly described by SM (Figures 7.5a and 7.5b) suggesting that an additional compositional factor is required.

The anomalous behaviour of peralkaline and peraluminous liquids in terms of their B and C parameters is also evident in the patterns of isothermal viscosity versus SM parameter (Figures 7.6a and 7.6b). At high temperatures (> 1200 °C, Figures 7.6a and 7.6b) and low values of viscosity (< 10^5 Pa s, if pure silica is excluded) viscosity varies coherently as SM changes, regardless of whether the melts are metaluminous, peraluminous or peralkaline. The model isothermal viscosities at 1400 and 2000 °C are predicted simply as a function of the SM parameter. Even at 1000°C there is a coherent trend between viscosity and SM for most

melts; the exceptions are two of the peralkaline composition (SFB40, SFB60), represented by the two crossed squares under the 1000 °C isothermal viscosity curve in Figure 7.6b. The discrepancies between model isothermal viscosity curves and the measured values of viscosity increase as temperature decreases. The discrepancies are mainly related to the peralkaline and peraluminous liquids and they become substantial at temperatures below 800°C (Figures 7.6a and 7.6b). At these low temperature, the peralkaline samples show viscosities significantly smaller than thet metaluminous samples, whereas the peraluminous samples have higher viscosities compared to the metaluminous samples. According to these observations it seems suitable to use the value of the difference between the alkali and the alumina content, on a molar basis (AE= $Na_2O+K_2O-Al_2O_3$) as a useful chemical parameter to discriminate between the compositional suites. These discrepancies can be attributable to the different roles played by the network modifying and network forming cations in the silicate network, in particular the mutual role played by the alkali and alumina.

Figure 7.6 also shows that the isothermal curves become parallel when a critical ratio of network modifiers (e.g., SM) is reached. The fact that the trends of the isothermal viscosity versus the SM parameter are almost parallel indicate that they are insensitive to temperature, possibly indicating that the effect of temperature on the structural rearrangement of silicate melts is quite limited. This is most apparent for melts with high SM values where the system is very depolymerised.

7.4. Viscosity model

Following the methods of Giordano and Dingwell (2003a), the empirical equations were fitted to the predicted values of viscosity for all melts at specific temperatures. For each melt composition (N=44) were computed the viscosity at a series of temperatures using a value of the A of -4.07 and the appropriate values of B and C (Table 7.3). Thus, for each specific temperature (see Figure 7.6a) were computed 44 model values of viscosity corresponding to each of the different melt compositions represented by SM.

Isothermal curves were then generated by fitting equations of the form:

$$\log_{10}\eta = a_1 + \frac{a_2 * a_3}{a_3 + SM} \tag{7.2}$$

to the $\log\eta$ - SM datasets computed for each temperature. Thus, the isothermal variation in viscosity is described as a function of SM by the values of a_1, a_2, a_3 (Table 7.4). The present

model uses a discrete number of isothermal viscosity curves at intervals of 100 °C over the range 700 °C to 2000 °C plus one at 630°C. The temperature interval (630 to 2000 °C) investigated here is significantly larger than that used by Giordano and Dingwell (2003a).
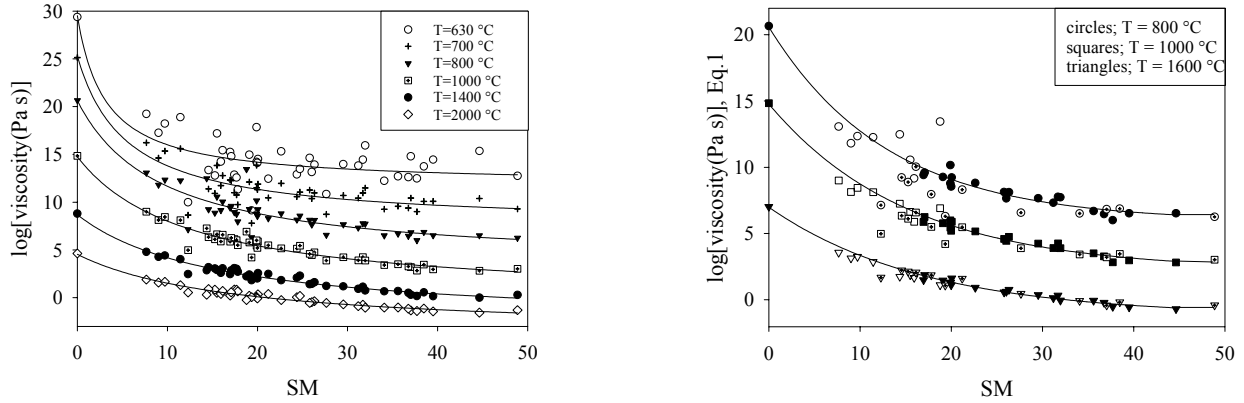
FIGURES 7.6. (**a**) Isothermal viscosity at six different temperatures (630, 700, 800, 1000, 1400, 2000 °C) versus the SM parameter. Numbers in the legend are temperatures (°C). Symbol positions are calculated from composition (SM) and from Equation 7.1 using ideal values of B, C and A=-4.07. (**b**) Circles, squares and triangles correspond to a detail of the 800, 1000 and 1600 isothermal curves respectively. Symbols are also differentiated to show metaluminous (filled) peraluminous (open), and peralkaline (crossed) melts compositions.

Figures 7.6a and 7.6b compare the values of viscosity (symbols) recalculated using the appropriate VFT functions at each temperature (630, 700, 800, 1000, 1400, and 2000 °C) to the model curves fitted to those data (curves) as a function of compositions (e.g., SM). The parameters (i.e., a_1, a_2, a_3) used for each isothermal viscosity curve are summarized in Table 7.4. These parameters allow melt viscosity to be predicted as a function of composition for specific temperatures. The values of these compositional parameters (a_1, a_2, a_3) vary with temperature (Figure 7.7). This figure shows the values of these coefficients computed for discrete temperatures:

$$a_1 = \frac{[-35.8816 + 0.0367110 \cdot T(^{\circ}C)]}{[1 - 0.0022362 \cdot T(^{\circ}C) - 0.00000166697 \cdot T(^{\circ}C)^2]} \tag{7.3}$$

$$a_2 = \frac{[-93.6494 + 0.2317411 \cdot T(^{\circ}C)]}{[1 - 0.0054597 \cdot T(^{\circ}C) + 0.00001361072 \cdot T(^{\circ}C)^2]} \tag{7.4}$$

$$a_3 = \frac{[45.575455 - 0.0780935 \cdot T(°C)]}{[1 - 0.0036108 \cdot T(°C) - 0.00000002170 \cdot T(°C)^2]} \tag{7.5}$$

In order to compute melt viscosity as a function of temperature and composition the following steps are taken: i) the coefficients a_1, a_2, and a_3 are calculated at specified temperatures using Equations 7.3 - 7.5; ii) the value of SM for the specific melt composition is calculated, and iii) the values of $\log\eta$ are calculated using the a_1, a_2, a_3 and SM values in Equation 7.2

Table 7.5 presents an example calculation that shows how to compute the viscosity for a fixed temperature and composition.

Figures 7.8a - 7.8c compare experimentally measured values of the viscosity and the values predicted by the model using Equations 7.2 - 7.5. The model reproduces the viscosities of metaluminous liquids with RMSE of 0.38 logunits. However, the model is less accurate in reproducing the viscosities of peraluminous and peralkaline compositions with RMSE values of 0.66 and 1.70, respectively (Figures 7.9b and 7.9c). Consequently, the RMSE value for the entire dataset (e.g. 44 composition) is 0.84 logunits.
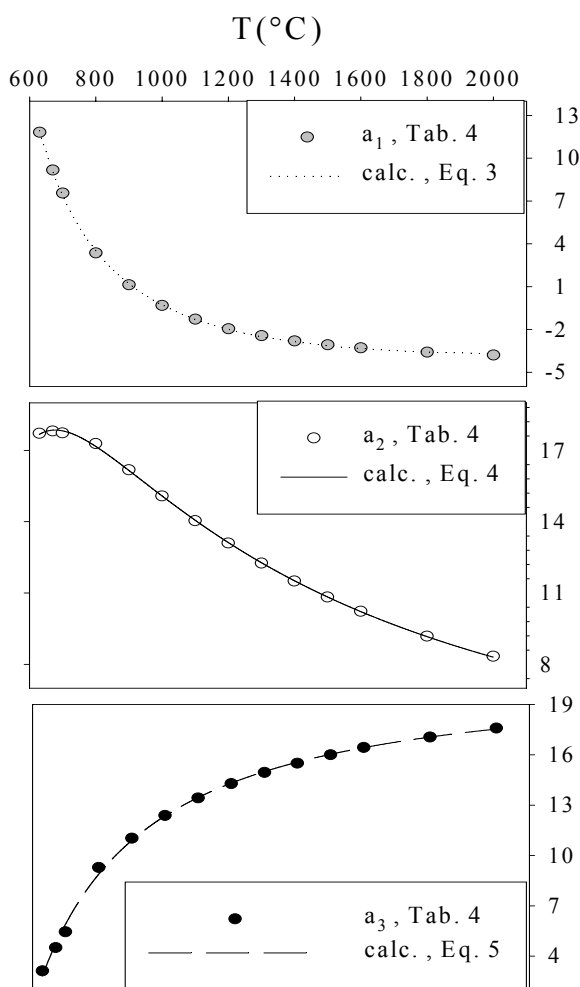
Nevertheless, these values are significantly lower than the RMSE values associated with the original Giordano and Dingwell (2003a) model; suggesting that these modifications significantly improve it.

FIGURES 7.7. Temperature dependence of the $a_{1, 2, 3}$ parameters obtained by fitting isothermal viscosity values (Figure 7.6). Curves in the figures correspond to (**a**) Equation 7.3; (**b**) Equation 7.4; (**c**) Equation 7.5.

7.5. Extension to peralkaline and peraluminous melts

In order to be able to apply this model to natural systems, it is critical to find a means of accurately predicting the viscosity for peraluminous and peralkaline melts. Figure 7.9 shows the discrepancies from the measured values for metaluminous, peralkaline and peraluminous melts that the recalibrated model (Equations 7.2 - 7.6) exhibits as a function of the experimental reciprocal temperature. From examining Figure 7.9 the following critical phenomena can be observed: 1) the model overestimates the viscosity of peralkaline melts (negative value of the residuals), 2) the model underestimates the viscosity of peraluminous (positive value of the residuals), 3) the largest residuals are associated with peralkaline liquids, 4) metaluminous melts have very small random residuals and 5) the residuals are temperature dependent and their absolute values increase with decreasing temperature. Along with these observations I believe that the observed discrepancies are strongly governed by the mutual relationships between alkali and alumina. In particular, as discussed below, the
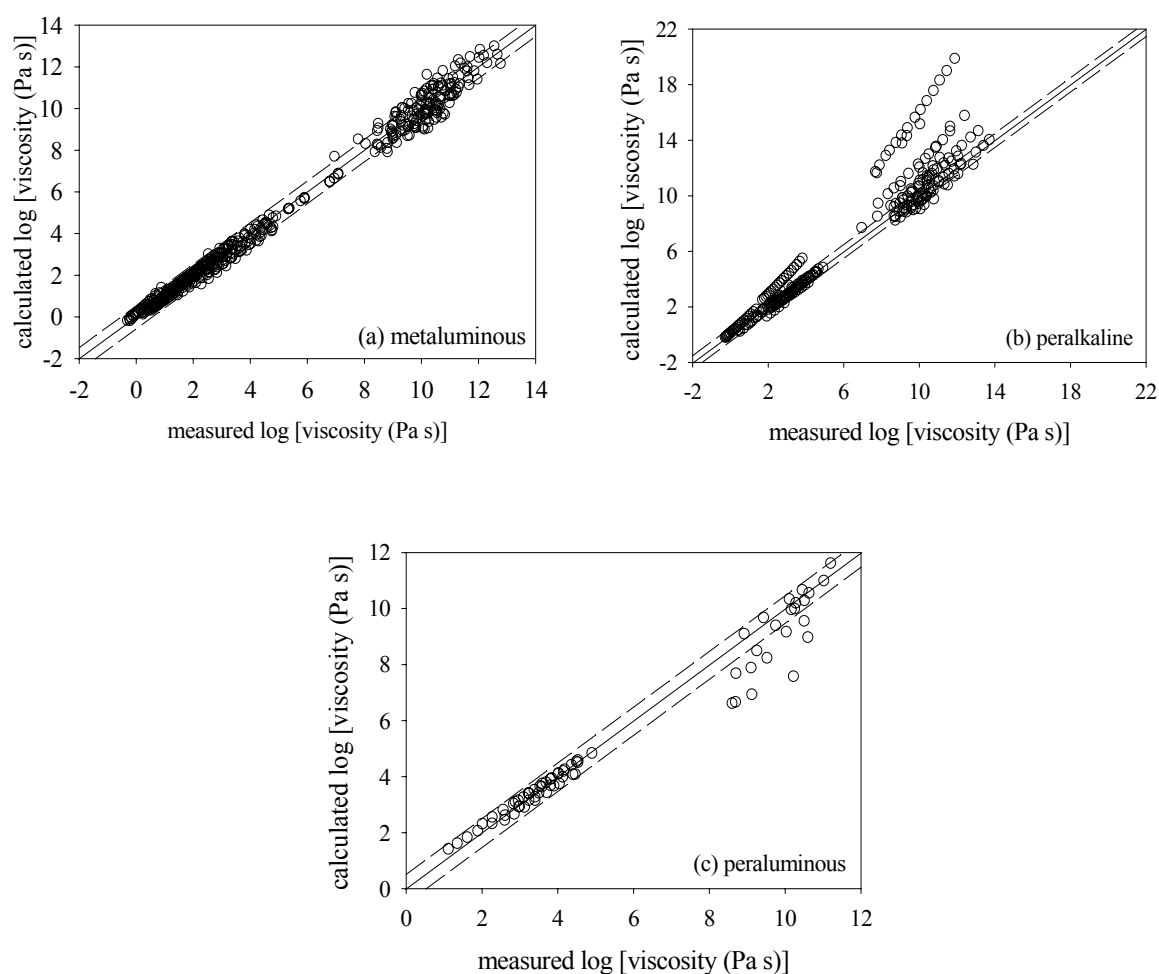
FIGURES. 7.8. Predicted vs. measured viscosity calculated by Equations 7.2 - 7.5. (**a**) metaluminous; (**b**) peralkaline; (**c**) peraluminous liquids.
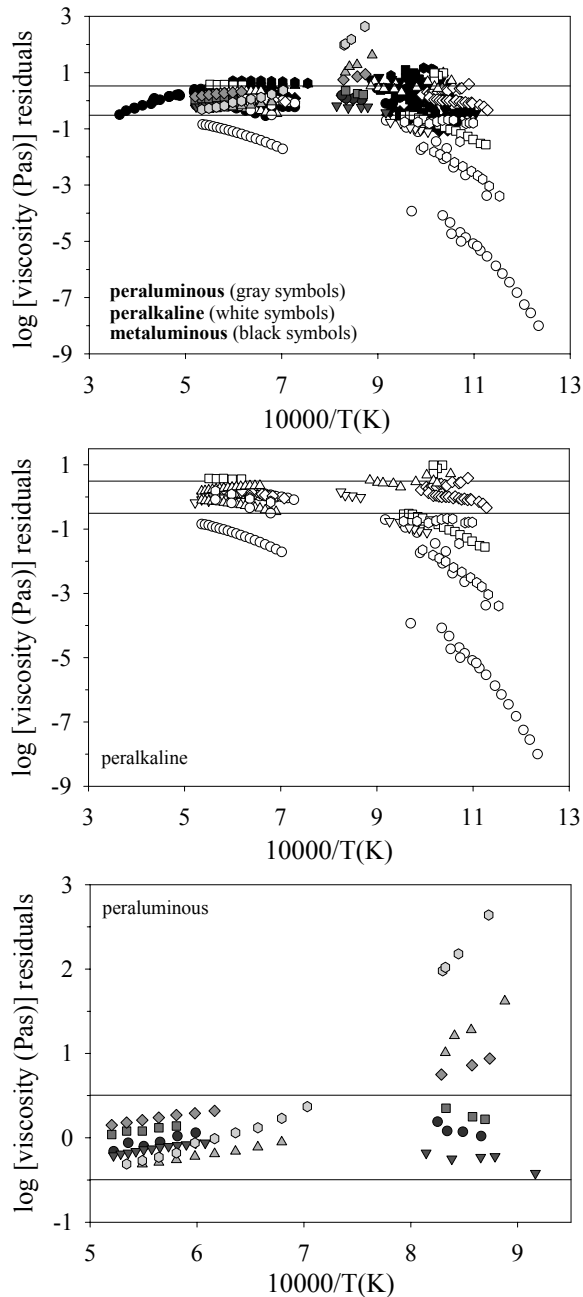
discrepancies were found to be related to the alkali excess over the alumina content (AE), the network modifiers content. Figure 7.9 constitutes a first step in the analysis and provides a guide towards the form of the equation that could be used to modify the current model reproduces the viscosities of peraluminous and peralkaline melts. For example, on the basis of Figure 7.9 it was noticed that the magnitude of the misfit between the model and the measured data increases as a function of: i) increasing excess of alkali (AE) contents, and for melts having low SM, of ii) AE. The goal at this point is to refine the model represented by Equations 7.2 - 7.6 so that it can be extended in a "continuous" way to reproduce all of the experimental data. A simple temperature-

FIGURES 7.9. Temperature-dependence of the residuals obtained for difference between the viscosities calculated using Equations.7.2 - 7.5 and the measured values. Lines in the figure constrain the 2 σ error interval.

dependent parabolic equation was adopted to describe the residuals for the peralkaline and the peraluminous melts as a function of composition. Compositional variation is treated as different amounts of excess alkali (AE) and the number of structural modifiers (SM). The equation has the form:

$$\Delta \log \eta = \log \eta_{meas} - \log \eta_{SMmodel} = -0{,}000012923 \cdot T^2 \cdot \left(\frac{AE}{SM}\right) + 0.03578 \cdot T \cdot \left(\frac{AE}{SM}\right) - 24.337 \cdot \left(\frac{AE}{SM}\right)$$

(7.6)

where $\log \eta_{meas.}$ is the measured value of viscosity, $\log \eta_{SM\text{-}model}$ is the viscosity predicted by Equations 7.2 - 7.5, T is the temperature in °C, AE is the excess of alkalies over the alumina

and SM is the "structure modifier" parameter (Giordano and Dingwell 2003a). The resulting parabolic equation provides a T-dependent correction factor as a function of the ratio AE/SM which can be added to equation 7.4 (see Equation 7.7 below). As previously described equations (7.2 - 7.5) were calibrated against parameters derived for a discrete number of isothermal viscosity (logη) vs. SM curves (i.e., Table 7.4) over the temperature interval (630 - 2400 °C). This temperature interval was chosen because for most of the compositions analysed over that interval there is a sufficient number of experimental data. At lower temperature only few composition were measured.

The final regression of the experimental data for the model parameters is performed on the experimental database, rather than on discrete model values (e.g. Figure 7.10 and Table 7.2). The resulting model is given by the equation:

$$\log_{10}\eta = b_1 + \frac{b_2 * b_3}{b_3 + SM} + b_4 \tag{7.7}$$

where

$$b_1 = \frac{[-33.5556 + 0.0351623 \cdot T]}{[1 - 0.0022362 \cdot T - 0.00000166697 \cdot T^2]} \tag{7.8}$$

$$b_2 = \frac{[-93.6494 + 0.2317411 \cdot T]}{[1 - 0.0054597 \cdot T + 0.00001361072 \cdot T^2]} \tag{7.9}$$

$$b_3 = \frac{[45.5755 - 0.0780935 \cdot T]}{[1 - 0.0036108 \cdot T - 0.00000002170 \cdot T^2]} \tag{7.10}$$

$$b_4 = -0{,}00001292391 \cdot \left(\frac{AE}{SM}\right) \cdot T^2 + 0.03577545 \cdot \left(\frac{AE}{SM}\right) \cdot T - 24.3366274 \cdot \left(\frac{AE}{SM}\right) \tag{7.11}$$

T(°C) being the temperature in °C and AE and SM as defined above.

Equation 7.11 comprised of 15 empirical parameters that reproduce very well the entire database of measured viscosities, including the peralkaline and peraluminous samples (Figure 7.10). The resulting fit has RMSE = 0.45 logunits. Figure 7.11 shows residuals as a function of SM. The largest differences between the observed and modelled viscosities (Equations. 7.7 - 7.11) are in the peralkaline melts.
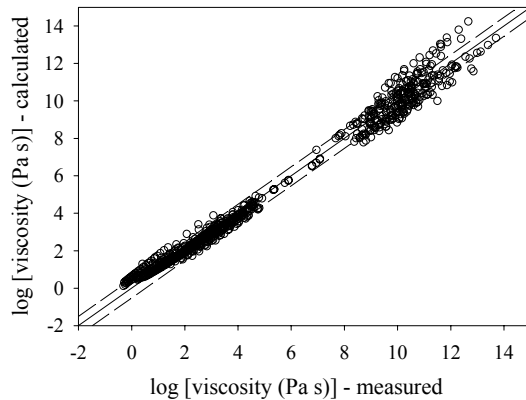
FIGURE 7.10. Comparison between the viscosity calculated by Equations. 7.2 −7.7 (corrected for the compositional dependence of the residuals) and the viscosity measured. The total RMSE value is 0.45 logunits.

7.6. Discussion

It is clear that the metaluminous, peraluminous and peralkaline melts analysed in this work, define three different domains/regimes of viscous flow. At constant T, the metaluminous melts are more viscous than the peralkaline and less viscous than the peraluminous. It is also clear that such differences are determined by how the alumina and the alkalies enter the silicate structure of the melts. In particular, as discussed by Dingwell et al. (1998), the viscosity for the haplogranitic composition (HPG8) increases with the addition of the first few percent of normative corundum, whereas it remains constant with further addition of Al_2O_3 (up to 5 wt%). A smooth variation of viscosity, in this compositional range, would require a viscosity maximum for a slightly peraluminous melt (between HPG8Al02 and HPG8Al05). Such a maximum, shifted with respect to the metaluminous composition was also found along the stoichiometrically similar join in the system Na_2O-Al_2O_3-SiO_2 and was accounted for by the presence of triclusters in the melt (Toplis et al., 1997).

Unfortunately, the lack of viscosity data on strongly peraluminous melts prevent me from investigating the tricluster hypothesis in more detail. In contrast to what was observed by Toplis et al. (1997) for simple systems, I find that peralkaline melts show a more complex relationship between viscosity and chemical composition. The viscosity maximum is not shifted to the peralkaline field and the decrease in viscosity with addition of alkali is more pronounced than what is expected by a simple depolymerization process as defined by either the SM, or the NBO/T (Mysen, 1988) parameters. This decrease in viscosity correlates to the ratio AE/SM.

As already argued by Giordano and Dingwell (2003a, b), this anomalous behaviour might be explained using the notion that percolation channels in silicate melts affecttheir medium-range order. This notion has arisen from experimental studies (e.g., Brown et al., 1995; Greaves and Ngai, 1995; Poggemann et al., 2003) and supported by molecular dynamics simulations (e.g., Horbach et al., 2001; Meyer et al., 2002). It is possible that for strongly peralkaline melts, the depolymerization of the structure is accompanied by modifications in the configurations of the percolation channels leading to changes in the viscous regime of these melts. Additional data on strongly peraluminous natural melts and strongly peralkaline natural melts are necessary in order to further explore these interpretations.
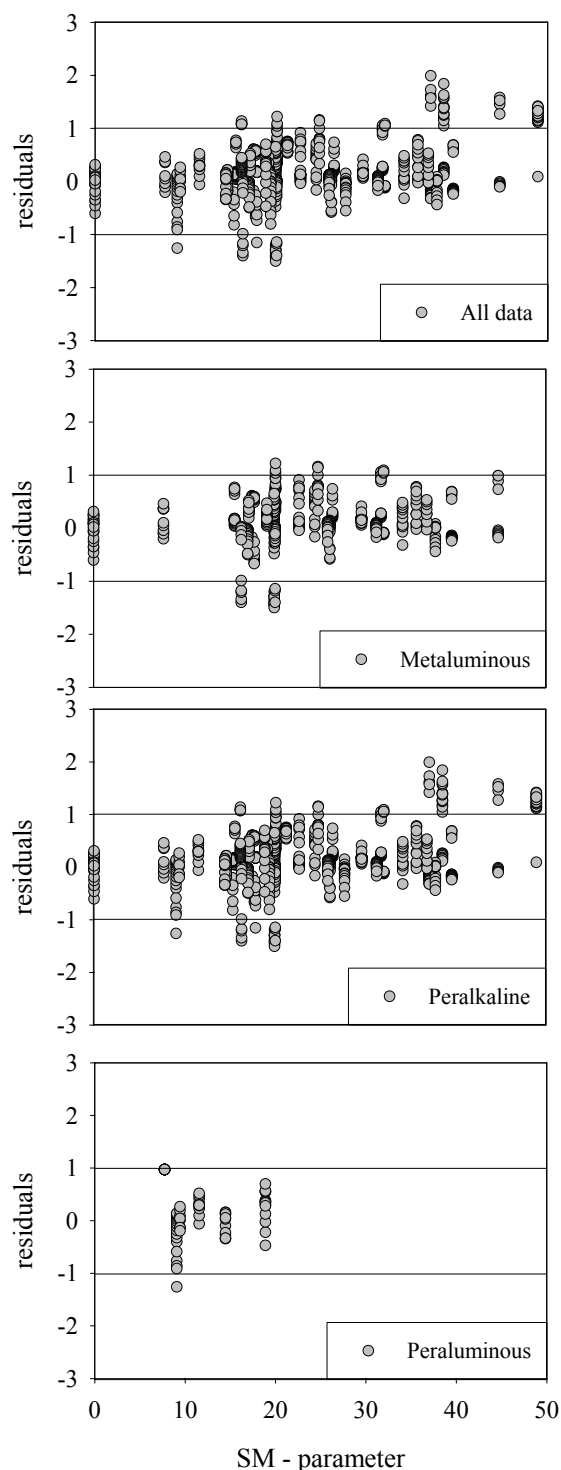
FIGURES 7.11. Residual viscosity values calculated according to Equations 7.7 - 7.11 vs the SM-parameter. Figures refer to all data together and separately to metaluminous, peralkaline and peraluminous melts. Figure shows that residuals increase toward higher values of the SM parameter. Lines in the figures constrain the 2σ interval.

8. Outlook

Based on the previous work on volume-temperature relationships of silicate and borosilicate melt properties, the following steps should be undertaken to improvie our understanding:

At the beginning of Chapter 4 it was discussed that existing multicomponent volumetric models are generally restricted to the major and minor oxide components present in naturally occurring igneous rocks. Clearly, there is a need for detailed studies and analysis of the material containing other trace elements. These elements might, for example, be useful in the petrogenetic modelling of magmatic differentiation where these elements are far more important than is apparent from their relative abundance in nature. Their partitioning behaviour as a function of phase composition, their temperature and pressure dependence as well as precise densitometry of silicates with high viscosity and high melting point, combined with in-situ spectroscopic measurements remain a challenge.

The supercooled liquid volumes and expansivity determined using the combined dilatometric/calorimetric method have confirmed that some binary and ternary systems have temperature independent thermal expansivities from the supercooled liquid temperature to the superliquidus temperature. However, in the AnDi system and the multicomponent natural samples studied here $\partial V/\partial T$ depends on temperature (Gottsmann and Dingwell, 2000; Knoche et al., 1994; Knoche et al., 1992b; Toplis and Richet, 2000). In addition, the change from a temperature independent thermal expansivity for wollastonite to a temperature dependent thermal expansivity for diopside (Knoche et al. 1992), despite similarity in degree of polymerisation and silica content, seems to be related to Mg content and its position in the silicate structure. A structural explanation for the temperature-dependent expansivity of AnDi melts is not yet available, further detailed investigation is required to develop a model.

This work also showed that there is a lack of precise densitometry data on Fe-bearing silicates at different $f\mathrm{O}_2$. I would like to urge more in-situ spectroscopic studies to be conducted on levitated Fe-bearing materials at different $f\mathrm{O}_2$ conditions. Such measurements might be combined with non-contact volumetric measurements. These measurements in scanning mode would help us to better understand the effect of the structural parameters on volumes and expansivities of silicate melts.

I would like also to challenge researchers to attempt further viscosity measurements on silicate melts containing volatile species (e.g. CO_2, SO_x, F, Cl), along with measurements of multiphase (liquid + crystals + vesicles) systems that are relevant in true volcanic scenarios.

Reference List

Adam, G. and Gibbs, J.H. (1965) On the temperature dependence of cooperative relaxation properties in glass-forming liquids. Journal of Chemical Physics, 43, 139-146.

Alibidirov, N., Dingwell, D.B., Stevenson, R.J., Hess, K-U, Webb, S.L., Zinke, J. (1997) Physical properties of the 1980 Mount St. Helens cryptodome magma. Bull. Volc. 59, 103-111.

Angell, C.A. (1985) Strong and fragile liquids. In Ngai, K.L., Wright, G.B., Eds., Relaxations in complex systems, p. 3-11. U.S. Department of Commerce National Technical Information Service, Springfield, Virginia.

Baker, D.R., Vaillancourt, J. (1995) The low viscosities of $F+H_2O$-bearing granitic melts and implications for melt extraction and transport. Earth Planet. Sci. Lett. 132, 199-211.

Bockris J. O. M., Tomlinson J. W., and White J. L. (1956) The structure of the liquid silicates: Partial molar volumes and expansivities. Transaction of the Faraday Society 53, 299-310.

Bottinga Y. (1985) On the isothermal compressibility of silicate liquids at high pressure. Earth and Planetary Science Letters 74(5), 350-360.

Bottinga, Y., Richet, P., Sipp, A. (1995) Viscosity regimes of homogeneous silicate melts. Am. Mineral. 80, 305-318.

Bottinga Y., Richet P., and Weill D. F. (1983) Calculation of the density and thermal expansion coefficient of silicate liquids. Bulletin de la Mineralgie 106, 129-138.

Bottinga Y. and Weill D. F. (1970) Densities of liquid silicate systems calculated from partial molar volumes of oxide components. American Journal of Science 269, 169-182.

Bottinga Y. and Weill, D. (1972) The viscosity of magmatic silicate liquids: a model for calculation. American Journal of Science, 272, 438-475.

Bottinga Y., Weill D., and Richet P. (1982) Density calculations for silicate liquids. - I. Revised method for aluminosilicate compositions. Geochimica et Cosmochimica Acta 46, 909-919.

Bouhifd, M.A., Whittington, A., Richet, P. (2001) Partial molar volume of water in phonolitic glasses and liquids. Contrib. Mineral. Petrol., 142, 235-243.

Bouhifd, M.A., Richet, P., Besson, P., Roskosz, M., Ingrin, J. (2004) Redox state, microstructure and viscosity of partially crystallized basalt melts. Earth Planet. Sci. Lett., 218, 31-34.

114

Brown, G.E., Farges, F., Calas, G. (1995) X-ray scattering and X-ray spectroscopy studies of silicate melts, Rev. Mineral. 32, 317-410

Calas, G., Cormier, L., Galoisy, L., and Jollivet, P. (2002a) Structure-property relationship in multicomponent oxide glasses. Comtes Rendus Chimie, 5, 831-843.

Cameron M., Sueno S., Prewitt C. T., and Papike J. J. (1973) High-Temperature Crystal-Chemistry of Acmite, Diopside, Hedenbergite, Jadeite, Spodumene, and Ureyite. American Mineralogist 58(7-8), 594-618.

Civetta, L., Orsi, G., Pappalardo, L., Fisher, R.V., Haiken, G., Ort, M. (1997) Geochemical zoning, mingling, eruptive dynamics and depositional processe.The Campanian Ignimbrite, Campi Flegrei caldera, Italy. J. Volcanol. Geoth. Res. 75, 183-219.

Cormier L., Neuville, D.R., and Calas, G. (2000). Structure and properties of low-silica calcium aluminosilicate glasses. Journal of Non-Crystalline Solids 274, 110-114.

Courtial P. and Dingwell D. B. (1995) Nonlinear composition dependence of molar volume of melts in the $CaO-Al_2O_3-SiO_2$ system. Geochimica et Cosmochimica Acta 59(18), 3685-3695.

Courtial P. and Dingwell D. B. (1999b) Densities of melts in the $CaO-MgO-Al_2O_3-SiO_2$ system. American Mineralogist 84, 465-476.

Courtial, P., and Dingwell, D.B. (2004) High-temperature density of lanthanide-bearing sodium silicate melts: Partial molar volumes for Ce_2O_3, Pr_2O_3, Nd_2O_3, Sm_2O_3, Eu_2O_3, Gd_2O_3, Tb_2O_3, Dy_2O_3, Ho_2O_3, Er_2O_3,Tm_2O_3 and Yb_2O_3. American Mineralogist, (submited).

Courtial, P., Gottsmann, J., Holzheid, A., Dingwell, D.B. (1999b). Partial molar volumes of NiO and CoO liquids: Implication for the pressure dependence of metal-silicate partitioning. Earth Planet. Sci. Lett., 171, 171-183.

Deino, A.L., Orsi, G., Piochi, M., de Vita, S. (2004) The age of the Neapolitan Yellow Tuff caldera-forming eruption Campi Flegrei caldera – Italy. assessed by 40Ar/39Ar dating method. J. Volcanol. Geoth. Res., 133, 157-170.

Della Mea, M., Gasparotto, A., Bettinelli, M., Montenero, A., and Scaglioni, R. (1986) Chemical durability of zinc-containing glasses. Journal of Non-Crystalline Solids, 84, 443-451.

Dingwell, D.B. (1991) The density of Titanium(IV) Oxide Liquid. Journal of the American Ceramic Society, 74(10), 2718-2719.

Dingwell, D.B. (1992) Density of some titanium-bearing silicate liquids and the compositional dependence of the partial molar volume of TiO_2. Geochimica et Cosmochimica Acta, 56, 3403-3407.

Dingwell, D.B. (1995) Relaxation in silicate melts: Applications. In J. Stebbins, P.F. McMillan and D.B. Dingwell, Eds., Structure, Dynamics and Properties of Silicate Melts, 32, 21-66. Reviews in Mineralogy, Mineralogical Society of America, Washington, D.C.

Dingwell, D.B., Brearley, M. (1988) Melt densities in the CaO-FeO-Fe_2O_3-SiO_2 system and the compositional dependence of the partial molar volume of ferric iron in silicate melts. Geochim. Cosmochim. Acta, 52, 2815-2825.

Dingwell, D.B., Brearley, M., Dickinson, J.E., Jr. (1988) Melt densities in the Na_2O-FeO-Fe_2O_3-SiO_2 system and the partial molar volume of tetrahedrally-coordinated ferric iron in silicate melts. Geochim. Cosmochim. Acta, 52, 2467-2475.

Dingwell, D.B., Hess, K.U., Romano, C. (1998a) Viscosity data for hydrous peraluminous granitic melts: Comparison with a metaluminous model. Am. Mineral. 83, 236-239.

Dingwell, D.B., Hess, K.U., Romano, C. (1998b) Extremely fluid behaviour of hydrous peralkaline rhyolites. Earth Planet. Sci. Lett. 158, 31-38

Dingwell, D.B., Hess, K.U, Romano, C. (2000) Viscosities of granitic sensu lato.: Influence of the anorthite component. Am. Mineralogist. 85, 1342-1348

Dingwell, D.B., Romano, C., Hess, K.U. (1996) The effect of water on the viscosity of a haplogranitic melt under P-T-X- conditions relevant to silicic volcanism. Contrib. Mineral. Petrol. 124, 19-28.

Dingwell, D.B., Virgo, D. (1988) Melt viscosities in the Na_2O-FeO-Fe_2O_3-SiO_2 system and factors controlling the relative viscosities of fully polymerised silicate melts. Geochim. Cosmochim. Acta 52, 395-403.

Dingwell, D.B., Webb, S.L. (1989) Structural Relaxations in Silicate Melts and Non-Newtonian Melt Rheology in Geologic Processes. Physics and Chemistry of Minerals, 16, 508-516.

Dingwell, D.B., Webb, S.L. (1990) Relaxations in silicate melts. European J.Mineral. 2, 427-449.

Di Vito, M.M., Isaia, R., Orsi, G., Southon, J., de Vita, S., D'Antonio, M., Pappalardo, L., Piochi, M. (1999) Volcanism and deformation since 12,000 years at the Campi Flegrei caldera Italy. J. Volcanol. Geoth. Res. 91, 221-246

Doroshev, A.M., Olesch, M., Logvinov, V.M., and Malinovsky, I.J. (1983) High pressure stability of zinc clinopyroxene $ZnSiO_3$ and the occurrence of a new polytype of zinc orthosilicate Zn_2SiO_4 as a breakdown product. Neues Jahrbuch für Mineralogie, 6, 277-288.

Dumas, T., and Petiau, J. (1986) EXAFS study of titanium and zinc environments during nucleation in a cordierite glass. Journal of Non-Crystalline Solids, 81, 201-220.

Ehlers E. G. (1972) The interpretation of geological phase diagrams, 280.

Ennas, G., Musinu, A., Piccaluga, G., Montenero, A., and Gnappi, G. (1990) Structure and chemical durability of zinc-containing glasses. Journal of Non-Crystalline Solids, 125, 181-185.

Essene, E.J., and Peacor, D.R. (1987) Petedunnite ($CaZnSi_2O_6$), anew zinc clinopyroxene from Franklin, New Jersey, and phase equlibria for zincian pyroxenes. American Mineralogist, 72, 157-166.

Fehr, K.T., and Hobelsberger, B. (1997) Experimentelle Bestimmung der chemischen Potentiale von Hedembergit in der Mischreihe Hedenbergit-Petedunnite. Beiheft zum European Journal of Mineralogy, 9, 98.

Fehr, K.T., and Huber, A.L. (2001) Stability and phase relations of $Ca[ZnSi_3]O_8$, a new phase with feldspar structure in the system $CaO-ZnO-SiO_2$. American Mineralogist, 86, 21-28.

Frenkel, Y.I. (1959) The kinetic theory of liquids. Selected works, Vol. 3 [in Russian], Izd. Akad. Nauk SSSR, Moscow-Leningrad

Fulcher, G.S. (1925) Analysis of recent measurements of the viscosity of glasses. J. Am. Ceramic Soc. 8, 339-355.

Galoisy, L., Cormier, L., Calas, G., and Briois, V. (2001) Environment of Ni, Co and Zn in low alkali borate glasses: information from EXAFS and XANES spectra. Journal of Non-Crystalline Solids, 293-295, 105-111

Gentile A. L. and Foster W. R. (1963) Calcium hexaluminate and its stability relations in the system $CaO-Al_2O_3-SiO_2$. Journal of American Ceramic Society 46, 74-76.

Ghiorso M.S., and Kress V.C., 2004, An Equation of State for Silicate Melts. II. Calibration of volumetric properties at 105 Pa, American Journal of Science 304, 679-751

Glasstone, S., Laidler, K., Eyring, H. (1941) Theory of Rate Processes, McGraw-Hills, New York.

Greaves, G.N., Ngai, K.L. (1995) Reconciling ionic-transport properties with atomic structure in oxide glasses. Phys. Rev. B 52, 6358-6380.

Grillot, H., Béguinot, J., Boucetta, M., Rouquette, C., Sima, A. (1964) Méthode d´analyse quantitative appliquées aux roches et aux prélèvements de la prospection géochemique. Mémoire du BRGM, 30, 3319.

Gottsmann J. and Dingwell D. B. (2000) Supercooled diopside melt: confirmation of temperature-dependent expansivity using container-based dilatometry. Contributions to Mineralogy and Petrology 139, 127-135.

Gottsmann J. and Dingwell D. B. (2002) Thermal expansivities of supercooled haplobasaltic liquids. Geochimica et Cosmochimica Acta 66(12), 2231-2238.

Gottsmann J., Dingwell D. B., and Gennaro C. (1999) Thermal expansion of silicate liquids: Direct determination using container-based dilatometry. American Mineralogist 84, 1176-1180.

Haermon J. (1979) The elastic constant of crystals an other anisotropic materials, in Landolt-Börnstein tables. 1-244.

Hazen R. M. (1976) Effects of Temperature and Pressure on Cell Dimension and X-Ray Temperature Factors of Periclase. American Mineralogist 61(3-4), 266-271

Herzberg C. T. (1987) Magma density at high pressure Part 1: The effect of composition on the elastic properties of silicate liquids. The Geochemical Society: Special Publication No.1, 25-46.

Hess, K.U., Dingwell, D.B. (1996) Viscosities of hydrous leucogranitic melts: A non-Arrhenian model. Am. Mineral. 81, 1297-1300

Hess, K.U., Dingwell, D.B., Gennaro, C., Mincione, V. (2001) Viscosity-temperature behaviour of dry melts in the Qz-Ab-Or system. Chem. Geol. 174, 133-142.

Hess, K.U., Dingwell, D.B. & Rossler, E. (1996) Parameterization of viscosity-temperature relations of aluminosilicate melts. Chemical Geology, 128, 155-163.

Hess, K.U., Dingwell, D.B. and Webb, S.L. (1995) The Influence of Excess Alkalis on the Viscosity of a Haplogranitic Melt. American Mineralogist, 80(3-4), 297-304.

Hodge, I.M. (1994) Enthalpy relaxation and recovery in amorphous materials. J. Non-Crystal. Solids, 169, 211-266.

Holzapfel, C., Courtial, P., Dingwell, D.B., Chakraborty, S., and Palme, H. (2001) Experimental determination of partial volumes of Ga_2O_3 and GeO2 in silicate melts: implication for the pressure dependence of metal-silicate partion coefficients. Chemical Geology, 174, 33-49.

Horbach, J., Kob, W., Binder, K. (2001) Structural and dynamical properties of sodium silicate melts: an investigation by molecular dynamics computer simulation. Chem. Geol. 174, 87-102.

Hummel, W., Arndt, J. (1985) Variation of viscosity with temperature and composition in the plagioclase system. Contrib. Mineral. Petrol. 90, 83-92.

Hurt, J.C., and Phillips, C.J. (1971) Structual Role of Zinc in Glasses in the System Na_2O-ZnO-SiO_2. Journal of American Ceramic Society, 53, 269-273.

Knoche R., Dingwell D. B., Seifert F. A., and Webb S. L. (1994) Non-linear properties of supercooled liquids in the system Na_2O-SiO_2. Chemical Geology 116(1-2), 1-16.

Knoche R., Dingwell D. B., and Webb S. L. (1992a) Non-linear temperature dependence of liquid volumes in the system albite-anorthite-diopside. Contributions to Mineralogy and Petrology 111, 61-73.

Knoche, R., Dingwell, D.B., Webb, S.L. (1992b) Temperature-dependent thermal expansivities of silicate melts: The system anorthite-diopside. Geochim. Cosmochim. Acta, 56, 689-699.

Knoche, R., Dingwell, D.B., and Webb, S.L. (1995) Melt densities for leucogranites and granitic pegmatites: Partial molar volumes for SiO_2, Al_2O_3, Na_2O, K_2O, Li_2O, Rb_2O, Cs_2O, MgO, CaO, SrO, BaO, B_2O_3, P_2O_5, F_2O_{-1}, TiO_2, Nb_2O_5, Ta_2O_5, and WO_3. Geochimica et Cosmochimica Acta, 59(22), 4645-4652.

Kress, V.C., Carmichael, I.S.E. (1991) The compressibility of silicate liquids containing Fe_2O_3 and the effect of composition, temperature, oxygen fugacity and pressure on their redox states. Contrib. Mineral. Petrol., 108, 82-92.

Lange R. A. (1996) Temperature independent thermal expansivities of sodium aluminosilicate melts between 713 and 1835 K. Geochimica et Cosmochimica Acta 60(24), 4989-4996.

Lange R. A. (1997) A revised model for the density and thermal expansivity of K_2O-Na_2O-CaO-MgO-Al_2O_3-SiO_2 liquids from 700 to 1900 K: extension to crustal magmatic temperatures. Contributions to Mineralogy and Petrology 130, 1-11.

Lange R. A. and Carmichael I. S. E. (1987) Densities of Na_2O-K_2O-CaO-MgO-FeO-Fe_2O_3-Al_2O_3-TiO_2-SiO_2 liquids: New measurements and derived partial molar properties. Geochimica et Cosmochimica Acta 51, 2931-2946.

Lee S. K. and Stebbins J. F. (1999a) Al-O-Al oxygen sites in crystalline aluminates and aluminosilicate glasses: High-resolution oxygen-17 NMR results. American Mineralogist 84, 983-986.

Lee S. K. and Stebbins J. F. (1999b) The degree of aluminum avoidance in aluminosilicate glasses. American Mineralogist 84, 937-945.

Le Grand, M., Ramos, A.Y., Calas, G., Galoisy, L., Ghaleb, D., and Pacaud, F. (2000) Zinc environment in aluminoborosilicate glasses by Zn K-edge extended x-ray absorption fine structure spectroscopy. Journal of Material Research, 15(9), 2015-2019.

Lepage Y., Calvert L. D., and Gabe E. J. (1980) Parameter Variation in Low-Quartz between 94 and 298k. Journal of Physics and Chemistry of Solids 41(7), 721-725.

Liu Q. and Lange R. A. (2001) The partial molar volume and thermal expansivity of TiO_2 in alkali silicate melts: Systematic variation with Ti coordination. Geochimica et Cosmochimica Act. 65(14), 2379-+2393.

Loewenstein W. (1954) The distribution of aluminum in the tetrahedra of silicates and aluminates. American Mineralogist 39, 92-96.

Maier C. G. and Kelley K. K. (1932) An equation for the representation of high temperature heat content data. Journal of American Ceramic Society 54, 3243-3345.

Mangiacapra, A., Giordano, D., Potuzak, M., Dingwell, D. B., (2005a) Modelling non-Arrhenian multicomponent melt viscosity: the effect of the iron oxidation state (in progress)

Mangiacapra, A., Di Matteo, V., Giordano, D., Nichols, A.R.L., Dingwell, D.B., Orsi, G. (2005b) Water and the viscosity of shoshonitic and latitic melts (in progress)

Meyer, A., Schober, H., Dingwell, D.B. (2002) Structure, structural relaxation and ion diffusion in sodium disilicate melts Eur. Lett. 59, 708-713.

Moynihan C. T., Easteal A. J., Tran D. C., Wilder J. A., and Donvan E. P. (1976) Heat Capacity and Structural Relaxation of Mixed-Alkali Glasses. Journal of the American Ceramic Society 59(3-4), 137-140.

Moynihan, C.T., Grupta, P.K. (1978) Order parameter for structural relaxation in glass. J. Non-Crystal. Solids, 29(2), 143-158.

Murdoch J. B., Stebbins J. F., and Carmichael I. S. E. (1985) High-resolution Si-29 NMR-study of silicate and aluminosilicate glasses - the effect of network-modifying cations. American Mineralogist 70, 332-343.

Mysen B.O. (1988) Structure and properties of silicate melts. Elsevier Science Publishers B.V., Amsterdam. 354 pp.

Myuller, R.L. (1955) A valence theory of viscosity and fluidity for high-melting glass-forming materials in the critical temperature range. Zh. Prikl. Khim. 28, 1077-1087.

Narayanaswamy, O.S. (1971) A model of structural relaxation in glass. J. Am. Ceramic Soc., 54(10), 491-498.

Nelson S. A. and Carmichael I. S. E. (1979) Partial Molar Volumes of Oxide Components in Silicate Liquids. Contribution to Mineralogy and Petrology 71, 117-124.

Neuville, D. (1992) Proprietes thermodynamiques et rheologiques des silicates fondus Translated Title: Rheologic and thermodynamic properties of silicates melts.

Neuville, D.R., Courtial, P., Dingwell, D.B., Richet, P. (1993) Thermodynamic and rheological properties of rhyolite and andesite melts. Contib. Mineral. Petrol. 113, 572-581.

Ohlhorst, S., Behrens, Holtz, F. (2001) Compositional dependence of molar absorptivities of near-infrared OH- and H_2O bands in rhyolitic to basaltic glasses. Chem. Geol. 174, 5-20.

Osborn E. F. and Muan A. (1960) Phase equilibrium diagram of oxide systems. The system CaO-Al_2O_3-SiO_2. Plate1. The American Ceramic Society and the Edward Orto Jr. Ceramic Foundation. Columbus, Ohio.

Ottonello, G., Moretti, R., Marini, L., Zuccolini, M. V. (2001) Oxidation state of iron in silicate glasses and melts: a thermochemical model. Chem. Geol., 174, 157-179.

Pacltová, B., Žert, B. (1958) Oligocenní pylové společenstvo v nadloží čedičového výlevu v Chebské pánvi. Věstník ÚÚG, 33, 350-353.

Poggemann, J.F., Heide, G., Frischat, G.H. (2003) Direct view of the structure of different glass fracture surfaces by atomic force microscopy. J. Non-cryst. Solids 326/327, 15-20.

Persikov, E.S. (1991) The viscosity of magmatic liquids: experiment generalized patterns, a model for calculation and prediction, applications. In Physical Chemistry of Magmas, Advances in Physical Chemistry eds., Perchuk, L.L., Kushiro, I., Springer Berlin, pp. 1-40.

Reznichenko, S.V., Belousova, V.Yu., Zemlyanoi, K.G. (2002) The viscosity of molten material in pores and capillary channels of the matrix phase of high-alumina castables employed in thermal power units of ferrous metallurgy. 1. viscosity analysis of melts in the $CaO - Al_2O_3 - FeO - Fe_2O_3 - SiO_2$ system. Refractories and Industrial Ceramics 46,167-171

Richet, P. (1984) Viscosity and configurational entropy of silicate melts. Geochimica et Cosmochimica Acta, 48, 471-483.

Richet, P. (1987) Heat Capacity of Silicate glasses. Chemical Geology 62, 111-124.

Richet, P. and Bottinga, Y. (1995) Rheology and configurational entropy of silicate melts. In: J.F. Stebbins, P.F. McMillan and D.B. Dingwell (Editors), Structure, dynamics and properties of silicate melts. Reviews in Mineralogy. Mineralogical Society of America, Washington, DC, United States, pp. 67-93.

Richet, P., Lejeune, A.M., Holtz, F., Roux, J. (1996) Water and the viscosity of andesite melts. Chem. Geol. 128, 185-197.

Richet, P.., Robie R. A., and Hemingway B. S. (1993) Entropy and structure of silicate glasses and melts. Geochimica et Cosmochimica Acta 57, 2751-2766.

Rekhson, S.M., Bulaeva, A.V., Mazurin, O.V. (1971) Changes in the linear dimensions and viscosity of window glass during stabilization. Inorganic Material (Engl. Trans), 7, 622-623.

Rivers, M.L., Carmichael, I.S.E. (1987) Ultrasonic Studies of Silicate Melts. J. Geophys. Res., 92(B9), 9247-9270.

Robie R. A., Hemingway B. S., and Fisher J. R. (1979) Thermodynamic properties of minerals and related substances at 298.5 K and 1 bar (10^5) Pascals and at higher temperatures. 456.

Roy B.N. and Navrotsky A. (1984) Thermochemistry of charge-coupled substitutions in silicate glasses: - The systems $M_{1/n}{}^{n+} AlO_2-SiO_2$ (M=Li, Na, K, Rb, Cs, Mg, Ca, Sr, Ba, Pb). J. Am. Ceram. Soc. 67, 606-610.

Rosenthal, A.B., and Garofalini, S.H. (1987) Structural Role of Zinc Oxide in Silica and Soda-Silica Glasses. Journal of American Ceramic Society, 70(11), 821-826.

Russell, J.K., Giordano, D. (2005) A model for silicate melt viscosity in the system $CaMgSi_2O_6-CaAl_2Si_2O_8-NaAlSi_3O_8$. Geochim. Cosmochim. Acta, in press.

Russell, J.K., Giordano, D., Dingwell, D.B., Hess, K.U. (2002) Modelling the non-Arrhenian rheology of silicate melts: Numerical considerations. Eur. J. Mineral. 14, 417-427.

Russell, J.K., Giordano, D., Dingwell, D.B. (2003) High-temperature limits on viscosity of non-Arrhenian silicate melts. Am. Mineral. 88, 1390-1394.

Sasabe, H., DeBolt, M.A., Macedo, P.B., Moynihan, C.T. (1977) Structural relaxation in an alkali-lime-silicate glass. *in* Proceedings of the 11th International Congress on Glass, Prague, 1, 339-348.

Sasaki S., Takeuchi Y., Fujino K., and Akimoto S. (1982) Electron-Density Distributions of 3 Orthopyroxenes, $Mg_2Si_2O_6$, $Co_2Si_2O_6$, and $Fe_2Si_2O_6$. Zeitschrift Fur Kristallographie 158(3-4), 279-297.

Sato R.K., McMillan, P.F., Dennison, P., and Dupree, R. (1991). A structural investigation of high alumina glasses in the CaO-Al$_2$O$_3$-SiO$_2$ system via Raman and magic angle spinning nuclear magnetic resonance spectroscopy. Physics and Chemistry of Glasses 32(4), 149-156.

Segnit, E.R. (1954) The system CaO-ZnO-SiO$_2$. Journal of The American Ceramic Society, 37, 273-277.

Stein, D.J., Stebbins, J.F., and Carmichael, I.S.E. (1986) Density of Molten Sodium Aluminosilicates. Journal of The American Ceramic Society, 69(5), 396-399.

Scherer, G.W. (1984) Use of the Adam-Gibbs Equation in the Analysis of Structural Relaxation. J. Am. Ceramic Soc., 67(7), 504-511.

Scherer, G.W. (1986) Volume Relaxation Far from Equilibrium. J. Am. Ceramic Soc., 69(5), 374-381.

Shaw, H.R. (1972) Viscosities of magmatic silicate liquids: An empirical model of prediction. Am. J. Sci. 272, 438-475.

Sipp A. (1998) Propriétés de relaxation des silicates vitreux et fondus. PhD thesis. Université Paris VII, 231.

Sipp A., Richet P. (2002) Equivalence of the kinetics of volume, enthalpy and viscosity relaxation in glass forming silicate liquids. J. Non-cryst Solids, 298, 202-212.

Solvang M., Yue Y. Z., Jensen S. L., and Dingwell D. B. (2004) Rheological and thermodynamic behaviors of different calcium aluminosilicate melts with the same non-bridging oxygen content. Journal of Non-Crystalline Solids 336, 179-188.

Solvang M., Yue Y. Z., Jensen S. L., and Dingwell D. B. (2005) Rheological and thermodynamic behavior of calcium aluminosilicate melts within the anorthite-wollastonite-gehlenite compatibility triangle. Journal of Non-Crystalline Solids 351, 499-507.

Stebbins J. F. and Xu Z. (1997) NMR Evidence for Excess Non-Bridging Oxygen in an Aluminosilicate Glass. Nature 390, 60.

Tammann, G. and Hesse, W. (1926) Die Abhängigkeit der Viskosität von der Temperatur bei unterkühlten Flüssigkeiten. Zeitschrift für anorganische und allgemeine Chemie, 156: 245-257.

Tangeman J. A. and Lange R. A. (2001) Determination of the limiting fictive temperature of silicate glasses from calorimetric and dilatometric methods: Application to the low-temperature liquid volume measurements. American Mineralogist 86, 1331-1344.

Tool A. Q. and Eichlin C. G. (1931) Variation caused in the heating curves of glass by heat treatment. Journal of the American Ceramic Society 14, 276-308.

Toplis M. J. and Dingwell D. B. (2004) Shear viscosities of $CaO-AL_2O_3-SiO_2$, and $MgO-Al_2O_3-SiO_2$ liquids: Implications for the structural role of aluminium and the degree of polymerisation of synthetic and natural aluminosilicate melts. Geochimica et Cosmochimica Acta 68(24), 5169-5188.

Toplis, M.J., Dingwell, D.B., Hess, K-U., Lenci, T. (1997) Viscosity, fragility, and configurational entropy of melts along the join $SiO2-NaAlSiO4$. American Mineralogist 82, 979-990.

Toplis, M.J., Dingwell, D.B., and Libourel, G. (1994) The effect of phosphorus on the iron redox ratio, viscosity, and density of an evolved ferro-basalt. Contributions to Mineralogy and Petrology, 117(3), 293-304.

Toplis M. J. and Richet P. (2000) Equilibrium density and expansivity of silicate melts in the glass transition range. Contribution to Mineralogy and Petrology 139, 672-683.

Toyoda, S., Fujino, S., and Morinaga, K. (2003) Density, viscosity and surface tension of $50RO-50P_2O_5$(R: Mg, Ca, Sr, Ba, and Zn) glass melts. Journal of Non-Crystalline Solids, 321, 169-174.

Vogel, H. (1921) Temperaturabhängigkeitsgesetz der Viskosität von Flüssigkeiten. Physikalische Zeitschrift, 22: 645-646.

Wilson, A.D. (1960) The Micro-determiantion of Ferrous Iron in Silicate Minerals by a Volumetric and Colorimetric Method. Analyt., 85, 823-827.

Whittington, A., Richet, P., Linard, Y., Holtz, F. (2000) Water and the viscosity of depolymerised aluminosilicate melts. Geochim. Cosmochim. Acta 64, 3725-3736.

Whittington, A., Richet, P., Linard, Y., Holtz, F. (2001) The viscosity of hydrous phonolites and trachytes. Chem. Geol. 174, 209-223.

Webb S. L. (1992) Shear, volume, enthalpy and structural relaxation in silicate melts. Chemical Geology 96, 449-457.

Webb, S. L. and Knoche, R. (1995) The glass transition, structural relaxation and shear viscosity of silicate melts. Chemical Geology, 128, 165-183.

Webb S. L., Knoche R., and Dingwell D. B. (1992) Determination of silicate liquid thermal expansivities using dilatometry and calorimetry. European Journal of Mineralogy 4, 95-104.

Webb, S.L., Müller, E., Büttner, H. (2004) Anomalous rheology of peraluminous melts Am. Mineral. 89, 812-818.

APPENDIX

TABLE 4.1.
Analyzed compositions* of the investigated materials (wt%)

Samples	SiO_2	Al_2O_3	Na_2O	CaO	MgO	ZnO	gfw #
NS2 (Courtial et al. 1999)							
NOM	66.37(0.44)	-	31.95(0.35)	-	-	-	60.69
HT	66.59(0.31)		31.98(0.20)				60.69
LT	66.44(0.41)		31.33(0.31)				60.68
NS2+1mol%							
NOM	65.09	-	33.58	-	-	1.34	60.92
HT(9)	67.19(0.95)		31.09(0.98)			1.72(0.14)	60.94
AS(21)	66.24(1.71)		32.32(1.69)			1.45(0.13)	60.92
NS2+5mol%							
NOM	61.62	-	31.79	-	-	6.59	61.75
HT(30)	63.87(1.36)		29.03(1.33)			7.10(0.33)	61.78
AS(20)	62.61(1.17)		30.57(0.86)			6.82(0.48)	61.77
NS2+25mol%							
NOM	45.59	-	23.52	-	-	30.89	65.89
HT(39)	45.63(1.01)		24.08(0.74)			30.29(0.64)	65.79
AS(21)	44.58(0.97)		26.081(0.61)			29.34(0.58)	65.65
AnDi							
NOM	50.33	15.37	-	23.50	10.80	-	59.69
HT							
AS							
AnDi+1mol%							
NOM	49.65		-	23.18	10.65	1.36	59.90
HT(10)	50.27(0.51)	14.63(0.19)		23.24(0.22)	10.31(0.29)	1.54(0.13)	59.90
AS(18)	50.21(0.54)	14.69(0.25)		23.33(0.21)	10.32(0.29)	1.45(0.18)	59.89
AnDi+5mol%							
NOM	46.96	14.34	-	21.93	10.08	6.70	60.77
HT(26)	47.60(0.51)	13.51(0.25)		21.96(0.27)	9.90(0.21)	7.02(0.55)	60.67
AS(20)	47.61(0.51)	12.89(0.23)		22.42(0.23)	9.93(0.23)	7.15(0.32)	60.50
AnDi+20mol%							
NOM	37.53	11.46	-	17.53	8.05	25.43	64.03
HT(51)	38.16(0.66)	10.07(0.23)		18.01(0.23)	8.13(0.21)	25.64(0.67)	63.63
AS(20)	38.48(1.98)	10.47(0.56)		18.14(0.94)	8.00(0.44)	24.92(3.80)	63.65
Zn-Diopside							
NOM	46.65		-	21.76	-	31.59	64.42
HT(10)	46.45(0.64)			21.88(0.17)		31.67(0.66)	64.42
AS(20)	46.55(0.60)			22.03(0.31)		31.42(0.56)	64.37

*Analyses made with an automated Cameca SX 50 electron microprobe operated at 15 kV and 15nA with a defocused beam. The number within parentheses represent the error based on the standard deviation of the replicate analyses.

NOM=nominal composition AS=composition after synthesis, HT= composition and after high-temperature densitometry experiments, The number within parentheses represent the number of analyses.

#gfw = gram formula weight.

TABLE 4.2.

Experimental density results (g.cm^{-3}) of the investigated materials at room temperature (RT) and high-temperature (stable melts).

Sample	T (K)	ρ (g.cm^{-3})
AnDi	1840	2.591 (0.010)
	1793	2.595 (0.004)
	1746	2.602 (0.006)
	1696	2.613 (0.008)
	1639	2.617 (0.012)
	1594	2.626 (0.005)
	1542	2.630 (0.006)
	1496	2.648 (0.007)
RT	297.96	2.7351 (0.0003)
AnDi	1842	2.596 (0.008)
(Holzapfel et al. 2001)	1793	2.601 (0.006)
	1745	2.615 (0.006)
	1698	2.615 (0.004)
	1651	2.629 (0.008)
	1605	2.6324 (0.0071)
AnDi	1873	2.590
(Lange & Carmichael 1987)	1773	2.605
	1673	2.622
	1573	2.636
AnDi + 1mol%	1850	2.621 (0.013)
	1653	2.648 (0.009)
	1555	2.649 (0.007)
	1507	2.661 (0.012)
RT	298.65	2.7955 (0.0025)
AnDi + 5mol%	1822	2.698 (0.009)
	1729	2.726 (0.007)
	1637	2.733 (0.010)
	1501	2.751 (0.016)
RT	298.65	2.8803 (0.0017)
AnDi + 20mol%	1828	2.972 (0.011)
	1733	3.006 (0.011)
	1640	3.025 (0.011)
	1547	3.037 (0.011)
	1455	3.058 (0.010)
RT	298.65	3.2185 (0.0011)

Note: The numbers within parentheses represent the errors based on the standard deviation of three replicate mass determination by using buoyancy measurements for each bob for the high-temperature densitometry.
*Stable liquid densities of the AnDi were also calculated by using Lange and Carmichael (1987) model and the measurements of Holzapfel et al., (2001) are also listed.

TABLE 4.3.

Experimental density results (g.cm^{-3}) of the investigated materials at room temperature (RT) and high-temperature (stable melts).

Sample	T (K)	ρ (g.cm^{-3})
NS2	1637	2.226 (0.010)
(Courtial et al.1999)	1541	2.255 (0.013)
	1447	2.277 (0.015)
	1400	2.285 (0.015)
	1353	2.290 (0.019)
RT	298	2.4915 (0.0015)
NS2	1873	2.166
(Lange & Carmichael 1987)	1773	2.185
	1673	2.205
	1573	2.225
NS2 + 1mol%	1558	2.260 (0.005)
	1505	2.271 (0.003)
	1460	2.281 (0.004)
	1412	2.294 (0.004)
	1363	2.299 (0.005)
RT	297.15	2.5164 (0.0008)
NS2 + 5mol%	1556	2.325 (0.006)
	1509	2.337 (0.009)
	1463	2.348 (0.007)
	1417	2.359 (0.006)
	1371	2.363 (0.009)
RT	297.15	2.5859 (0.0001)
NS2 + 25mol%	1556	2.759 (0.007)
	1509	2.770 (0.006)
	1463	2.784 (0.005)
	1417	2.795 (0.005)
	1371	2.811 (0.005)
RT	297.15	3.0243 (0.0002)
Zn - Diopside	1816	3.045 (0.008)
	1723	3.069 (0.009)
	1631	3.090 (0.010)
	1540	3.110 (0.010)
	1450	3.132 (0.010)
RT	298.05	3.3032 (0.0005)

Note: The numbers within parentheses represent the errors based on the standard deviation of three replicate mass determination by using buoyancy measurements for each bob for the high-temperature densitometry.
*Stable liquid densities of the NS2 were also calculated by using Lange and Carmichael (1987) model and the measurements of Courtial et al. (1999) are also listed.

TABLE 4.4.
Linear fit parameters of the experimental density (g.cm^{-3}) of the investigated melts as a function of absolute temperature $\rho_{liquid}(T) = A^{density} + B^{density}\,T(K)$ within temperature range investigated (ΔT).

Samples	$A^{density}$ (intercept density)	$B^{density}$ x 10^{-4} (g.cm^{-3}.K)	R^2	ΔT (K)
AnDi	2.8751	-1.5554	0.96752	1840-1496
AnDi (*Holzapfel et al. 2001*)	2.8913	-1.6045	0.96452	1842-1605
AnDi (*Lange & Carmichael 1987*)	2.8804	-1.5479	0.99958	1773-1573
AnDi+1mol%	2.8219	-1.0795	0.94095	1850-1507
AnDi+5mol%	2.9864	-1.5514	0.93050	1822-1501
AnDi+20mol%	3.3772	-2.1799	0.96961	1828-1455
NS2 (*Courtial et al.1999*)	2.6041	-2.2872	0.97749	1637-1353
NS2 (*Lange & Carmichael 1987*)	2.5312	-1.9458	0.99993	1873-1573
NS2+1mol%	2.5860	-2.0899	0.98592	1558-1363
NS2+5mol%	2.6569	-2.1220	0.97757	1556-1371
NS2+25mol%	3.1923	-2.7917	0.99564	1556-1371
Diopside (*Knoche et al. 1992b*)	2.9138	-1.6500	0.99989	1895-1695
Diopside (*Lange & Carmichael 1987*)	2.9230	-1.6840	0.99874	1873-1573
Zn-Diopside	3.4727	-2.3499	0.99928	1816-1450

TABLE 4.5.
Linear fit parameters of the experimental molar volume of the investigated melts as a function of absolute temperature $V_{liquid}(T) = a_{vol} + b_{vol}\,T(K)$ within temperature range investigated (ΔT).

Samples	A^{volume} (intercept molar volume)	B^{volume} x 10^{-3} (cm^3.mol^{-1}.K)	R^2	ΔT (K)
AnDi	20.559	1.3554	0.96906	1840-1496
AnDi (*Holzapfel et al. 2001*)	20.485	1.4060	0.96440	1842-1605
AnDi (*Lange & Carmichael 1987*)	20.507	1.3526	0.99949	1773-1573
AnDi +1mol%	21.127	0.9284	0.94116	1850-1507
AnDi +5mol%	20.164	1.2693	0.92765	1822-1501
AnDi +20mol%	18.689	1.5349	0.96697	1828-1455
NS2 (*Courtial et al.1999*)	22.764	2.7205	0.97544	1637-1353
NS2 (*Lange & Carmichael 1987*)	23.431	2.4502	0.99994	1873-1573
NS2 +1mol%	23.135	2.4491	0.98555	1558-1363
NS2 +5mol%	22.831	2.3833	0.97666	1556-1371
NS2 +25mol%	20.198	2.3726	0.99618	1556-1371
Diopside (*Knoche et al. 1992b*)	18.406	1.3084	0.99980	1895-1695
Diopside (*Lange & Carmichael 1987*)	18.361	1.3202	0.99852	1873-1573
Zn-Diopside	18.264	1.5872	0.99897	1816-1450

TABLE 4.6.
Regression fit parameters* provided on samples molar composition (after HT measurements).

i	$V_{i, 1300}$	$\partial V_i/\partial T \, x10^{-3}$
NS2	26.470 (0.061)	2.525 (0.5)
ZnO	13.482 (0.453)	1.642 (3.7)
R^2	0.99628	
Adjusted R^2	0.99140	
S	0.1240	
	$V_{i, 1300}$	$\partial V_i/\partial T \, x10^{-3}$
AnDi	22.331 (0.027)	1.131 (0.1)
ZnO	13.438 (0.248)	2.943 (0.8)
R^2	0.99436	
Adjusted R^2	0.99351	
S	0.0585	
i	$V_{i, 1300}$	$\partial V_i/\partial T \, x10^{-3}$
SiO_2	25.099 (0.356)	0.000 (1.2)
Al_2O_3	39.754 (0.774)	0.000 (2.6)
MgO	11.850 (0.700)	4.171 (2.3)
CaO	16.540 (0.415)	4.178 (1.4)
Na_2O	29.214 (0.900)	7.176 (4.9)
ZnO	14.141 (0.730)	2.836 (1.8)
R^2	0.96765	
Adjusted R^2	0.96473	
S	0.3897	

Fit parameters derived from separate regressions for four liquids in the binary ZnO - $Na_2Si_2O_5$ system (NS2) and four liquids in the binary ZnO - $CaAl_2Si_2O_8$-$CaMgSi_2O_6$ system ($An_{42}Di_{58}$). Fit parameters for multi-component system were calculated using all our HT density data (i.e., NS2-ZnO, AnDi-ZnO, and petedunnite) and the HT density data from Lange and Carmichael, (1987, i.e., samples LC2-15) and all HT density data from Courtial and Dingwell (1995, 1999a).

TABLE 5.1.
Composition of the investigated CAS samples reported as wt% and normalized mol% of oxides.

Samples	SiO_2 (wt%)	Al_2O_3 (wt%)	CaO (wt%)	Total	SiO_2 (mol%)	Al_2O_3 (mol%)	CaO (mol%)	NBO/T	gfw (g mol^{-1})
CAS1	47.7	13.5	38.1	99.3	49.44	8.25	42.31	1.03	61.843
CAS2	43.4	16.9	39.0	99.3	45.62	10.47	43.92	1.01	62.709
CAS3	38.8	20.2	40.4	99.4	41.28	12.66	46.05	1.00	63.544
CAS4	34.6	23.2	41.5	99.3	37.31	14.74	47.95	0.99	64.338
CAS5	30.3	25.6	43.3	99.2	33.02	16.44	50.55	1.04	64.943
CAS6	45.8	23.6	30.1	99.5	49.81	15.12	35.07	0.50	65.013
CAS7	40.0	26.8	32.6	99.4	44.09	17.41	38.50	0.54	65.833
CAS8	35.4	30.3	33.9	99.6	39.52	19.93	40.55	0.52	66.808
CAS9	30.6	33.6	35.0	99.2	34.81	22.53	42.66	0.50	67.809
Wo	50.9	0.2	48.1	99.2	49.63	0.11	50.25	2.01	58.120

The oxides were measured using XRF and are given in wt%. Data from Solvang et al. (2004 and 2005).

TABLE 5.2.
Density (g cm^{-3}) of the investigated materials at room temperature measured on glasses in air and ethanol. The numbers within parentheses represent the errors based on the standard deviation of three replicate mass determinations.

Samples	a	b * 10^{-4}	c	R^2	Standard Error	ΔT (K)
CAS1	0.92762	2.36541	-23900.795	0.99866	0.0032	298-1014
CAS2	1.00398	1.65507	-28139.408	0.99857	0.0032	298-1024
CAS3	0.91464	3.10086	-20569.448	0.99757	0.0048	298-1034
CAS4	0.94667	2.02091	-22136.687	0.99822	0.0034	298-1044
CAS5	0.89349	2.54394	-19570.683	0.99647	0.0052	298-1054
CAS6	0.95467	1.94693	-24772.988	0.99727	0.0044	298-1038
CAS7	0.90165	2.60633	-22492.289	0.99870	0.0033	298-1043
CAS8	0.94113	2.11327	-24194.172	0.99714	0.0046	298-1053
CAS9	0.98702	1.31906	-27306.309	0.99858	0.0029	298-1063
Wo	1.01636	0.59786	-33855.738	0.99901	0.0023	298-1014

TABLE 5.3.
Least squares fit parameters of the heat capacity glass state curves obtained using a modified Maier-Kelley equation (i.e., $c_p=a+bT+cT^{-2}$)

Samples	Temperature (K)	Density (g cm^{-3})
CAS1	298.05	2.8325 (0.0023)
CAS2	297.65	2.8504 (0.0025)
CAS3	297.65	2.8682 (0.0016)
CAS4	297.35	2.8857 (0.0028)
CAS5	297.55	2.9062 (0.0052)
CAS6	297.75	2.7627 (0.0037)
CAS7	298.05	2.7972 (0.0035)
CAS8	298.05	2.8186 (0.0038)
CAS9	298.15	2.8395 (0.0042)
Wo	298.15	2.9128 (0.0055)

Up to three different glass samples from each composition were heated at least 65 K above their T_g at 10 K min^{-1} after undergoing cooling at the same rate. From these data an average c_p was calculated (J g^{-1} K^{-1}). Regressions were performed on the average heat capacity curves of the glassy state for each composition. The onset of the glass transition area defines the high temperature end of the glassy state. ΔT is the temperature range of glassy state.

TABLE 5.4.

Least squares fit parameters for $\partial L/L_0$ (cm) dilatomeric traces. T_g temperature peaks obtained by dilatometry and calorimetry.

Samples	$a^{dil} \times 10^{-3}$	$b^{dil} \times 10^{-6}$	R^2	ΔT^a (K)	T_g^{dil} (K)	T_g^{cal} (K)
CAS1	-2.777	8.870	0.9988	298.5-1014.5	1068	1071
CAS2	-2.785	8.969	0.9986	297.7-1024.5	1081	1082
CAS3	-2.902	9.183	0.9987	297.7-1034.5	1092	1092
CAS4	-2.940	9.311	0.9970	297.4-1044.5	1103	1103
CAS5	-2.964	9.399	0.9989	297.6-1054.5	1113	1113
CAS6	-2.420	7.422	0.9981	297.8-1038.6	1093	1096
CAS7	-2.521	7.797	0.9986	298.1-1043.5	1103	1106
CAS8	-2.577	7.946	0.9985	298.1-1053.5	1110	1111
CAS9	-2.656	8.168	0.9988	298.2-1063.3	1120	1120
Wo	-3.445	10.732	0.9992	298.2-1014.4	1065	1064

Linear fit parameters for $\partial L/L_0$ (cm) as a function of temperature ($\partial L/L_0 = a^{dil} + b^{dil}T(K)$), for the investigated glasses across the temperature interval ΔT, which were heated and cooled at 10 K min^{-1} together with the glass transition temperatures obtained by dilatometry (T_g^{dil}) and calorimetry (T_g^{cal}).

^{a} The upper limit of ΔT was defined by the onset of the glass transition.

TABLE 5.5.

The thermal expansion coefficients, α_0 and α_1 of the investigated glasses.

Samples	V_{glass}^{298} (cm³ mol⁻¹)	$\alpha_0 \times 10^{-5}$	$\alpha_1 \times 10^{-9}$	$\overline{\partial V_{glass}}/\partial T \times 10^{-4}$ (cm³ mol⁻¹ K⁻¹)	ΔT (K)
CAS1	21.833	2.07157	8.80637	5.847	298-1014
CAS2	22.000	2.13776	8.35953	5.958	298-1024
CAS3	22.155	2.07761	9.91997	6.145	298-1034
CAS4	22.295	2.11887	9.82553	6.270	298-1044
CAS5	22.347	2.17697	9.26436	6.346	298-1054
CAS6	23.532	1.43553	11.4702	5.268	298-1038
CAS7	23.535	1.60309	10.5976	5.536	298-1043
CAS8	23.703	1.62295	10.8624	5.683	298-1053
CAS9	23.881	1.68102	10.8296	5.887	298-1063
Wo	19.953	2.30149	13.3134	6.472	298-1014

These coefficients were obtained by performing a least squares fit of Equation 2.14 in the temperature range ΔT. The molar thermal expansion coefficient α_{glass} can then be expressed empirically as $\alpha_{glass} = \alpha_0 + \alpha_1 T(K)$ within temperature range ΔT. A first approximation of the glassy molar thermal expansion $\overline{\partial V_{glass}}/\partial T$ was obtained as a regression coefficient from the linear relationship between the molar volume of the glass and absolute temperature (in the temperature range ΔT). Precise molar thermal expansion of the glass at temperature T can be calculated using Equation 2.12.

TABLE 5.6.

Molar volume ($cm^3\ mol^{-1}$), molar thermal expansivity ($cm^3\ mol^{-1}\ K^{-1}$) and molar thermal expansion coefficient (K^{-1}) of each melts at their supercooled liquid temperature (T_{sc}), the temperature at which the melt becomes relaxed, indicated by constant c_p.

Samples	V_{mol}^{Tsc} ($cm^3\ mol^{-1}$)	$\dfrac{\partial V^{Tsc}}{\partial T} x10^{-4}$ ($cm^3\ mol^{-1}\ K^{-1}$)	$\alpha_{mol}^{(Tsc)}\ x\ 10^{-6}$ (K^{-1})	T_{sc} (K)	T_{sc}- T_g (K)
CAS1	22.485 (0.01)	17.10	76.051 (2.1)	1150	79
CAS2	22.650 (0.01)	17.20	75.938 (1.7)	1150	68
CAS3	22.790 (0.01)	17.30	75.911 (2.2)	1160	68
CAS4	22.950 (0.01)	17.40	75.817 (0.6)	1172	69
CAS5	23.010 (0.01)	17.50	76.054 (1.5)	1178	65
CAS6	24.120 (0.01)	14.01	58.085 (2.0)	1170	74
CAS7	24.130 (0.01)	14.30	59.262 (1.9)	1180	74
CAS8	24.400 (0.01)	14.20	58.436 (2.6)	1185	74
CAS9	24.500 (0.01)	14.20	57.959 (2.4)	1200	80
Wo	20.620 (0.01)	20.50	99.418 (3.1)	1135	71

The number between the parentheses is the standard deviation from repeated measurements of the samples.

TABLE 5.7.

Parameters to fit the linear relationship between liquid molar volume and temperature for all compositions which were obtained in temperature interval ΔT.

Samples	a	$b\ x\ 10^{-3}$	R^2	ΔT (K)
CAS1	20.532	1.703	0.9999	1150-1973
CAS2	20.690	1.704	0.9999	1150-1973
CAS3	20.808	1.712	0.9999	1160-1973
CAS4	20.924	1.729	0.9999	1172-1973
CAS5	21.084	1.679	0.9990	1178-1973
CAS6	22.486	1.396	0.9999	1170-1973
CAS7	22.457	1.417	0.9999	1180-1973
CAS8	22.624	1.415	0.9999	1185-1973
CAS9	22.801	1.417	0.9999	1200-1973
Wo	18.437	1.973	0.9994	1135-1973

The molar volumes can be expressed empirically, using $V_{mol\_liq} = a + bT(K)$ in the temperature interval ΔT.

The lower temperature limit of ΔT is defined as the temperature of the supercooled liquid, obtained from the combined calorimetry/dilatometry method and upper temperature limit was taken as 100 K higher then the reference temperature used in the model of Courtial and Dingwell (1995).

TABLE 5.8.

Regression fit parameters provided using samples molar composition to calculate partial molar volume and molar thermal expansivity of each component (i).

1st regression i	$V_i, 1200$ $(cm^3\,mol^{-1})$	$\partial V_i/\partial T\,x10^{-3}$ $(cm^3\,mol^{-1}\,K^{-1})$
SiO_2	27.280 (0.234)	0.000 (0.5)
Al_2O_3	36.700 (0.194)	0.000 (0.4)
CaO	19.095 (0.228)	2.033 (0.5)
SiO_2-CaO	-3.197 (0.309)	1.308 (0.6)
R^2	0.99994	
Adjusted R^2	0.99993	
S	0.0092	

2nd regression i	$V_i, 1200$ $(cm^3\,mol^{-1})$	$\partial V_i/\partial T\,x10^{-3}$ $(cm^3\,mol^{-1}\,K^{-1})$
SiO_2	27.295 (0.396)	0.000 (0.7)
Al_2O_3	36.328 (0.352)	0.000 (0.6)
CaO	19.005 (0.248)	2.778 (0.4)
SiO_2-CaO	-3.056 (0.398)	0.121 (0.7)
R^2	0.99678	
Adjusted R^2	0.996593	
S	0.0882	

The fit parameters were derived from separate regressions of Eq.16 for liquids in the ternary CaO-Al_2O_3.SiO_2 system (CAS). The temperature ranges from 1200 to 1873 K in steps of 100 K. V_i is the partial molar volume of component i at reference temperature 1200 K. $\partial V_i/\partial T$ is molar thermal expansivity of the component i. Note that the partial molar volumes for the first regression analysis were obtained from all our molar volume data at T_{sc} together with the HT molar volume data calculated using the model of Courtial and Dingwell (1995). In the second regression, the partial molar volumes of SiO_2, Al_2O_3, and CaO were calculated using all our molar volume data at T_{sc}, together with the HT molar volume data of our samples calculated using Courtial and Dingwell (1995) model and finally all samples relevant to CAS system used in both models of Lange and Carmichael (1987) (LC3-LC8) and Courtial and Dingwell (1995) (Ca_{YX} samples).

TABLE 5.9.

Comparison of the fitted partial molar volumes and molar thermal expansivities calculated from the data presented in this study to the models of Lange and Carmichael (1987), Lange (1997) and Courtial and Dingwell (1995) at reference temperature of 1873 K.

$T_{ref}=1873K$	$V_i\,(cm^3\,mol^{-1})$ $\partial V_i/\partial T\,x10^{-3}(cm^3\,mol^{-1}\,K^{-1})$				
i	This study (1st regression)	This study (2nd regression)	L&C '87[a]	L'97[b]	C&D'95[c]
SiO_2	27.28	27.29	26.90	26.86	27.61
	0.00	0.00	0.00	0.00	1.85
Al_2O_3	36.70	36.33	37.63	37.42	36.36
	0.00	0.00	2.62	0.00	-2.06
CaO	20.46	20.88	17.15	17.27	20.84
	2.03	2.78	2.92	3.74	4.33
SiO_2-CaO	-2.32	-2.98	-	-	-8.35
	1.31	0.12	-	-	-4.14

[a] L&C '87 – from Table 8 in Lange and Carmichael (1987)
[b] L'97 – from Table 4 in Lange (1997)
[c] C&D '95 – from Table 5 in Courtial and Dingwell (1995)

134

TABLE 6.1.
The chemical composition of the investigated natural sample analysed by electron microprobe.

Sample / Oxide	Slapany (σ) basanite (wt%)	Etna (σ) trachybasalt (wt%)	Vesuvius (σ) tephriphonolite (wt%)
SiO_2	45.76 (0.15)	47.50 (0.81)	49.75 (0.39)
Al_2O_3	12.52 (0.20)	17.39 (1.42)	19.66 (0.18)
FeO_{tot}	11.30 (0.13)	10.27 (0.87)	5.84 (0.20)
TiO_2	2.27 (0.06)	1.70 (0.12)	0.71 (0.05)
MnO	0.25 (0.05)	0.21 (0.06)	0.17 (0.04)
MgO	11.42 (0.12)	5.54 (1.05)	2.95 (0.10)
CaO	11.45 (0.10)	10.35 (0.40)	8.79 (0.24)
Na_2O	2.65 (0.06)	3.96 (0.29)	3.81 (0.07)
K_2O	1.07 (0.04)	1.94 (0.19)	7.34 (0.13)
P_2O_5	0.86 (0.06)	0.63 (0.07)	0.53 (0.06)
Sum	99.55 (0.41)	99.49 (0.41)	99.55 (0.18)

The numbers within parentheses represent the errors based on the standard deviation of replicate measurements. The microprobe operating conditions: 15 kV acceleration voltage, 10nA beam current, 20 μm defocused beam diameter, counting time 20 s on the peak and 10 s on the background. A ZAF correction was undertaken. The calibration was based on mineral standards.

.

TABLE 6.2.
Linear fit parameters of the measured FeO (wt%) data as a function of absolute temperature ($FeO\ (wt\%) = A^{FeO} + B^{FeO} T(K)$) within the temperature range investigated ΔT.

Samples	A^{FeO}	$B^{FeO}\ x10^{-4}$	R^2	ΔT (K)
Slapany	-3.006	33.681	0.999	1796-1512
Etna	2.051	8.946	0.999	1803-1571
Vesuvius	-0.565	12.578	0.999	1803-1696

TABLE 6.3.

Experimental density results (g cm^{-3}) of the investigated materials.

Measurement at high-temperature were performed on stable melts in air. The numbers within parentheses represent the errors based on the standard deviation of three replicate buoyancy measurements.

Samples	Temperature (K)	Density (g cm^{-3})
Slapany		
RT	298.7	2.873 (0.003)
HT.1	1796.2	2.655 (0.002)
HT.2	1741.2	2.663 (0.004)
HT.3	1693.2	2.671 (0.005)
HT.4	1642.2	2.682 (0.006)
HT.5	1594.2	2.690 (0.003)
HT.6	1546.2	2.700 (0.003)
HT.7	1521.2	2.705 (0.005)
HT.8	1512.2	2.708 (0.012)
Etna		
RT	298.7	2.768 (0.003)
HT.1	1803.2	2.573 (0.002)
HT.2	1757.2	2.578 (0.002)
HT.3	1711.2	2.583 (0.001)
HT.4	1617.2	2.596 (0.002)
HT.5	1571.2	2.601 (0.002)
Vesuvius		
RT	298.7	2.621 (0.002)
HT.1	1803.2	2.458 (0.006)
HT.2	1757.2	2.463 (0.005)
HT.3	1745.2	2.463 (0.005)
HT.4	1712.2	2.465 (0.004)
HT.5	1696.2	2.467 (0.002)

TABLE 6.4.

Fit parameters for the average heat capacity curves across the glassy state were obtained by least squares fit method of the Maier - Kelley equation.

Samples	a	$b * 10^{-4}$	c	R^2	Standard Error
Slapany	0.792	4.851	- 15513.834	0.996	0.0068
Etna	0.812	3.980	- 16687.680	0.997	0.0053
Vesuvius	0.859	3.908	- 19616.695	0.993	0.0078

Three different glass samples from each composition were heated between 46 to 69 K above T_g at 5 K min^{-1} after undergoing cooling at the same rate.

TABLE 6.5.

Linear fit parameters of the $\partial L/L$ (cm) as a function of temperature for the investigated glasses which were heated and cooled at 5 K.min^{-1} obtained in temperature interval [a]ΔT. ($\partial L/L = a^{dil} + b^{dil}T(K)$), together with the glass transition temperatures obtained by dilatometry (T_g^{dil}) and calorimetry (T_g^{cal}).

Samples	a x 10^{-3}	b x 10^{-6}	R^2	[a]ΔT (K)	T_g^{dil} (K)	T_g^{cal} (K)
Slapany	-2.593	8.002	0.997	298-900	946	948
Etna	-2.566	7.994	0.997	298-886	945	947
Vesuvius	-2.771	8.752	0.999	298-878	940	942

[a] The glass dilatometric data were fitted within the temperature interval ΔT, until the occurrence of the onset of the glass transition.

TABLE 6.6.

The thermal expansion coefficients α_0 and α_1 of the investigated glasses obtained as least square fit parameters of Equation 2.14 in the temperature range ΔT.

Samples	$V_{glass}^{(298)}$ $(cm^3\,gfw^{-1})$	α_0 x 10^{-5}	α_1 x 10^{-8}	$\partial V_{glass}/\partial T$ x 10^{-4} $(cm^3\,mol^{-1}\,K^{-1})$	ΔT (K)
Slapany	21.374	1.286	1.825	5.389	298-900
Etna	23.355	1.363	1.720	5.825	298-886
Vesuvius	26.556	1.732	1.483	6.896	298-878

The thermal molar expansion coefficient α_{glass} can be expressed empirically as $\alpha_{glass} = \alpha_0 + \alpha_1\,T(K)$ within temperature range ΔT . As a first approximation glassy thermal molar expansion $(\partial V_{glass}/\partial T)$ was obtained from the linear fit between the molar volume of the glass and the absolute temperature (in the temperature range ΔT). Precise thermal molar expansion of the glass $(\partial V_{glass}/\partial T)$ at temperature T can be calculated using Equation 11.

TABLE 6.7.

Linear fit parameters of the experimental data of the investigated melts as a function of absolute temperature ($\rho = A^x + B^x\,T(K)$) within the temperature range investigated (ΔT).

Samples	$A^{density}$	$B^{density}$ x 10^{-4}	R^2	ΔT (K)
Slapany	3.001	-1.938	0.992	1796-1512
Etna	2.800	-1.262	0.999	1803-1571
Vesuvius	2.605	-0.813	0.986	1803-1696
	$A^{M.volume}$	$B^{M.volume}$ x 10^{-3}	R^2	ΔT (K)
Slapany	21.491	1.374	0.989	1796-1512
Etna	23.790	1.152	0.999	1803-1571
Vesuvius	26.394	0.754	0.980	1803-1696
	$A^{S.volume}$	$B^{S.volume}$ x 10^{-5}	R^2	ΔT (K)
Slapany	0.329	2.694	0.993	1796-1512
Etna	0.355	1.885	0.999	1803-1571
Vesuvius	0.383	1.340	0.986	1803-1696

[x] is density, molar volume or specific volume. $B^{M.volume}$ parameters correspond to the thermal molar expansivity $(\partial V/\partial T)$ within temperature range ΔT.

TABLE 6.8.

Molar volume (cm^3 gfw^{-1}), thermal molar expansivity (cm^3 mol^{-1} K^{-1}) and molar thermal expansion coefficient (K^{-1}) of the melts at their supercooled liquid temperature (Tsc).

Samples	[a] V_{mol}^{Tsc}	[a] $\dfrac{\partial V^{Tsc}}{\partial T}$ x10^{-4}	[a] $\alpha_{mol}^{(Tsc)}$ x 10^{-6}	[b] T_{sc} (K)
Slapany	22.858 (0.01)	16.859 (0.48)	73.753 (2.1)	993 (46)
Etna	24.716 (0.01)	18.996 (0.47)	76.857 (1.9)	995 (49)
Vesuvius	26.788 (0.01)	20.981 (0.62)	78.320 (2.3)	1010 (69)

[a] The number between parentheses represent the errors based on the standard deviation of replicate measurements for samples under the same conditions (i.e., heating/ cooling rate of 5 K min^{-1}).
[b] is defined as the temperature at which the supercooled liquid is relaxed. The number in parentheses represents the difference between Tsc and the glass transition temperature Tg (defined as c_p peak).

TABLE 6.9.

Regression coefficients from the equation: $V = a + b\ ln(T)$ where T is the absolute temperature.

Samples	a	b	R^2	ΔT (K)
Slapany	8.706	2.041	0.961	993-1796
Etna	11.045	1.979	0.999	995-1803
Vesuvius	14.982	1.707	1.000	1010-1803

Use of this equation allows, the molar volume of the liquid to be calculated as a function of the natural logarithm of absolute temperature.

TABLE 7.1.

List of samples used in this study including: rock type, sample label, composition (wt% oxides) and reference source. Compositions were measured at the IPGP (Istitut du Physique du Globe Parìs) using the conditions reported at the bottom of the table.

Location	Sample	Composition	SiO_2	TiO_2	Al_2O_3	FeO_{tot}	MnO	MgO	CaO	Na_2O	K_2O	P_2O_5	SUM	SM	NBO/T	ref.	
Nyiragongo (DRC)	NYI	Foidite	41.07	2.75	14.97	11.99	0.32	3.72	10.39	6.89	5.61	1.22	98.93	37.10	0.73	0	Scoria from February 2002 eruption
Stromboli, I	STB*	Trachybas.	49.07	0.98	16.91	8.36	0.22	5.73	10.88	2.63	2.20	0.00	96.98	31.26	0.45	*	Scoria from April 2003 eruption
Monserrat	MST	Andesite	60.71	0.58	18.29	6.38	0.19	2.58	7.10	3.57	0.85	0.00	100.24	20.06	0.15	*	Tephra from the 1997 vulcanian eruption
PF, I	Min2a	Shoshonite	52.26	0.75	16.06	7.45	0.10	5.56	9.92	2.33	3.67	0.00	98.11	29.60	0.43	*	Tephra from the (10.3 - 9.5 ky) Minopoli eruption [10]
PF, I	Min2b	Shoshonite	53.72	0.64	17.47	7.22	0.17	3.78	8.07	3.63	3.53	0.00	98.23	26.11	0.30	*	Tephra from the (10.3 - 9.5 ky) Minopoli eruption [10]
PF, I	Fra	Latite	55.41	0.72	18.38	7.31	0.16	2.39	5.76	4.23	4.58	0.00	98.95	22.70	0.19	*	Tephra from the (10.3 - 8 ky) Fondo Riccio eruption [10]
PF, I	NYT*	Trachyte	58.77	0.50	18.39	4.96	0.06	1.43	4.03	3.38	7.67	0.00	99.18	19.16	0.12	*	Tephra from the 15 ky Napolitean Yellow Tuff eruption [11]
PF, I	CI_OF*	Trachyte	68.80	0.23	12.58	3.17	0.14	1.24	3.43	4.01	6.18	0.03	99.84	16.20	0.16	*	Tephra from the 39 ky Campanian Ignimbrite eruption [12]
Slapany, CZ	SLP*	Basanite	45.76	2.27	12.52	11.30	0.25	11.42	11.45	2.65	1.07	0.86	99.55	39.57	0.90	*	Slapany Lava flow
Merapi (Indonesia)	MRP	Andesite	53.53	0.82	18.95	9.03	0.19	3.42	9.23	3.45	1.64	0.00	100.26	25.87	0.26	*	Tephra from the 1993 dome eruption
Moldavite	MDV	Moldavite	79.43	0.20	9.94	1.89	0.03	1.64	2.42	0.49	3.42	0.00	99.44	9.08	0.05	*	Tectite analogue
PF, I	IGC	Trachyte	60.74	0.27	19.22	3.37	0.18	0.28	2.11	5.28	6.32	0.06	97.83	15.58	0.04	1	
PF, I	MNV	Trachyte	63.88	0.31	17.10	2.90	0.13	0.24	1.82	5.67	6.82	0.05	98.93	15.35	0.07	1	
PF, I	AMS_B1	Trachyte	60.10	0.38	18.03	3.43	0.14	0.73	2.92	4.49	7.89	0.16	98.27	17.51	0.10	1	
PF, I	AMS_D1	Trachyte	59.98	0.39	18.01	3.82	0.11	0.88	2.91	4.06	8.37	0.21	98.75	17.75	0.11	1	
Vesuvius (I)	Ves_W	Phonolite	52.02	0.59	19.28	4.65	0.14	1.72	6.58	4.53	7.69	0.65	97.82	24.45	0.26	1	
Vesuvius (I)	Ves_G	Phonolite	51.24	0.58	19.14	4.55	0.12	1.71	6.51	4.60	7.99	0.71	97.14	24.80	0.28	1	
Montana Blanca E)	Td_ph	Phonolite	60.46	0.56	18.81	3.31	0.20	0.36	0.67	9.76	5.45	0.06	99.64	17.88	0.10	1	
Unzen (Japan)	UNZ	Dacite	66.00	0.36	15.23	4.08	0.10	2.21	5.01	3.84	2.16	0.14	99.13	17.03	0.14	1	
Vesuvius, I	Ves_Gt	Phonoteph.	49.70	0.84	16.57	7.27	0.13	5.15	10.30	2.73	6.57	0.73	99.98	31.77	0.53	1	
Vesuvius, I	VesW_t	Tephriphon.	51.94	0.68	18.87	6.19	0.13	2.54	7.41	3.80	8.01	0.41	99.98	26.40	0.31	1	
Povocao, P	PVC	Trachyte	65.26	0.45	17.30	2.60	0.14	0.32	0.85	6.46	6.52	0.09	99.98	14.63	0.06	1	
Eifel, D	EIF	Basanite	41.14	2.74	12.10	10.11	0.18	11.24	15.66	2.76	3.04	1.02	99.98	44.71	1.17	1	
Etna, I	ETN	Trachybas.	47.03	1.61	16.28	10.13	0.20	5.17	10.47	3.75	1.94	0.59	97.18	32.04	0.51	1	
PF, I	ATN	Trachyte	60.66	0.47	18.82	3.66	0.17	0.66	2.85	3.95	8.59	0.15	99.98	17.15	0.09	1	
Mt Peleé (Martiniq)	ME1311e	Andesite	62.46	0.55	20.03	0.03	0.02	3.22	9.09	3.52	0.93	0.12	99.98	19.97	0.16	2	
Mt. St Helens Wa.)	MSHD	Dacite	65.28	0.59	17.05	4.97	0.08	1.82	4.70	4.34	1.29	0.13	100.25	16.34	0.10	3	
	SiO_2		100	0.00	0.00	0.00	0.00	0.00	0.00	0.00	0.00	0.00	100.00	0.00	0.00	4	
	HPG8	Haplogran.	78.60	0.00	12.50	0.00	0.00	0.00	0.00	4.60	4.20	0.00	99.90	7.73	0.02	5	
	W_T	Trachytic	64.45	0.50	16.71	0.00	0.00	2.92	5.36	6.70	3.37	0.00	100.01	20.12	0.21	6a	
	W_ph	Phonolitic	58.82	0.79	19.42	0.00	0.00	1.87	2.35	9.31	7.44	0.00	100.00	21.27	0.19	6a	
	W_Tf	Tephritic	50.56	2.35	14.03	0.00	0.00	8.79	15.00	7.04	3.01	0.00	100.78	38.53	0.86	6b	
	NIQ	Basanitic	43.57	2.97	10.18	0.00	0.00	9.17	26.07	7.59	0.96	0.00	100.51	48.93	1.51	6b	
	N_An	Andesitic	62.40	0.55	20.01	0.03	0.02	3.22	9.08	3.52	0.93	0.12	99.88	19.97	0.16	7	
Stein Frentz , D	SFB	Tephritic	46.58	2.45	13.28	11.20	0.00	9.15	10.00	5.60	1.38	0.00	99.64	37.77	0.75	8	
Stein Frentz , D	SFB5	Tephritic	48.23	2.32	13.10	10.24	0.00	8.91	10.01	5.63	1.45	0.00	99.89	36.82	0.72	8	
Stein Frentz , D	SFB10	Phonoteph.	49.34	2.12	12.80	9.86	0.00	8.10	9.62	6.10	1.52	0.00	99.46	35.67	0.69	8	
Stein Frentz , D	SFB20	Mugearitic	51.58	1.51	12.12	8.94	0.00	7.24	9.24	6.48	1.76	0.00	98.87	34.14	0.66	8	
Stein Frentz , D	SFB40	Trachytic	58.97	1.58	9.86	7.24	0.00	4.56	5.33	8.99	2.34	0.00	98.87	27.71	0.50	8	
Stein Frentz , D	SFB60	Rhyolitic	74.84	0.50	4.24	1.20	0.00	1.98	1.96	11.34	3.39	0.00	99.45	19.41	0.40	8	
	HPG8An10	Synthetic	73.60	0.00	15.60	-1.00	0.00	0.00	2.10	4.40	3.80	0.00	98.50	9.42	-0.01	9	
	HPG8An20	Synthetic	71.50	0.00	17.30	0.00	0.00	0.00	4.00	4.20	3.50	0.00	100.50	11.54	0.01	9	
	HPG8An50	Synthetic	64.00	0.00	23.10	0.00	0.00	0.00	8.70	2.60	1.90	0.00	100.30	14.46	-0.01	9	
	HPG8An75	Synthetic	56.20	0.00	27.20	0.00	0.00	0.00	13.30	1.60	1.50	0.00	99.80	18.89	0.02	9	

0.Giordano et al. (2005); **1.** Giordano and Dingwell (2003a); **2.** Richet et al. (1996); **3.** Alibidirov et al. (1997); **4.** Toplis et al. (1997); **5.** Dingwell et al. (1996); **6.** Whittington et al. (2000. 2001); **7.** Neuville et al. (1993); **8.** Bouhifd et al. (2004); **9.** Dingwell et al. (2000); **10.** Di Vito et al.. (1999); **11.** Deino et al. (2003); **12.** Civetta et al. (1988); *this study. Experimental conditions used during microprobe analysis are: 15 kv, 10nA, spot 5μm. The standard crystals and the counting time (in seconds) are as it follows: TAP [Si (10); Al (10)]; LIF [Fe (20); Mn(60); Ti (60)]; PET [K(10)]; TAP [Na (10); Mg (10)].

TABLE 7.2.
Measured values of viscosity for individual melt compositions at specified temperatures.

Sample name	T (°C)	log η (Pa s)	Sample name	T (°C)	log η (Pa s)	Sample name	T (°C)	log η (Pa s)
IGC	1495.5	2.37	STB*	1200.2	2.02	SLP*	1495.5	-0.19
IGC	1470.9	2.49	STB*	1175.6	2.21	SLP*	1470.9	-0.12
IGC	1446.3	2.63	STB*	1151.0	2.39	SLP*	1446.3	-0.03
IGC	1421.7	2.77	STB*	729.5	9.35	SLP*	1421.7	0.05
IGC	1397.1	2.92	STB*	697.9	10.51	SLP*	1397.1	0.15
IGC	1372.5	3.08				SLP*	1372.5	0.24
IGC	1347.8	3.24	Fra	1593.9	1.02	SLP*	1347.8	0.34
IGC	1323.2	3.4	Fra	1569.3	1.08	SLP*	1323.2	0.45
IGC	1298.6	3.58	Fra	1544.7	1.19	SLP*	1298.6	0.56
IGC	1274.0	3.76	Fra	1520.1	1.29	SLP*	1274.0	0.68
IGC	1249.4	3.94	Fra	1495.5	1.40	SLP*	1249.4	0.81
IGC	1224.8	4.14	Fra	1470.9	1.50	SLP*	730.1	9.01
IGC	1200.2	4.34	Fra	1446.3	1.62	SLP*	719.3	9.42
IGC	1175.6	4.54	Fra	1421.7	1.72	SLP*	688.3	10.53
IGC	782.5	10.83	Fra	1397.1	1.85	SLP*	696.6	10.08
IGC	803.1	10.44	Fra	1372.5	1.97			
IGC	835.6	9.84	Fra	1347.8	2.10	MRP	1593.9	0.61
IGC	860.7	9.32	Fra	1323.2	2.24	MRP	1569.3	0.70
			Fra	1298.6	2.38	MRP	1544.7	0.80
MST	1618.6	1.04	Fra	1274.0	2.52	MRP	1520.1	0.89
MST	1593.9	1.11	Fra	1249.4	2.67	MRP	1495.5	0.99
MST	1569.3	1.21	Fra	1224.8	2.83	MRP	1470.9	1.09
MST	1544.7	1.32	Fra	1200.2	2.99	MRP	1446.3	1.20
MST	1520.1	1.43	Fra	1175.6	3.16	MRP	1421.7	1.31
MST	1495.5	1.53	Fra	1151.0	3.35	MRP	1397.1	1.43
MST	1470.9	1.65	Fra	771.3	10.11	MRP	1372.5	1.56
MST	1446.3	1.76	Fra	765.7	10.05	MRP	1347.8	1.68
MST	1421.7	1.89	Fra	753.3	10.45	MRP	1323.2	1.82
MST	1397.1	2.01	Fra	749.1	10.52	MRP	1298.6	1.97
MST	1372.5	2.15	Fra	741.4	10.55	MRP	1274.0	2.12
MST	1347.8	2.29	Fra	734.0	10.65	MRP	1249.4	2.28
MST	1323.2	2.43	Fra	713.7	10.99	MRP	1224.8	2.44
MST	1298.6	2.58	Fra	711.9	10.98	MRP	1200.2	2.62
MST	1274.0	2.73				MRP	1175.6	2.81
MST	1249.4	2.90	CI_OF*	1593.9	2.02	MRP	1151.0	3.01
MST	1224.8	3.06	CI_OF*	1569.3	2.14	MRP	1126.4	3.22
MST	1200.2	3.25	CI_OF*	1544.7	2.26	MRP	722.9	10.5
MST	753.4	9.74	CI_OF*	1520.1	2.39	MRP	716.0	10.6
MST	739.6	10.18	CI_OF*	1495.5	2.52			
MST	688.7	11.60	CI_OF*	1470.9	2.66	MDV	1643.2	2.83
			CI_OF*	1446.3	2.80	MDV	1618.6	2.96
STB*	1593.9	0.21	CI_OF*	1421.7	2.94	MDV	1593.9	3.10
STB*	1569.3	0.28	CI_OF*	1397.1	3.10	MDV	1569.3	3.24
STB*	1544.7	0.37	CI_OF*	1372.5	3.25	MDV	1544.7	3.38
STB*	1520.1	0.45	CI_OF*	1347.8	3.42	MDV	1520.1	3.53
STB*	1495.5	0.54	CI_OF*	1323.2	3.59	MDV	1495.5	3.69
STB*	1470.9	0.64	CI_OF*	1298.6	3.76	MDV	1470.9	3.84
STB*	1446.3	0.74	CI_OF*	1274.0	3.94	MDV	1446.3	4.01
STB*	1421.7	0.84	CI_OF*	1249.4	4.13	MDV	1421.7	4.18
STB*	1397.1	0.95	CI_OF*	856.3	9.00	MDV	1397.1	4.36
STB*	1372.5	1.06	CI_OF*	836.3	9.31	MDV	1372.5	4.53
STB*	1347.8	1.16	CI_OF*	822.8	9.56	MDV	919.6	9.43
STB*	1323.2	1.29	CI_OF*	797.2	10.08	MDV	882.3	10.11
STB*	1298.6	1.42	CI_OF*	780.3	10.35	MDV	864.7	10.45
STB*	1274.0	1.56				MDV	817.8	11.20
STB*	1249.4	1.70	SLP*	1544.7	-0.31	MDV	954.7	8.92
STB*	1224.8	1.86	SLP*	1520.1	-0.24			

TABLE 7.3.

Model fits of VFT equation to individual data sets. Model parameter values are reported for independent fits of each melt composition (A, B, C) and fits coupled by a common value of A (-4.07) and independent values of B and C. Also reported N, χ^2 and RMSE (Root Mean Square Error)

		Single fits values (Eq. 1)								
		-7.38	27568.73	-24.48		0.07				
		Individual fit parameters					Common A parameters			
Sample	N	Avft	Bvft	Cvft	χ^2	RMSE	Bvft	Cvft	χ^2	RMSE
SiO$_2$	26	-7.38	27568.73	-24.48	0.07	0.05	16110.07	421.44	0.45	0.13
IGC	18	-4.77	9184.30	473.71	0.12	0.08	7999.62	526.70	0.13	0.09
MNV	19	-6.05	13653.62	165.01	0.02	0.03	9513.13	338.71	0.12	0.08
AMS_B1	11	-3.82	9055.89	362.24	0.07	0.08	9527.53	340.61	0.07	0.08
AMS_D1	14	-3.86	9107.49	350.21	0.09	0.08	9515.45	331.46	0.09	0.08
Ves_W	14	-6.76	12183.32	265.80	0.09	0.08	7460.75	463.58	0.25	0.13
Ves_G	14	-6.34	11559.47	304.76	0.35	0.16	7685.78	464.96	0.52	0.19
Td_ph	22	-4.94	11068.55	220.81	0.02	0.03	9356.47	295.80	0.05	0.05
UNZ	20	-3.63	6878.87	545.14	0.02	0.03	7581.79	510.68	0.03	0.04
Ves_Gt	16	-4.98	6986.95	531.98	0.05	0.06	5591.25	601.23	0.10	0.08
VesW_t	12	-5.05	8069.69	467.16	0.03	0.05	6410.60	546.93	0.05	0.06
HPG8	10	-7.32	18859.18	128.39	0.01	0.04	11013.98	430.56	0.06	0.08
PVC	25	-5.68	13003.54	205.44	0.04	0.04	9574.11	353.78	0.12	0.07
EIF	10	-4.24	4171.47	687.90	0.05	0.07	3958.80	699.35	0.05	0.07
ETN	10	-4.84	6019.41	602.37	0.03	0.06	4893.52	658.69	0.04	0.07
W_T	24	-3.61	7201.13	510.12	0.02	0.03	7957.46	474.82	0.06	0.05
W_ph	20	-3.22	7009.47	458.59	0.01	0.03	8372.12	396.59	0.14	0.08
W_Tf	22	-3.93	4662.72	639.99	0.08	0.06	4830.22	631.92	0.08	0.06
NIQ	20	-5.06	5289.38	605.55	0.02	0.03	4541.56	633.26	0.17	0.09
N_An	14	-3.97	7184.27	508.67	0.03	0.05	7355.36	500.77	0.03	0.05
ATN	17	-4.99	10078.07	382.53	0.09	0.07	8428.82	456.38	0.11	0.08
MSHD	12	-5.08	10008.47	372.45	0.02	0.04	8093.43	461.17	0.04	0.06
ME1311e	36	-4.36	7360.71	567.14	0.02	0.03	6905.56	588.03	0.05	0.04
NYI	23	-3.97	4257.07	677.48	0.34	0.12	4390.20	670.42	0.34	0.12
STB_B30	21	-3.70	4816.41	632.70	0.00	0.01	5331.53	605.24	0.02	0.03
MST	21	-4.25	7308.32	503.02	0.02	0.03	7021.19	516.73	0.02	0.03
Min_2a	25	-4.10	5749.19	584.80	0.16	0.08	5707.24	586.88	0.16	0.08
Min_2b	25	-3.66	5629.01	572.09	0.03	0.04	6237.55	541.20	0.06	0.05
FR_a	27	-4.66	7436.51	523.86	1.15	0.21	6530.46	566.17	1.20	0.21
NYT_lm*13*	24	-3.97	7390.22	514.10	0.02	0.03	7565.79	505.75	0.03	0.03
CI_OF104	20	-5.44	11387.42	336.00	0.02	0.03	8683.52	457.97	0.07	0.06
Slapany	17	-4.44	4680.09	650.73	0.15	0.10	4209.57	675.93	0.17	0.10
MRP	22	-3.84	5636.13	600.77	0.01	0.02	5976.23	583.66	0.02	0.03
MDV_snt	17	-6.43	16039.36	184.00	0.01	0.02	10558.22	408.32	0.09	0.07
SFB	11	-3.47	3641.66	678.94	0.04	0.06	4380.17	638.49	0.05	0.07
SFB5	13	-3.56	4290.31	639.86	0.11	0.09	4856.70	612.16	0.18	0.12
SFB10	14	-4.50	5635.45	573.37	0.57	0.20	5114.99	598.16	0.60	0.21
SFB20	15	-3.41	4390.19	625.01	0.45	0.17	5138.79	587.84	0.56	0.19
SFB40	15	-3.15	5105.35	538.97	0.01	0.02	6318.20	479.64	0.18	0.11
SFB60	18	-1.82	4762.12	461.56	0.07	0.06	8206.66	282.26	0.96	0.23
HPG8An10	8	-6.20	15552.56	221.44	0.01	0.03	10576.73	428.68	0.02	0.05
HPG8An20	10	-4.37	10213.29	456.98	0.00	0.00	9631.14	483.67	0.00	0.01
HPG8An50	12	-4.12	7235.99	636.87	0.02	0.05	7166.01	640.21	0.03	0.05
HPG8An75	14	-4.21	6076.60	727.36	0.04	0.05	5894.99	736.49	0.04	0.05

TABLE 7.4.
Isothermal viscosity curve values for the a_i coefficients of Equation 7.2.

$T(°C)$	a_1	a_2	a_3
630	11.7979	17.715	3.116
670	9.15816	17.813	4.507
700	7.54986	17.731	5.450
800	3.3433	17.288	9.2741
900	1.1136	16.185	11.020
1000	-0.3258	15.078	12.378
1100	-1.2886	14.039	13.423
1200	-1.9651	13.099	14.269
1300	-2.4516	12.258	14.936
1400	-2.8139	11.508	15.491
1500	-3.0908	10.828	15.998
1600	-3.3099	10.231	16.432
1800	-3.6018	9.1890	17.058
2000	-3.8001	8.3428	17.587

TABLE 7.5.
Example of viscosity calculation for the Campanian Ignimbrite sample (IGC) at 1200°C. Inputs are the temperature in degree Celsius and the composition in wt%.

Sample name (IGC)	Input values Composition (wt. %)	Output values Composition (moles %)		Calculated parameters (Eqs. 8-11)			
SiO$_2$	60.74	70.31					
TiO$_2$	0.27	0.24	b_1	-2.115425225			
Al$_2$O$_3$	19.22	13.11	b_2	13.12945529			
Fe$_2$O$_3$*	1.69	0.73	b_3	14.30849252			
FeO*	1.69	1.63	b_4	0.002671818			
MgO	0.28	0.48					
CaO	2.11	2.62	logη(Pas)	**4.173**			
Na$_2$O	5.28	5.93					
K$_2$O	6.32	4.67					
P$_2$O$_5$	0.06	0.03					
MnO	0.18	0.18					
H$_2$O**	0.02	0.08					
sum	97.83	100.00					
FeO$_{tot}$*	3.37				Model coefficients		
		molar amount		Eq. 7.8	Eq. 7.9	Eq. 7.10	Eq. 7.11
SM		15.58		-33.5556	0.03516228	-0.0022362	-1.66697E-06
AE		-2.52		-93.6494	0.2317411	-0.0054597	1.36107E-05
AE/SM		-0.1618		45.575455	-0.0780935	-0.0036108	-2.17E-08
T(°C)	1200			-1.29239E-05	0.03577545	-24.3366274	

* FeO and Fe$_2$O$_3$ are arbitrarily calculated assuming that half of the total iron FeO$_{tot}$ (wt. %) is partioned as FeO and the remaining half is partioned as Fe$_2$O$_3$.
**According to the observations from Ohlhorst et al. (2001), that a residual amount of water is always present also in remelted liquid, we have added a fixed amount of water of 200 ppm to the chemical analysis for "virtually dry" samples.

Curriculum Vitae

<u>Persönliche Daten:</u>

Marcel Potužák, geboren am 17. Dezember 1972 in Sušice, Tschechoslowakei, wohnhaft in Kolinec, Tschechische Republik

<u>Schulbildung:</u>

1979 – 1987 Besuch der Grundschule Příbram, Tschechoslowakei

1987 – 1991 Besuch der technischen Fachschule Příbram, Tschechoslowakei

Juli 1991 Erwerb des Abiturs

<u>Studium:</u>

- September 1991 - September 1996: Studium am Institut für Geochemie, Mineralogie und Mineral Quellen der Karls Universität Prag (UK Praha), Tschechische Republik
- September 1994: Abschluss in Geologie (Titel: „Bakalar [Bc.])
- September 1996: Erwerb des Diploms in Geochemie (Titel: Magister [Mgr.])
- November 1997 – Juni 1999: Studium am Institut für Hydrogeologie, Ingenieurgeologie und angewandte Geophysik der Karls Universität Prag (UK Praha), Tschechische Republik
- Juni 1999: Erwerb des Diploms in Ingenieurgeologie (Titel: Magister [Mgr.])
- July 1999: Sommer-Ausbildung an der Linguistik-Schule der Universität Bamberg, Deutschland
- Seit Juni 2001: Promotion am Institut für Mineralogie, Petrologie und Geochemie der Ludwig-Maximilians-Universität (LMU) München (seit 2002 Sektion Mineralogie am Department für Geo- und Umweltwissenschaften der LMU München)

<u>Berufstätigkeit und Stipendien:</u>

- Juli 1989 – August 1989: Praktikum als Juniorforscher bei der UD Příbram an der Uran-Lagerstätte Příbram, Tschechoslowakei
- Juli 1990 – August 1990: Praktikum als Juniorforscher bei der Geoindustria Praha an der Gold- and Wolfram-Lagerstätte im Südwesten des Böhmischen Massifs, Tschechoslowakei

- August 1997 - Dezember 1997: Praktikum als Junior-Ingenieur-Geologe am Institut für Geotechnik, Frankfurt am Main, Deutschland

- April 2000 – August 2000: Erasmus/Socrates Stipendium

- November 2000 – Dezember 2001: "EU research training network"-Stipendium "Volcano dynamics in relation to monitoring, hazards mitigation and volcano crisis response"

- Dezember 2001 – März 2002: Stipendium des DAAD

- April 2002 - Juni 2002: Wissenschaftliche Arbeit am Observatoire Volcanologique de la Soufrière, Guadeloupe, (French West Indies)

- April 2002 – August 2002: Stipendium von "NATO Science Fellowships Programme"

- Seit September 2005: Mitglied des „**Elite Network Bayern -** International graduate school, THESIS"

- zur Zeit: wissenschaftlicher Angestellter am Department für Geo- und Umweltwissenschaften der LMU München